



Review

# Perspectives and Research Challenges in Wireless Communications Hardware for the Future Internet and Its Applications Services

Dimitrios G. Arnaoutoglou <sup>1</sup>, Tzichat M. Empliouk <sup>1</sup>, Theodoros N. F. Kaifas <sup>1</sup>, Constantinos L. Zekios <sup>2</sup> and George A. Kyriacou <sup>1,\*</sup>

<sup>1</sup> Department of Electrical and Computer Engineering, Democritus University of Thrace, 67100 Xanthi, Greece; darnaout@ee.duth.gr (D.G.A.); templiou@ee.duth.gr (T.M.E.); tkaifas@ee.duth.gr (T.N.F.K.)

<sup>2</sup> Department of Electrical and Computer Engineering, Florida International University, Miami, FL 33174, USA; kzekios@fiu.edu

\* Correspondence: gkyriac@ee.duth.gr

**Abstract:** The transition from 5G to 6G wireless systems introduces new challenges at the physical layer, including the need for higher frequency operations, massive MIMO deployment, advanced beamforming techniques, and sustainable energy harvesting mechanisms. A plethora of feature articles, review and white papers, and roadmaps elaborate on the perspectives and research challenges of wireless systems, in general, including both unified physical and cyber space. Hence, this paper presents a comprehensive review of the technological challenges and recent advancements in wireless communication hardware that underpin the development of next-generation networks, particularly 6G. Emphasizing the physical layer, the study explores critical enabling technologies including beamforming, massive MIMO, reconfigurable intelligent surfaces (RIS), millimeter-wave (mmWave) and terahertz (THz) communications, wireless power transfer, and energy harvesting. These technologies are analyzed in terms of their functional roles, implementation challenges, and integration into future wireless infrastructure. Beyond traditional physical layer components, the paper also discusses the role of reconfigurable RF front-ends, innovative antenna architectures, and user-end devices that contribute to the adaptability and efficiency of emerging communication systems. In addition, the inclusion of application-driven paradigms such as digital twins highlights how new use cases are shaping design requirements and pushing the boundaries of hardware capabilities. By linking foundational physical-layer technologies with evolving application demands, this work provides a holistic perspective aimed at guiding future research directions and informing the design of scalable, energy-efficient, and resilient wireless communication platforms for the Future Internet. Specifically, we first try to identify the demands and, in turn, explore existing or emerging technologies that have the potential to meet these needs. Especially, there will be an extended reference about the state-of-the-art antennas for massive MIMO terrestrial and non-terrestrial networks.



Academic Editor: Gianluigi Ferrari

Received: 15 April 2025

Revised: 19 May 2025

Accepted: 28 May 2025

Published: 31 May 2025

**Citation:** Arnaoutoglou, D.G.; Empliouk, T.M.; Kaifas, T.N.F.; Zekios, C.L.; Kyriacou, G.A. Perspectives and Research Challenges in Wireless Communications Hardware for the Future Internet and Its Applications Services. *Future Internet* **2025**, *17*, 249. <https://doi.org/10.3390/fi17060249>

**Copyright:** © 2025 by the authors.

Licensee MDPI, Basel, Switzerland. This article is an open access article distributed under the terms and conditions of the Creative Commons Attribution (CC BY) license

(<https://creativecommons.org/licenses/by/4.0/>).

**Keywords:** Internet of Things; multifunctional antennas; beamforming networks; passive components; 5G systems

## 1. Introduction

Wireless communication has grown rapidly, leading to the development and widespread use of 5G networks. However, 6G wireless systems aim to achieve much

higher ambitions, targeting ubiquitous ultra-high-speed connectivity, ultra-low latency, and full integration with artificial intelligence and extended reality services. Meeting these objectives requires overcoming profound challenges at the physical layer, particularly regarding efficient spectrum utilization, severe propagation losses, energy sustainability, and scalable system design. Critical technologies such as beamforming, massive MIMO, RIS, terahertz communications, wireless energy harvesting, and digital twins are pivotal. Although many studies have been conducted, a comprehensive and systematic review consolidating these advancements has been lacking.

The rollout of 5G, especially in the sub-6 GHz spectrum, has significantly enhanced network performance and reliability, offering scalable support for the pre-existing Internet of Things (IoT) ecosystem [1,2]. The importance is highlighted by the European Union's allocation of 150 million euros to support further research and advancements in the field of IoT [3]. Despite the efforts of service providers and manufacturers, 5G has not fully achieved its true capabilities. For example, in most European countries, the mmWave band (FR-2) has not yet been deployed [4]. However, numerous articles can already be found in the literature proposing the structure and functionalities of next-generation mobile communications, namely, those beyond 5G and 6G [5–9]. A motivation behind the rush for the standardization of 6G is the emerging Society 5.0 and its demand for broadband, low-latency, and ultra-reliable communications [10].

The early generations of mobile communications (1G–3G) primarily focused on expanding and upgrading communication infrastructure. In contrast, long-term evolution (LTE) or 4G transformed mobile communications into an integral part of daily life by delivering significantly higher data rates. 5G represents a significant evolution from a technology that enhances daily life (4G) to a comprehensive social infrastructure, enabling connectivity not only between people but also with animals and machines through the IoT [11]. As envisioned by many researchers, time and space will become controllable at a high level in the Beyond 5G/6G era [5]. This implies that, through emerging technologies such as augmented reality and digital twins, users will be able to transcend certain limitations of the physical world. Specifically, the real world (physical space) will seamlessly merge with cyberspace (the Internet), unlocking novel capabilities that were unattainable with previous generations of mobile communications [12,13].

The term physical space encompasses all communication infrastructures, extending beyond terrestrial networks [5]. On the other hand, cyberspace refers to all software-driven methods used to process and manage the vast amount of data collected from the physical space. In such a cyber–physical system, humans, animals, and machines will seamlessly interact through cyberspace, fostering enhanced connectivity and automation. Moreover, cyber–physical systems are expected to become deeply integrated with various social activities, contributing to the development of a more “human-centered” society. In fact, many experts foresee that communication networks will soon serve as the foundational infrastructure of society, functioning as its neural network [5,14].

The complexity and abstractness of 6G has led to an ongoing debate among service providers, infrastructure manufacturers, researchers, and governments worldwide about how to proceed with the transition to this new generation. For this reason, a wide range of white papers has been published, offering key insights and guidelines on recent research and developments in the field [14,15]. The goal is to encourage the development of an open system that enables participation from various corporations, recognizing the critical importance of this ecosystem. As Beyond 5G/6G evolves into an open platform, key stakeholders, including service developers, end users, communication device manufacturers, network operators, and algorithm providers, will be able to collaborate more freely to improve

its capabilities [14]. This collaborative environment will foster the continued growth of Beyond 5G/6G, positioning it as a cornerstone of global social infrastructure.

In the physical space, 6G aims to expand beyond the conventional 2D terrestrial network by integrating non-terrestrial networks into a fully immersive 3D infrastructure. This evolution will take us beyond traditional mobile networks based primarily on smartphones to a comprehensive ecosystem that seamlessly connects private wireless systems, next-generation wireless local access networks, high-altitude platform stations (HAPS), and satellites [5]. In addition to wireless networks, optical networks will be seamlessly integrated to enable ultra-low latency and high-capacity communication between edge computing devices, edge clouds, and data centers. Establishing such a unified network will allow for the adaptive utilization of all available resources, ensuring uninterrupted service for all users. Notably, the management and orchestration of these interconnected networks will enable the dynamic selection of the optimal communication channel, whether terrestrial or non-terrestrial, ensuring users' connectivity needs are met anytime and anywhere across diverse environments.

The three primary service scenarios anticipated for 6G are enhanced mobile broadband (eMBB), ultra-reliable and low latency communication (URLLC), and machine-type communication (MTC) [14]. Enhanced mobile broadband [16] aims to support ultra-high data rate applications such as virtual reality (VR), extended reality (XR), and high resolution streaming (e.g., 4K video). URLLC [17] targets real-time applications requiring both high reliability and low latency, including remote surgery, autonomous vehicles, digital twins, and industrial automation. MTC [18], on the other hand, focuses on massive-scale, low-power connectivity for IoT devices, characterized by sporadic but highly diverse traffic patterns. While these categories are based on the same types of services that were first introduced in 5G, real-world deployment has shown that achieving widespread adoption is more complex than initially projected. In many cases, the absence of use cases and viable business models has limited the practical realization of these capabilities. Therefore, in the context of 6G, it is important not only to focus on advancing the technical foundations of these service types but also to consider the ecosystem readiness, economic reasons, and user demand that are essential for turning these ambitions into reality.

To meet the growing demands of wireless communication systems, higher frequency bands such as millimeter-wave and sub-terahertz must be utilized to achieve higher data rates with lower spectrum efficiency for short-range applications. Additionally, tapping into unused spectrum resources will significantly enhance network capacity, which is crucial for enabling emerging services such as the metaverse. One notable example of an underutilized yet highly valuable frequency band is FR-3 (7–24 GHz). Despite its immense potential, this band has largely been overlooked due to the presence of pre-existing critical wireless systems, such as satellite communications and radar. However, significant portions of its spectrum remain unexploited, presenting a unique opportunity for expansion. To harness the benefits of higher frequency bands, their inherent challenges, such as propagation losses and hardware limitations, must be addressed through innovative solutions. Beyond spectrum-related challenges, several critical aspects of communication networks, including power efficiency, computational resources, thermal management, and device packaging, also require strategic advancements to support the next generation of wireless technologies.

Furthermore, the currently separate mobile and satellite networks must be seamlessly integrated, unifying terrestrial and air-space domains with the support of emerging technologies such as high-altitude platform stations and drones [19]. This integration is expected to enhance both quality of service (QoS) and quality of experience (QoE), ensuring uninterrupted communication coverage even in the most remote areas of the world, including oceans, skies, and rural regions. The development of a 3D network will be instrumental

in achieving this goal by interconnecting multiple nodes, such as mobile network towers, HAPS, and satellites, creating new possibilities for communication pathways and data rates. An example of a smart city utilizing 3D integrated networks is shown in Figure 1, where diverse devices can be interconnected to enable seamless communication across various environments.

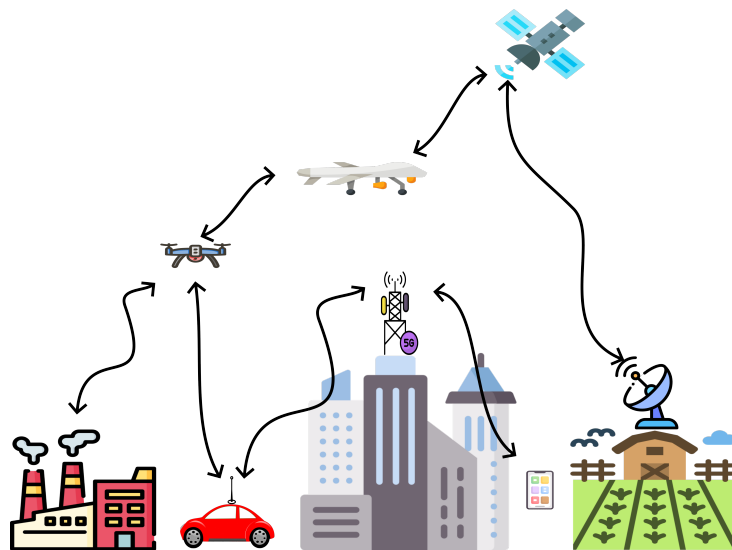


**Figure 1.** Example of a 3D integrated network in the 6G era.

This survey provides a comprehensive review of recent advancements in radio frequency (RF) hardware technologies, with particular emphasis on the physical layer infrastructure required to support next generation wireless networks. Compared to conventional 5G and 6G surveys, which often focus on system-level architectures or protocol design, this work highlights the enabling role of core hardware components. Specifically, it investigates sub-terahertz and millimeter wave systems for ultra-high throughput, line-of-sight communications, the evolution of multiple-input multiple-output (MIMO) systems operating at high frequencies, developments in phased-array antenna architectures, and emerging techniques in energy harvesting and RF front-end reconfigurability. Special attention is also given to analog, digital, and hybrid beamforming architectures, which are key to improving spectrum utilization, especially in dense network environments. The survey further discusses how technologies like reconfigurable intelligent surfaces and adaptable hardware platforms can make wireless systems more flexible and energy efficient. By focusing on these critical physical layer advancements, this work aims to support future research and development in the design of scalable and high-performance wireless communication hardware.

The content of this article is organized as follows. In Section 2, the main challenges at the physical layer of future wireless communication systems are discussed, including spectrum scarcity, propagation losses at mmWave and THz frequencies, and hardware limitations. In Section 3, a range of emerging technologies is presented, such as reconfigurable intelligent surfaces (RIS), massive MIMO, advanced beamforming techniques, wireless power transfer, and reconfigurable RF front-end systems, along with the role of digital twins in optimizing network performance. In Section 4, a comprehensive classification and analysis of antenna and antenna related technologies is provided, covering designs for user devices, centralized and distributed systems, and edge computing applications. Finally, conclusions are drawn in Section 6.

## 2. Physical Layer's Challenges for 6G

The immense demands of next-generation mobile communication have introduced numerous challenges in both the physical and cyberspace domains that must be addressed to enable the full deployment of 6G. This study focuses on the physical challenges arising from the need for increasingly higher throughput, particularly within the 6G eMBB scenario. This scenario is driven by the growing demand for ultra-high data rates, where any lack of connectivity, whether in remote locations or while in motion, is considered unacceptable. Achieving seamless connectivity becomes particularly challenging in the case of low Earth orbit (LEO) satellites, which operate at altitudes ranging from 200 to 2000 km and complete polar orbits within a few hours. These satellites traverse the sky at extremely high speeds, reaching several kilometers per second [19]. Consequently, such velocities result in Doppler shifts of hundreds of kilohertz for communication systems operating at frequencies above 10 GHz. Addressing these challenges effectively is crucial for the seamless integration of terrestrial and satellite communication networks. The expected peak data rates for 6G are projected to reach nearly 1 terabit per second (Tbps), more than 100 times the capacity of current 5G networks [5].

To meet these growing demands, ultra-wideband systems are essential. However, the sub-6 GHz spectrum is heavily congested, significantly limiting the available bandwidth. Consequently, mmWave and Terahertz communication technologies have been proposed to enhance the capacity, robustness, and security of mobile networks from a physical layer perspective [20,21]. In practical terms, it is necessary to explore new frequency bands to support these advanced services, as existing bands such as C, Ka, and Ku are heavily utilized by satellite communications. A promising solution lies in the largely unexploited FR-3 sub-bands, which offer significant potential for integration into advanced 5G and future 6G systems.

By definition, the mmWave band includes all frequencies corresponding to wavelengths between 1 to 10 mm, or equivalently, 30 to 300 GHz. The mmWave bands currently under investigation for mobile communications include the Q band (33–50 GHz), V band (50–75 GHz), W band (75–110 GHz), D band (110–170 GHz), and G band (170–300 GHz). Notably, the Q band overlaps with part of the Ka band, as it has not been officially defined by the International Telecommunication Union (ITU) or the Institute of Electrical and Electronics Engineers (IEEE) [22]. Among these bands, the D and G bands are particularly promising for future applications, as they remain largely unallocated and offer significant potential for ultra-high data rates due to their wide bandwidth availability.

It is well known that increasing the central frequency of transmission results in greater path loss, as described by the Friis equation representing energy diffusion due to the free space loss model [23]. Beyond traditional propagation losses, mmWave and, more critically, terahertz frequency bands are highly susceptible to atmospheric effects due to their short wavelengths. One of the key challenges is attenuation caused by energy absorption from atmospheric gases such as oxygen and water vapor, which varies significantly across different frequency bands, as shown in Figure 2 (attenuation measured in dB/km). The propagation of electromagnetic waves in the Q and V bands is particularly affected by atmospheric absorption [24]. However, there are specific frequency windows where absorption is minimized, making them viable for mobile communications. One such example is the 96 GHz window, where oxygen attenuation reaches a local minimum, highlighting its potential for applications such as sensing and communications in commercial or military operations. Additionally, the 77–81 GHz range is already licensed for automotive radar applications. Rain is another critical factor contributing to signal attenuation (absorption by water droplets), especially in higher mmWave bands. Rain-induced attenuation increases with frequency but eventually plateaus, becoming largely independent of rainfall intensity

at higher frequencies. Similar attenuation effects are observed with cloud cover, where vaporized water further contributes to energy absorption.

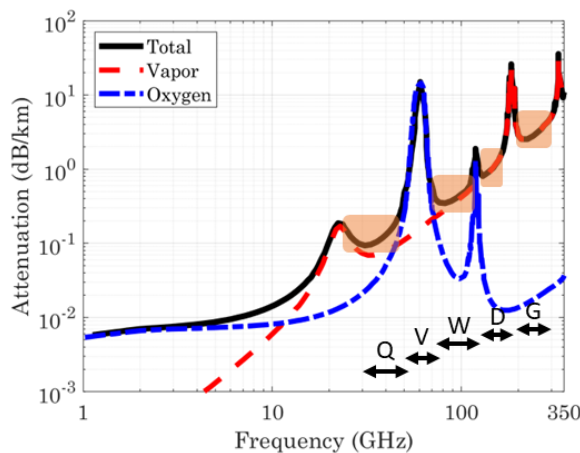


**Figure 2.** Atmospheric losses in dB/km for the range 1–350 GHz.

To mitigate these losses, various strategies must be implemented to enhance antenna and system gain while ensuring optimal efficiency levels. Techniques such as beamforming [9,25], the use of highly efficient high-power amplifiers based on GaN [26–28], MIMO systems with adaptive channel coding [29–32], and dynamic link budget control based on meteorological data can help overcome atmospheric effects [33,34]. Additionally, the integration of reconfigurable intelligent surfaces (RIS) can further optimize performance [35–38]. The key enabler of mmWave communications is the ability to maintain highly directional antenna radiation beams through beamforming. This capability serves as the fundamental mechanism underpinning the aforementioned techniques and is essential for ensuring efficient operation. Interestingly, mmWave bands also hold significant potential for applications such as inter-satellite, moon-to-satellite, or interplanetary communications due to their broad available bandwidth. Furthermore, the absence of weather-related effects, such as rain and clouds, in space further enhances their suitability for these long-range, high-data-rate applications [39].

Another significant challenge lies in massive machine-type communications (mMTC) within IoT systems, where millions of devices periodically transmit data such as status updates or sensor readings [40,41]. This results in vast amounts of data across extensive areas, requiring efficient management through either terrestrial base stations or satellite networks. In mMTC applications, lower operational frequencies are preferred, as they align with the relatively lower data rate requirements compared to the high-speed demands of eMBB scenarios. Promising frequency bands for mMTC include the C and S bands [42,43], which offer several advantages over mmWave frequencies. These bands are more resilient to weather conditions, support communication through multiple propagation paths, penetrate walls effectively, provide wider coverage areas, and benefit from well-established communication protocols such as Wi-Fi and LoRa. A key characteristic of this scenario is its diversity, encompassing a wide range of devices, data types, and geographic locations.

Examining the evolution of telecommunication hardware, the efficiency of RF components has not advanced as expected, resulting in 5G devices and base stations that are excessively power-hungry [44–46]. This challenge is expected to intensify with the advent of 6G, where the number of base stations and connected devices will significantly increase to ensure seamless broadband communication [47–49]. The widespread deployment of hundreds of thousands of IoT devices acting as sensors or actuators will require robust systems capable of supporting their communication demands within the machine-type communication framework of 6G. To enable efficient wireless data transfer, these devices must incorporate

efficient telecommunication technologies. Achieving high efficiency is critical, as many IoT devices will depend on energy harvesting (EH) or wireless power transfer (WPT) for their operation [50–52]. These technologies can potentially eliminate the need for conventional batteries in certain applications, such as ultra-low-power electromagnetic energy harvesting (EM-EH) techniques, which operate with minimal energy requirements. This approach not only enhances system versatility but also significantly reduces maintenance costs by minimizing battery-related replacements and environmental impact.

A holistic assessment of power requirements must consider all aspects of energy consumption across every stage of development and operation. This includes not only energy losses during network operation but also the energy expended in the production and deployment of hardware infrastructure. Despite advancements in energy-efficient RF hardware, network operators may choose to retain older equipment to minimize costs, especially if it remains within its operational lifespan. However, this approach could delay the adoption of energy-optimizing technologies, thereby slowing their potential impact on reducing network power consumption. To emphasize the importance of designing and manufacturing more energy-efficient hardware, it is essential to evaluate the overall energy footprint of the telecommunication industry. Recent studies [53,54] suggest that mobile networks, including components such as mobile phones and base stations, account for approximately 1% of global energy consumption, with base stations representing the largest share of this energy use. Therefore, various strategies must be implemented to improve the efficiency of RF front-end modules and reduce their energy demands. At this point, it is essential to note that digital processing devices (e.g., microprocessors, digital signal processors, microcontrollers, analog-to-digital converters, etc.) consume significantly more energy than their analog counterparts (e.g., the beamforming networks of the RF front-end system), with the exception of the RF power amplifier in the transmit chain [55]. Thus, adopting analog RF beamforming or hybrid analog–digital beamforming architectures could play a pivotal role in reducing the total energy consumption of next-generation communication systems.

Addressing the challenges of 6G networks, particularly in the deployment of radio towers, requires more comprehensive strategies. The use of higher frequency bands necessitates the placement of base stations in close proximity to compensate for the reduced coverage area of mmWave frequencies. It is well established that 5G base stations require high densification, with an initial coverage radius of approximately 100 m per station, which may eventually be reduced by half. To optimize energy efficiency and performance, electronically steerable, highly directive beams are crucial. These beams enable spatial domain multiple access (SDMA) [56], which not only increases channel capacity but also ensures efficient energy utilization by directing power exclusively toward the intended user, minimizing losses in other directions. Another promising solution is the deployment of massive MIMO, where multiple radio signals are connected to a single or a small number of antenna elements (sub-arrays) [7]. This approach reduces the transmit power required from each RF module, as massive MIMO stations distribute lower-power signals across multiple antennas, offering improved energy efficiency compared to traditional antenna systems. At this point, it must be noted that high-directive antennas (beamforming) and MIMO systems present competing priorities. In sub-7 GHz frequencies, MIMO is often prioritized due to its effective handling of multipath propagation. However, at mmWave frequencies, beamforming becomes essential to overcome significant propagation losses. As a result, mmWave systems prioritize beamforming, with a viable solution being hybrid digital-analog configurations, which allow for compact MIMO implementations with minimal losses. This hybrid approach also facilitates the development of power amplifiers with improved power added efficiency (PAE). In the near future, the design of base stations is

expected to transition toward integrating multiple low-power RF transceiver modules with high power amplifiers (HPA) in the transmitter and low noise amplifiers (LNA) in the receiver, rather than relying on a few high-power transmit components [57,58]. This modular approach is already well established in modern radar systems and is also compatible with the mmWave MIMO versus beamforming compromise. A foreseen viable solution is the employment of one transmit (HPA) and one receive (LNA) RF module per MIMO port. In this manner, a hybrid analog–digital beamforming system can be implemented, where each RF module feeds a directive sub-array (block), ensuring dense mmWave beamforming. In turn, multiple similar blocks may comprise the required MIMO system. This redesigned architecture will align with the emerging implementation paradigm, significantly reducing power losses in RF hardware. While hardware evolution is gradual, substantial improvements in energy efficiency and performance are anticipated in the mid-term future.

### 3. Emerging and State-of-the-Art Technologies

#### 3.1. Reconfigurable Intelligence Surface (RIS)

A highly promising and rapidly emerging technology for enabling ultra-high-throughput communication in the mmWave spectrum and for decoupling wireless communication KPIs from strict dependence on Tx-Rx distance is the reconfigurable intelligent surface (RIS). RIS has gained recognition as a key enabler in enhancing wireless networks, especially in the domains of massive MIMO, beamforming, and integrated sensing. The recent literature underscores rapid advancements in RIS architectures, performance optimization techniques, and deployment strategies. RIS encompasses a broad class of passive or active two-dimensional microwave surfaces that can dynamically manipulate incident RF signals [59]. These surfaces are capable of reflecting, diffracting, amplifying, focusing, or steering electromagnetic waves. The resulting directive beams help address the fundamental limitations of mmWave bands, such as high free-space path loss and poor penetration through obstacles.

What distinguishes RIS from comparable technologies such as transmitarrays, reflectarrays, or frequency-selective surfaces is its ability to electronically reconfigure its electromagnetic properties in real-time [59]. For example, an RIS installed on the exterior of a building and configured as a reflectarray can dynamically redirect incoming mmWave signals toward a targeted receiver at the optimal frequency and angle, thereby improving link quality and overall system performance. An example of such a scenario is illustrated in Figure 3. This transformative potential has sparked significant research interest and innovation in RIS development. A sharp rise in related publications highlights this growing attention [59–69]. For instance, in [70], the performance of a double-stacked intelligent metasurface integrated into massive MIMO systems is explored. This configuration, depicted in Figure 4, effectively enhances spatial diversity, thereby improving communication reliability and throughput.

A variety of innovative RIS architectures and applications have been explored in the recent literature, further highlighting the versatility and potential of this technology in next-generation communication systems. In [71], a simple stacked metasurface architecture with reconfigurable amplitude and phase is utilized to optimize downlink beamforming, significantly improving signal quality in multiuser environments. Active RIS with discrete phase shifts is examined in [72], demonstrating enhanced spectral efficiency in communication systems. Hybrid RIS configurations designed for integrated sensing and communication are presented in [73], underscoring the multifunctionality of RIS in future network paradigms. A location-driven beamforming strategy tailored for RIS-enabled near-field communications is proposed in [74], where beam patterns are dynamically optimized based on user position data to improve connectivity in dense urban settings.

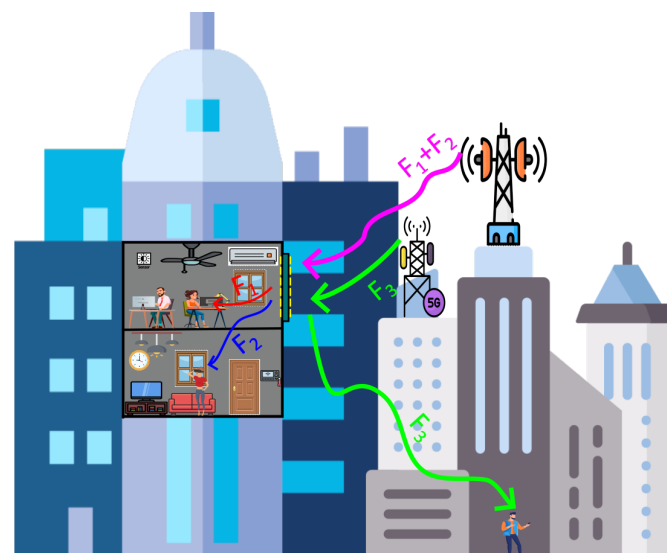


**Figure 3.** The operation of a reconfigurable intelligence surface in a 6G society.

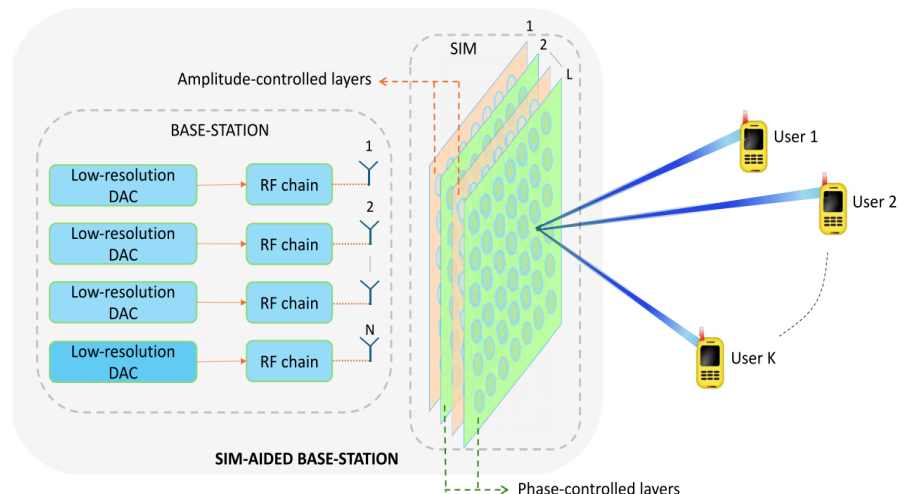


**Figure 4.** Stacked reconfigurable intelligent metasurface antenna, [71].

Deployment challenges in complex cellular networks are addressed in [75], which introduces a frequency-dependent RIS model applicable to multiband, multicell MIMO networks. In [76], the integration of RIS with spatial modulation is explored to enhance antenna selection for vehicular communications, leading to improvements in link robustness and data rate performance. Furthermore, ref. [77] presents a transparent, graphene-based RIS operating in the THz band for 6G systems, an innovative design that demonstrates the promise of advanced materials for supporting ultra-high-frequency communications. Despite these advances, several key challenges must be overcome to enable commercially viable RIS deployment. These include optimizing energy efficiency and scalability, refining real-time electronic control mechanisms, and addressing practical concerns such as cost, power consumption, and seamless integration with existing communication infrastructure. Table 1 lists some notable RIS works that span both passive and active architectures across a wide frequency range from sub 6 GHz to the terahertz band. The table summarizes key characteristics including the type of RIS (passive, active, or hybrid), the number of elements, physical dimensions, underlying manufacturing technology, and operating frequency range, as well as some reported performance metrics.

**Table 1.** Summary of RIS characteristics from recent works.

Reference	Type	# Elements	Size	Technology	Frequency Range (GHz)	Performance Metrics
[60]	Active	400 ( $20 \times 20$ )	$10 \times 10$ cm	6-layer PCB (Meteorwave 8000 + FR4), PIN diodes	27.5–29.5	30 dBi directivity, 25 dB gain, <8 W, $\pi$ phase tuning, >20% efficiency
[61]	Active	100 (94 reflective + 6 sensing)	$50 \times 50$ mm	LTCC + SIW + Rotman lens, varactors, MCU	27.5–28.5	DoA tracking, beam steering, <5 dB loss, 1-bit control
[65]	Passive	Single unit (scalable)	$20 \times 20$ mm	Rogers 5880 + FR4, varactor diodes	5–5.5	360° phase shift (TE/TM), 1.5–6 dB reflection loss depending on polarization
[67]	Passive	-	$12 \times 12$ mm per unit	Sawtooth metasurface on FR4	4.2–12.5	$2 \times 360^\circ$ phase shift, beam redirection, tested at 10 GHz
[68]	Active	196 ( $14 \times 14$ )	$362 \times 381$ mm	Multiport system with 3-bit varactors	2.6	Beam steering ( $22^\circ/34^\circ$ ), 94% simulation time reduction, low RMSE
[71]	Active + Passive	Theoretical analysis	Theoretical analysis	Stacked metasurfaces: passive (phase) + active (amplifier-based amplitude)	$f_0$	Wave-domain beamforming, sum-rate optimization, ZF beamforming, hybrid SIM
[77]	Passive	576 ( $24 \times 24$ )	$720 \mu\text{m} \times 720 \mu\text{m}$	Graphene on sapphire with gold backplane	1000–5000	Digital and analogical beam steering, mutual coupling optimization

### 3.2. Multiple-Input Multiple-Output (MIMO)

In recent years, the term *MIMO* has dominated the scientific discourse, promising to address the inherent losses of mmWave communication. However, strictly speaking, this is a widespread misconception, as it is the directional antenna beams that mitigate mmWave losses through their high gain, not merely the multiple ports of the antenna array. Among its key advantages, massive MIMO's ability to significantly enhance channel capacity stands out [78]. The term "massive" refers to the inclusion of a large number of antenna elements in the system, often exceeding hundreds and potentially reaching thousands [79]. This extensive array of elements forms the foundation for robust adaptive techniques aimed at mitigating noise and boosting received signal power. Furthermore, beamforming has become an integral component of MIMO systems, improving system gain and overall performance. Currently, MIMO systems typically employ configurations such as sub-arrays with  $4 \times 4$  antenna elements, particularly in the sub-6 GHz range, where physical size and system complexity remain limiting factors [80].

MIMO technology leverages multipath communication, exploiting the diverse propagation paths of RF signals to increase channel capacity. This phenomenon is more pronounced in the lower microwave frequency bands (e.g., sub-7 GHz) than at mmWave bands. Notably, multipath dominates at sub-7 GHz, while direct line-of-sight (LOS) is the principal link at mmWave frequencies. MIMO increases capacity by processing distinct signals through transceiver modules, transmitting them from individual elements or subarrays within an antenna array, and subsequently applying post-processing at the receiver to reconstruct the transmitted data. The efficiency of this process is heavily dependent on the algorithms that encode and decode signals based on the channel's characteristics [78]. Consequently, a significant body of research focuses on developing advanced algorithms and adaptive techniques to optimize MIMO system performance. One critical challenge is the requirement for real-time processing to accommodate the dynamic nature of the wireless environment. This necessitates continuous monitoring of the channel's characteristics and frequent updates to the channel matrix for each frequency component to ensure seamless operation. Massive MIMO's capacity to adapt to changing environments and enhance communication reliability makes it an indispensable technology for next-generation wireless networks. However, appropriate topologies combining MIMO and beamforming must be exploited to address the challenges of mmWave frequencies effectively.

A commonly cited advantage supporting the development of massive MIMO systems or massive element arrays at mmWave frequencies is the relative ease of fabricating antenna arrays with hundreds or even thousands of elements within a compact space, enabled by the short wavelengths at these frequencies [79,81–86]. However, this advantage is counterbalanced by a critical limitation. Specifically, the primary benefit of MIMO, its ability to exploit multipath propagation, is significantly diminished at mmWave frequencies due to increased free space path loss and substantial attenuation from atmospheric gases and water vapor (Figure 2). To compensate for these losses, antenna systems must achieve considerably higher gain, as the available power is inherently constrained at these frequencies. This requirement necessitates the use of beamforming techniques, which focus energy along a single LOS propagation path. While effective in overcoming propagation challenges, beamforming largely eliminates the ability to capitalize on multipath diversity, which is a key advantage of MIMO technology at lower frequencies. Consequently, at mmWave frequencies, the potential benefits of massive MIMO in harnessing multipath propagation are significantly diminished.

The complex interrelation between beamforming and MIMO at mmWave frequencies is elaborated by NTT-DOCOMO [87], which refers to “user and spatial multiplexing of massive-element antennas”. An indicative diagram (Figure 3) illustrates how the number of elements increases with the square of the frequency ratio, while the overall array size remains approximately constant.

For instance, at a range of approximately 490 m, a square array of size  $20\text{ cm} \times 20\text{ cm}$  comprises  $10 \times 10 = 100$  elements at 10 GHz, or  $20 \times 20 = 400$  elements at 20 GHz. Although the physical array size is retained, the dramatic increase in element count introduces major challenges in beamforming or antenna feeding network design. A practical solution lies in *hybrid beamforming*. In the example above, each  $20 \times 20\text{ cm}^2$  subarray could employ an analog beamforming circuit, e.g., switched-beam Butler, Nolen, or Blass matrices, while MIMO-based user multiplexing could be handled by an equal number of subarrays, each driven by a separate RF chain.

Another major challenge in implementing massive MIMO systems is the enormous complexity introduced by managing the envisioned millions of antenna elements. Controlling such a vast number of elements requires numerous fully controllable RF transceiver chains, each of which must be monitored and dynamically adjusted in real-time. Essentially, the challenge lies in managing and optimizing the individual radiated beams, typically achieved by controlling the excitation current of each antenna element in terms of amplitude and phase. However, some analog beamforming techniques, such as switched-beam systems, offer a more practical approach by simplifying control through the selection of the appropriate transmit/receive (Tx/Rx) beamforming network port. To address these issues, various research groups have proposed hybrid MIMO architectures that combine analog and digital signal processing, aiming to minimize the number of required RF chains without compromising performance. Despite these theoretical advancements, practical implementations of massive MIMO systems for mmWave frequencies remain scarce. The majority of published work focuses on simulations, with emphasis on developing and testing advanced algorithms for MIMO system optimization. The introduction of artificial intelligence (AI) and machine learning (ML) is expected to play a crucial role in addressing beam management challenges, offering enhanced adaptability and real-time optimization. However, the physical fabrication and experimental validation of such systems present significant challenges. These stem from intricate design requirements, complex manufacturing processes, and the demanding testing environments needed to ensure accurate performance validation.

Traditional microwave testing methods become impractical due to the extremely high number of ports. Thus, conductive path approaches involve high complexity and require excessive effort. In the sub-7 GHz band, these issues are reliably addressed through over-the-air (OTA) testing approaches. However, in the mmWave bands, the number of ports is expected to remain relatively small, making testing methods involving conductive techniques (e.g., cables or waveguides) potentially more practical and accurate.

### 3.3. Beamforming Networks at mmWaves and THz

The demand for high-gain antennas operating at mmWave frequencies has surged, driven by the need to extend the range of communication links in these bands, while meeting the performance requirements of 6G networks. As 6G aims to deliver ultra-high data rates, extreme coverage and reliability, and massive connectivity, beamforming has emerged as the most effective method for achieving these goals: not only enhancing signal gain, but also enabling dynamic real-time beam steering, thus optimizing link quality, reducing interference, and supporting massive connectivity. Additionally, 6G networks require highly adaptive and intelligent beamforming solutions that leverage AI and ML to predict user movement, optimize spectral efficiency, and manage complex multi-antenna

deployments. This adaptability makes beamforming a cornerstone technology in mmWave communication systems, ensuring robust and energy-efficient wireless transmission in next-generation networks [88,89].

Beamforming relies on two key components: a phased array (linear, conformal cylindrical, or planar) and a feeding network [23]. The phased array consists of multiple antenna elements, while the beamforming feeding network provides each element with the necessary signal characteristics, specifically, the amplitude and phase of the excitation current, to shape and direct the beam. Historically, fully passive beamforming networks were used (see Figure 5a). Switched beam networks, such as Butler matrices, Nolen matrices, Blass matrices, and Rotman lenses, introduced predefined phase shifts or time delays through fixed excitation ports [90–95]. While these systems were effective in early applications, their inherent inflexibility and lack of adaptability limited their functionality in dynamic environments. Particularly in the sub-7 GHz band, where multipath dominates and is exploited through MIMO, digital beamforming is preferably utilized, while matrix-switched beams are rarely adopted. However, these matrix-based beamforming networks (BFNs) have the potential to be effectively utilized in mmWave networks, particularly when modified to function as hybrid digital-analog beamformers, as indicatively presented in Figure 5d. By integrating multiple matrices, it is possible to construct three-dimensional beamforming networks capable of optimally steering highly directional radiation beams [96,97].

To understand the beamforming effect, we conduct the following study. Assuming a total transmission power of  $P_t = 40$  dBm from a 5G base station [98], and a received power of  $P_r = -50$  dBm for a conventional mobile phone with full reception [99], we consider communication in the 3.5 GHz, 10 GHz, and 20 GHz bands. The mobile phone antenna gain is assumed to be  $G_r = 0$  dBi. To maintain communication at the same distances across these frequency bands, we analyze different planar antenna array configurations at the base station: (1) at 3.5 GHz, we consider  $4 \times 4$ ,  $8 \times 8$ , and  $16 \times 16$  arrays; (2) at 10 GHz, we consider  $8 \times 8$ ,  $16 \times 16$ , and  $64 \times 64$  arrays; and (3) at 20 GHz, we consider  $16 \times 16$ ,  $64 \times 64$ , and  $128 \times 128$  arrays. The coverage estimation is based on the Friis transmission formula,  $P_r = P_t + G_t + G_r - L_m - L_p - L_s$ , where  $P_r$  is the received power at the mobile phone in dBm,  $P_t$  is the transmit power from the base station in dBm,  $G_t$  is the base station antenna gain in dBi,  $G_r$  is the mobile phone antenna gain in dBi,  $L_m$  represents penetration losses in dB,  $L_s$  accounts for shadowing and fading losses in dB, and  $L_p$  denotes path losses in dB, given by  $L_p = 32.4 + 20 \log_{10}(d) + 20 \log_{10}(f)$ , where  $d$  is the distance in km, and  $f$  is the signal frequency in MHz. The base station antenna gain is calculated using the maximum directivity of a planar array, assuming total efficiency  $\epsilon_{eff} = 1$ ; thus,  $G_t = \epsilon_{eff} D_{max}$ , where  $D_{max} = 4\pi A_{eff}/\lambda^2$ , with  $A_{eff}$  being the effective area [100]. For a realistic scenario, we incorporate penetration losses of 5.5, 6.2, and 7.8 dB at 3.5, 10, and 20 GHz, respectively, as reported in [101]. Similarly, we consider shadowing and fading losses of 6, 7, and 8 dB at 3.5, 10, and 20 GHz, respectively, based on findings from [102–104]. Figure 6 shows the range achieved by each antenna configuration under these conditions.

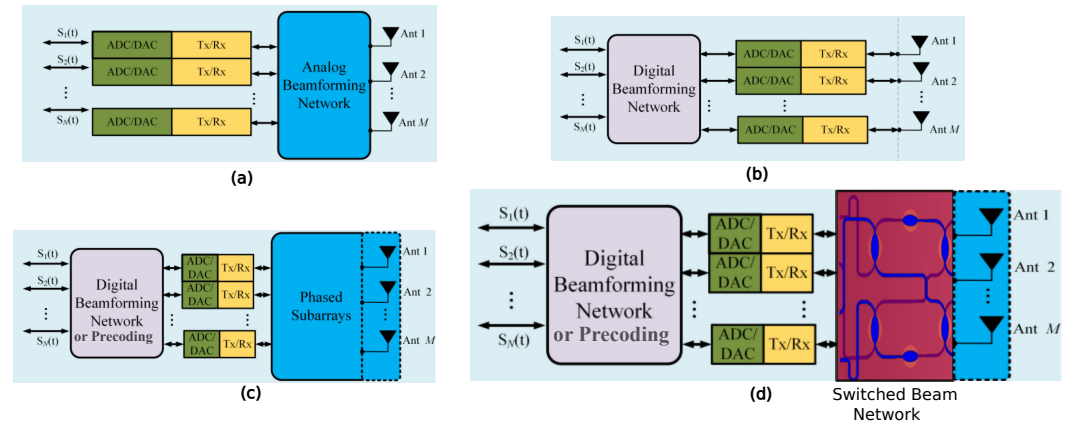


**Figure 5.** Types of BFN architectures [20]: (a) analog beamforming, (b) digital beamforming, (c) hybrid beamforming, and (d) switched-beam hybrid beamforming.

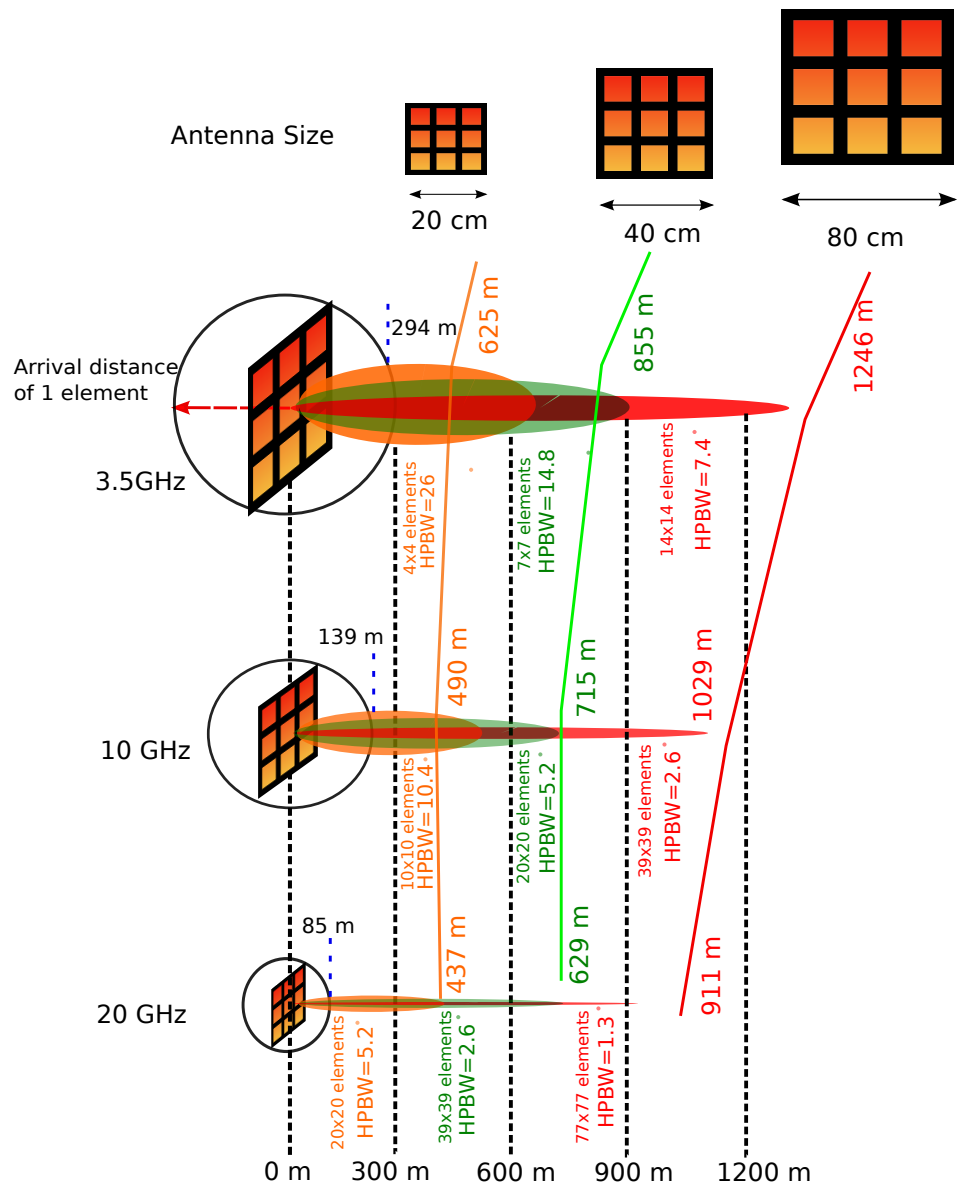


**Figure 6.** Maximum distance maintaining a link for three different antenna arrays' configurations. This figure was inspired by [87].

An example of a 3D beamforming topology [105] is illustrated in Figure 7, and it is utilized to enhance system capacity and efficiency by enabling precise transmit and receive functions with narrow beams in both azimuth and elevation angles. This analog 3D beamformer is constructed using a stack of vertical beamformers (BMs), which are driven by either a single horizontal BM or a stack of horizontal BMs. To achieve ultra-wideband performance, the planar array is composed of planar-printed Vivaldi antenna elements, ensuring high directivity and efficient spatial coverage. Both adaptive phased-array beamforming and switched beamforming will play a crucial role in coverage extension in 6G non-terrestrial networks (NTN), enabling seamless connectivity across air, sea, and space. This involves the integration of LEO (low Earth orbit) satellites, GEO (geostationary) satellites, and HAPS to provide global coverage. Since LEO satellites traverse the sky at high speeds and for short durations (up to 30 min), real-time beam steering is essential to continuously track mobile ground terminals, ensuring stable and seamless connectivity. Scalable, reconfigurable, and large antenna arrays are required to serve multiple ground terminals simultaneously. A relevant example of this is a 1024-element SATCOM phased array, as discussed in [106]. The key challenges for phased-array beamformers will be high power consumption and increased computational complexity, especially in large-scale systems, as well as cost-effective implementation, particularly for LEO terminals that require real-time tracking. On the other hand, less complex switched beam beamformers can be effectively deployed in GEO satellites to cover vast geographic areas with predefined beams and in HAPS platforms to provide extensive ground coverage without requiring continuous steering, thereby minimizing power consumption. They are also well suited for backhaul communication between terrestrial networks and NTN. A 3D beamformer featuring a  $16 \times 16$  (256 element) array or larger, powered by a stack of multiple beamform modules similar to the design shown in Figure 7b, is expected to significantly improve coverage and performance for 6G networks. Although the main issue in extreme coverage extension is long-distance signal propagation, particularly in NTN where signals must travel thousands of kilometers while maintaining low latency and high reliability, 3D beamforming is essential for handovers between terrestrial 6G networks and NTN systems, significantly enhancing spectral efficiency. Additionally, it enables high-gain directional beams, optimizing signal strength and ensuring efficient long-distance communication in NTN environments. To integrate 3D beamformers into the aforementioned platforms, a miniaturized and compact design with enhanced performance accuracy is essential for optimal efficiency and seamless deployment.

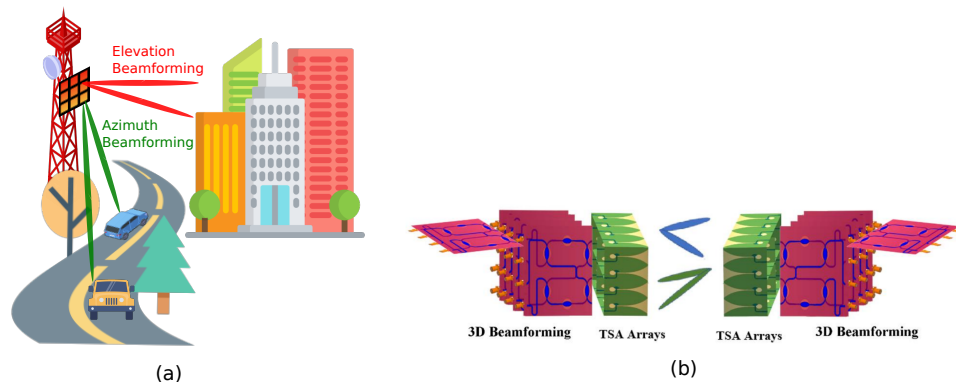


**Figure 7.** (a) 3D beamforming; (b) 3D beamforming utilizing Butler matrix and Vivaldi array.

The introduction of tunable and reconfigurable components, such as phase shifters [107], attenuators [108], and SPDT switches [109], marked a significant step forward. These devices enabled precise control over the phase and amplitude of the excitation currents feeding each

antenna element, while the SPDT switches enabled dual-port excitation of the beamformer to produce additional beams. However, their use in mmWave systems is constrained by their high insertion loss and limited tuning ranges, which degrade performance at higher frequencies [110]. To address these limitations, more advanced beamforming architectures have been developed, including fully digital [111–114] and hybrid analog–digital systems [115–117]. In a fully digital beamforming network, each antenna element receives a signal that is digitally processed and then converted to an analog signal using a digital-to-analog converter (DAC), as shown in Figure 5b. This approach provides unparalleled flexibility and precision in shaping the beam. However, at mmWave frequencies, fully digital systems face significant challenges. In general, DACs consume significant power, particularly at high sampling rates ( $f_s$ ). The sampling must obey the Nyquist minimum rate  $f_s > 2BW$ , where  $BW$  represents the operational channel bandwidth of the received signal. However, complex sampling techniques can be employed to reduce the required sampling rate by half, allowing  $f_s > BW$ . In practical implementations, commercial ADCs and DACs, especially those used in software-defined radio (SDR) applications, often operate at slightly higher sampling frequencies (approximately  $f_s = 2.2BW$  for real signals or  $f_s = 1.1BW$  for complex (IQ) signals) to ensure optimal performance [118]. Notably, current 5G systems support channel bandwidths of up to 200 or 400 MHz, whereas 6G is expected to accommodate bandwidths ranging from 0.5 GHz to 2 GHz, posing new challenges in power efficiency and signal processing capabilities. The DACs required to generate signals with these requirements must operate at extremely high sampling rates, which can result in substantial power consumption and reduced system efficiency.

Hybrid beamforming networks provide a practical solution for mmWave applications [113] and are essential for THz frequency bands. By integrating analog and digital processing, these systems efficiently handle the high data rates and massive connectivity demands of 6G while reducing power consumption and hardware complexity [119]. The signal undergoes initial digital processing before being converted into an intermediate analog form. Subsequent operations, including up-conversion, amplification, and filtering, take place in the analog domain before transmission through the antenna elements, as illustrated in Figure 5c. By minimizing the number of DACs and leveraging analog signal processing, hybrid architectures achieve an optimal balance among complexity, performance, and energy efficiency, making them well suited for high-frequency applications. However, implementing hybrid beamforming in 6G introduces several challenges. Propagation loss compensation at THz frequencies requires high-gain arrays to maintain reliable communication. The beam squint effect is also an important issue [120], where the wide bandwidths of THz communications cause beams to shift in different directions at varying frequencies, leading to array gain loss. Furthermore, hardware constraints pose a significant hurdle, as hybrid beamforming in ultra-massive MIMO (or multi-antenna) systems demands managing large numbers of antennas and RF chains, increasing both hardware complexity and power consumption. Lastly, beam management is crucial in dynamic environments [121], where user mobility and rapid changes in channel conditions require efficient beam alignment and tracking mechanisms to ensure seamless connectivity.

### 3.4. Angular Coverage

An important issue in mmWave hybrid or switched beam matrix beamformers is related to continuous angular coverage. Specifically, at mmWaves, increased gain is needed to mitigate propagation losses, thus corresponding to narrow beamwidth. When this is successfully achieved, the consecutive switched beams may overlap at very low levels, below  $-3$  dB. This problem can be mitigated by introducing a group of intermediate orthogonal beams, as suggested by Fakoukakis et al. [122], which is also shown in Figure 8. This is achieved by introducing constant-value phase shifters between the Nolen or Butler

matrix outputs and the antenna ports, selectable through digitally controlled RF switches. At even higher frequencies, a third or fourth group of additional orthogonal beams may be needed if the radiation pattern of the element is highly directive. As displayed in Figure 8, a  $4 \times 8$  Nolen matrix can be expanded by introducing an intermediate group of three additional beams, leading to a total of seven beams and improving the overlapping point to  $-3$  dB.

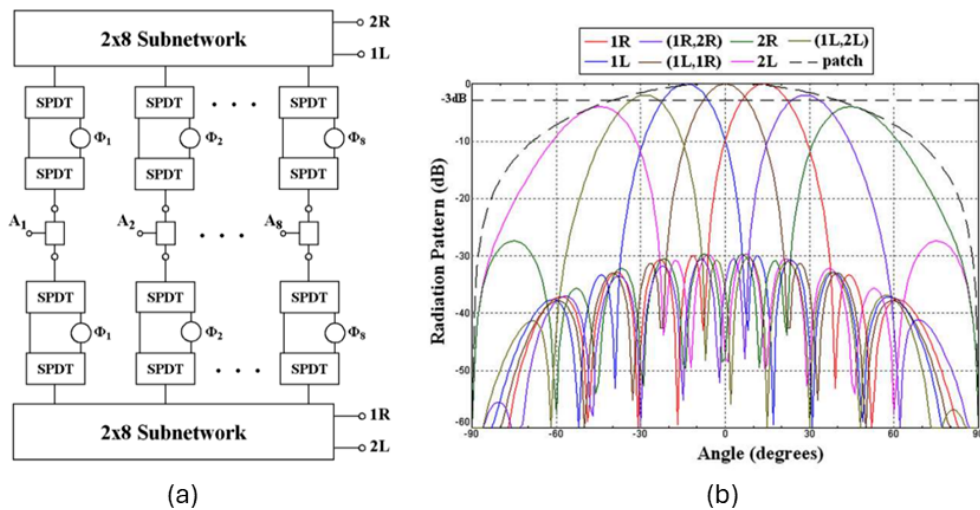


**Figure 8.** (a) Schematic diagram of the  $4 \times 8$  network implementing the switched-line-phase-shifter (SLPS) technique and (b) their corresponding results where three more beams were introduced [122].

As future 6G networks adopt larger antenna arrays and operate at higher frequencies, such as the THz band, beamforming will become increasingly complex. To address this challenge, AI, particularly ML, is being leveraged to optimize beamforming strategies, enhancing efficiency, adaptability, and overall network performance [123,124]. The optimization process involves several key aspects, including enhanced beam selection, where AI identifies the optimal transmission beam, reducing latency and improving signal quality. Additionally, adaptive beam management allows AI-driven algorithms to enable real-time beam tracking and selection, ensuring seamless communication in dynamic environments. Furthermore, Improved channel estimation leverages AI to predict channel conditions with greater accuracy, enabling more efficient and adaptive beamforming adjustments. However, several challenges must be addressed. One major issue is algorithm selection, as identifying the most suitable AI model for specific beamforming scenarios remains difficult. Another critical concern is security, as AI-based beamforming systems must be safeguarded against adversarial attacks to ensure network integrity and reliability.

The development of 6G technology presents substantial challenges in PCB manufacturing, particularly in ensuring signal integrity and minimizing losses. Advancements in digital and RF systems so far rely heavily on PCB technologies, where transmission lines are typically incorporated into planar or multilayer structures to support seamless integration and high-performance operation. However, at frequencies above 10 GHz, RF propagation through dielectric materials introduces significant losses. In the context of 6G communication systems, where power efficiency is paramount, minimizing transmission and insertion losses in devices is critical. Consequently, alternative transmission line technologies have been explored to address these challenges. One promising solution is substrate integrated waveguides (SIWs), a hybrid technology that combines the advantages of metallic rectangular waveguides and printed transmission lines [125]. An inevitable requirement for the selection of mmWave transmission lines is to avoid dielectric losses, which are unacceptably high even at microwave frequencies. Additionally, the metallic

surfaces must be made perfectly smooth (metal spreading) to minimize current paths, since at mmWaves, the penetration depth is very short. Thus, waveguides based on air or with isolated metallic parts are needed. The trend is to devise waveguides with a planar structure but with air or gap-isolated conductors.

SIWs are fabricated using a dielectric substrate with metalized top and bottom layers and vertical vias along the sides to form a pseudo-waveguide structure. This configuration reduces losses compared to traditional printed lines while supporting higher power handling, all while maintaining the benefits of printed circuits, such as compactness and easy integration [126]. Despite these advantages, SIWs still suffer from dielectric losses [127]. To mitigate this issue, air-filled SIWs have garnered significant interest. In these designs, the dielectric propagation medium is replaced by air, resulting in substantially lower losses. However, the fabrication process for air-filled SIWs is more complex, requiring precise techniques to maintain structural integrity and performance [128,129].

An even more advanced alternative is the use of full metallic waveguides with internal ridges or grooves [130–132]. These waveguides offer minimal propagation losses and compact designs suitable for mmWave frequencies.

The feasibility of such structures has been enabled by breakthroughs in micromachining technologies, which allow the precise milling of metallic blocks into intricate and sophisticated geometries. An example of a groove gap waveguide 3D beamformer fabricated using additive manufacturing is shown in Figure 9. By leveraging these innovations, passive beamforming networks for mmWave applications can be realized with ridge, groove, inverted microstrip, or microstrip ridge waveguides, which introduce negligible RF signal losses. This significant reduction in losses enhances the overall efficiency of the communication system, aligning with the stringent power efficiency requirements of 6G technologies. The development of mmWave beamformers, whether based on switched-matrix or hybrid topologies, has already garnered significant interest from researchers worldwide. However, progress in this area has been relatively slow compared to the rapid pace of 5G and anticipated advances of 6G. Table 2 lists some notable work on beamforming network implementations, highlighting various architectures such as Butler matrices, Nolen matrices, and fully digital phased arrays. For each case, the beamforming type, frequency range, physical dimensions, fabrication technology, and number of supported beams are summarized to provide a comparative overview of analog, digital, and hybrid approaches across different platforms.

**Table 2.** Summary of beamforming network characteristics.

Reference	BF Network Type	BF Type	Frequency Range (GHz)	Size (in $\lambda$ )	Technology	Beams
[95]	3 × 3 Nolen Matrix	Analog	2.52–4.2	0.82 $\lambda$ × 0.75 $\lambda$	Microstrip on FR4	3
[96]	Modified Blass Matrix	Analog TTD	24–40	2.6 $\lambda$ × 2 $\lambda$	Microstrip	8
[97]	Nolen	Analog	29.6–30.4	22 $\lambda$ × 9 $\lambda$	RGW	4 or 12
[105]	4 × 4 and 8 × 8 Butler Matrix	Analog	6–16	0.74 $\lambda^2$ (4 × 4), 2.26 $\lambda^2$ (8 × 8)	Microstrip to slot (multilayer)	8
[109]	4 × 4 Butler Matrix	Analog	26–30	0.16 $\lambda$ × 0.10 $\lambda$	28 nm CMOS	7
[111]	2D Planar Hhased Array	Digital	28	0.5 $\lambda$ × 4 $\lambda$	PCB/RFIC	20
[112]	SDR-Based 1 × 8 Linear Array	Digital	26–30	5.6 $\lambda$ × 14.2 $\lambda$	SIW + TSA + SDR	8
[122]	Dual Series Nolen Matrix	Analog	2.8–3.2	1.3 $\lambda$ × 1.75 $\lambda$	Microstrip	4

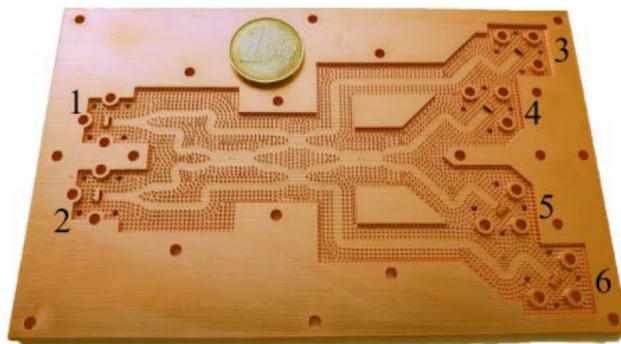


**Figure 9.** Groove gap waveguide 3D Butler matrix [94].

### 3.5. Wireless Power Transfer and Energy Harvesting

Energy efficiency is a critical consideration in 6G communication systems due to the large number of user devices and base stations. Specifically, in mMTC, millions of IoT devices will be deployed across metropolitan and rural areas, serving various purposes, such as environmental monitoring (e.g., temperature, humidity sensors) or operational control (e.g., lighting systems, sprinkler systems) [18,133–135]. These devices will be connected wirelessly, either with each other or with nearby base stations, necessitating energy-efficient operation and communication. A major challenge arises from the reliance on batteries, which have a limited lifespan and require periodic replacement, leading to increased maintenance efforts and costs. To overcome this limitation and achieve energy independence, two key techniques have been proposed, either as standalone solutions or in combination to support battery life extension and efficient energy harvesting [136–141].

Energy harvesting involves collecting ambient energy (e.g., electromagnetic, thermal, acoustic, solar) [138] from the environment and converting it into usable electrical energy. This energy is then utilized for the device operation and communication with other devices. This method is particularly crucial for devices that are not connected to the electrical grid. However, energy harvesting does not need to function as a standalone solution; it can be used in conjunction with either a wireless energy transfer unit or batteries to enhance system efficiency. By integrating these methods, battery life can be extended, reducing the energy footprint of the device. Wireless power transfer, on the other hand, refers to the deliberate transfer of electromagnetic energy from a power station to the device. This approach often leverages nearby radio towers operating in specific frequency bands (e.g., 5G) to supply energy [142]. Another innovative technique is to use a centralized radio tower to transmit electromagnetic waves to passive devices, utilizing the phenomenon of backscatter communication [143,144]. Backscatter devices, which resemble RFID tags, enable sensors to operate without batteries by reflecting ambient RF signals using various modulation schemes. This method eliminates the need for power-hungry components, such as oscillators, mixers, and amplifiers. Instead, it relies on low-cost, low-complexity devices that consume minimal power, often harvested from the surrounding environment. Notably, backscatter communication is particularly appealing as it enables batteryless operation and reduces overall system complexity and energy consumption.

### 3.6. Techniques for Reconfigurable RF Front-End Systems and Antennas

Following the emerging trends of low-cost, frequency-agile, and reconfigurable communication systems for 6G, the development of novel tunable devices is essential. Reconfigurable RF front-end will play a pivotal role in the miniaturization and simplification of future base stations. With 6G expected to unify various licensed spectra, including satellite communication, terrestrial networks, radar systems, and more, there will be a significant demand for wideband systems, particularly in base stations. The development

of such wideband systems poses considerable challenges, as it further complicates the design and operation of RF transceivers. To address this, an effective strategy is the design and implementation of tunable microwave devices and antennas. These devices would enable the dynamic adjustment of system response based on the utilized frequency band, reducing complexity and minimizing insertion losses particularly at mmWave frequencies. In microwave technology, tunability refers to the electronic control of different characteristic of a device. For example, in antennas, the ability to control the radiation pattern and operation frequency is a highly valuable asset.

Traditionally, the most widespread technique for introducing electronic control in microwave systems involves the use of semiconductors, such as PIN diodes, varactor diodes, or transistors acting as switches [145,146]. Typically, these switches connect or disconnect specific elements from the main structure of the device, or they introduce variable capacitance to modify its properties. For instance, a continuously tunable SIW filter was demonstrated using varactors integrated into a resonator patch [147], and a 1-bit reconfigurable metasurface was proposed in [148]. A tunable filtenna for X band applications were proposed in [149] where a novel superstrate-loading technique was applied permitting the frequency control using only one varactor. The measured antenna's tunability reached 35%, providing more than 20 dB out-of-band radiation suppression. As illustrated in Figure 10a, a PIN diode is employed between the arms of a Jerusalem cross, enabling the metasurface to switch between transmission and reflection modes.

However, a significant limitation of such tuning mechanisms lies in the discrete nature of their tuning states, which can restrict applications or require a large number of switches to achieve finer control [150,151]. The increased number of switching elements also leads to higher power consumption, particularly for diodes, as they require a bias voltage for their operation. Thus, minimizing the number of diodes is an active area of research. Moreover, as a two-terminal device, the PIN diode shares a single physical point for both the control port (biasing) and the RF signal. This dual use complicates the design of the biasing network, which must integrate the DC and RF signals while ensuring proper isolation between them. Designing effective solutions to these challenges is crucial for advancing reconfigurable microwave technology.

On the other hand, RF microelectromechanical systems (MEMS) offer superior isolation, lower insertion losses, and higher power-handling capabilities compared to traditional switching mechanisms [152]. Due to their compact size (typically smaller than 1 mm), MEMS devices are particularly attractive for miniature frequency-reconfigurable antennas [152,153], where the effective length of the antenna is adjusted by adding or removing parts of the radiating element. Recently, significant research efforts have focused on developing MEMS for mmWave bands, leveraging their advantages in the design of novel variable phase shifters [154] and attenuators [155] for beamforming networks [156,157]. Moreover, a new type of MEMS-based linear RF switches was fabricated and tested in [158] (see Figure 10b), demonstrating operation over a wide frequency range from 20 GHz to 110 GHz, thereby enabling high scalability for future communication systems. Despite these advantages, MEMS presents low switching speeds and challenges in integration.

The previously mentioned approaches involve external devices integrated into the structure. An alternative solution is the use of tunable materials, which exhibit properties that can be varied when biased with an appropriate DC field. Two of the most widely researched tunable materials are liquid crystals/ferroelectrics [159] and ferrites [160]. Liquid crystals and ferroelectrics enable permittivity tuning with applied voltage (see Figure 11a), while ferrites allow permeability tuning through the application of a DC magnetic field. These materials are generally considered cost-effective and technologically promising for mmWave frequencies, with applications spanning RIS [161,162], filters [163,164], tun-

able phase shifters [165,166] and reconfigurable phased arrays [167,168], among others. An example of a reconfigurable antenna is depicted in Figure 10f. However, at higher and particular at mmWaves frequencies, these materials face several challenges, such as increased insertion losses, reduced efficiency [168], higher power consumption, and the requirement for complex biasing networks [169]. To mitigate the increased losses, thin film ferroelectrics such as  $BaTiO_3$  and its composites [170] were utilized for the development of RF surface mount capacitors [171], RIS [172], and tunable phase shifters [173]. For ferrites, the switching speeds are limited by the capabilities and the bulkiness of the electromagnets employed. An example of a  $360^\circ$  phase shifter with ferrite slab developed utilizing SIW technology is presented in Figure 11b.

To address these issues, composite multiferroics have recently been proposed as an alternative solution. These materials combine the advantages of both ferroelectrics and ferrites, offering potential improvements in tunability [174]. The working principle of composite magnetoelectric/multiferroic materials can be described as follows: When an electric field is applied to a piezomagnetic material, the microscopic electric dipoles shift, causing mechanical deformation. This deformation is transmitted across the interface to the magnetic material, where a similar effect, such as magnetostriction or piezomagnetism, takes place, leading to an overall macroscopic magnetization. This process, known as converse magnetoelectric coupling, results in the modification of the material's magnetization by an external electric field, as seen in Figure 11c. Conversely, the direct magnetoelectric effect occurs when a magnetic field is applied to a magnetostrictive material, generating voltage or polarization due to strain-induced effects in the piezoelectric component. Some popular piezoelectric materials are PZT, barium strontium titanate (BST), and lithium niobate, while for magnetostrictive, there are YIG, Terfenol, Metglas, NFO, and Galfenol. Despite these advancements, the tuning range of currently available tunable microwave devices remains limited due to the low electromechanical coupling [175–179]. Another challenge is that the strong magnetostrictive materials such as Metglas and Terfenol are highly lossy at microwave frequencies, making them unfit for such applications.

For sub-THz and THz applications, graphene has been extensively exploited due to its intrinsic property of tunable conductivity via applied chemical potential [180–182]. Yasir et al. [180] proposed a tunable phase shifter where graphene alters both the amplitude and phase response of the device, as shown in Figure 11d. Another key application area is nano-antennas, where conventional metals such as copper and gold approach their plasma frequency and become extremely lossy, rendering them inefficient as radiating elements [183]. Consequently, graphene-based optical nanoantennas are widely integrated into optoelectronic devices for plasmonic applications and have become a focal point of research worldwide [184,185].

Furthermore, integrating graphene metal hybrid antennas [186,187] into optoelectronic platforms enables the realization of versatile photonic systems. Various techniques for frequency tuning [188] and active modulation [189] of optical properties particularly via *in situ* control using external electric fields have been explored. Additionally, multiple approaches for beam scanning and reconfigurable beam control have been proposed, including reflectarrays [190] and leaky-wave graphene antennas [191]. However, the relatively low conductivity of graphene introduces significant losses, which degrades device efficiency. Therefore, innovative methods are required to fully harness the potential of multiferroic and graphene-based structures for RF applications. To mitigate losses at mmWave frequencies, particularly for RIS applications, novel approaches utilizing the mechanical control of individual array elements have emerged [192–195]. These methods employ rotary actuators [192,193], electromagnets [194] (as shown in Figure 10c), or electric motors [196] for actuation. Similar to MEMS, such mechanical elements often function

as switches with discrete states [195]. One major advantage is their simplified biasing networks compared to semiconductor-based solutions. Nonetheless, these systems face inherent limitations due to the physical response times of mechanical actuators and electromagnetic mechanisms [193,194,196]. Additionally, the incorporation of larger mechanical components, as demonstrated in [194,196], can lead to bulky structures, which restrict their integration in compact base stations or large-scale RIS implementations. Ongoing and future research aims to overcome these constraints and enhance the practicality and scalability of mechanically reconfigurable RF systems.

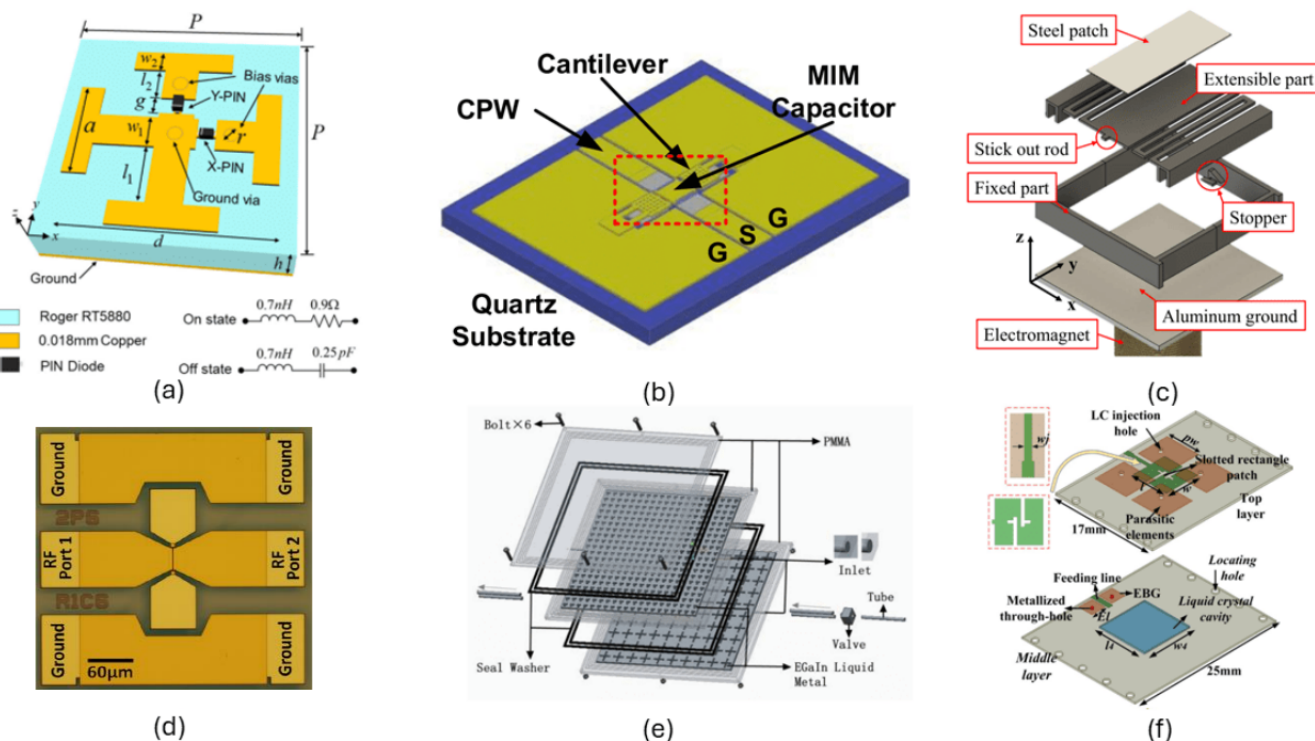


**Figure 10.** Examples of reconfigurable devices with (a) PIN diodes at Jerusalem cross unit cell [148], (b) MEMS as mm-waves switches [158], (c) an electromagnet-controlled element with varying height for RIS [194], (d) a PCM RF switch using coplanar waveguide technology [197], (e) a liquid metal double-layer FSS [198], and (f) a liquid crystal-based antenna [199].

As noted, mechanical RF components currently deliver exceptional performance and reliability. However, they are often bulky, expensive, and not easily scalable despite outperforming semiconductor-based switches in terms of RF characteristics due to reduced leakage and parasitic effects at mmWave frequencies [200]. While RF-MEMS offer superior RF performance, they typically require high DC actuation voltages and specialized packaging, which limits their integration into compact systems.

To address the growing demand for miniaturized mmWave devices, particularly for handheld and IoT applications, phase change materials (PCMs) have emerged as a promising alternative for RF switching [201,202]. PCMs can exhibit resistance changes spanning five orders of magnitude when subjected to nanosecond-scale voltage pulses, making them ideal for low-loss, high-speed switching at microwave and mmWave frequencies [201]. The two most widely studied PCMs are vanadium dioxide ( $\text{VO}_2$ ) and germanium telluride ( $\text{GeTe}$ ) [202]. Their operation relies on reversible changes in the crystal structure of chalcogenide materials between amorphous (high-resistivity) and crystalline (low-resistivity) states, typically triggered by thermal pulses.

This switching mechanism mirrors that of conventional electronic switches, enabling the development of fundamental PCM-based RF components such as SPDT, SP4T, and SP8T switches [203–205]. An optical image of a PCM-based RF SPDT switch fabricated on coplanar waveguide technology is shown in Figure 10d. By combining SPDT elements into more complex topologies, researchers have demonstrated advanced PCM-enabled systems, including crossbar switching matrices [206], tunable filters [207], tunable attenuators [185], and reconfigurable antennas [208]. Despite their significant potential, PCM-based devices face challenges that have limited their widespread commercialization, including moderate power handling, limited switching speed, and restricted cycling endurance [209]. Continued research is needed to address these issues and fully realize PCM-based RF switching technologies.

In recent years, liquid metals have emerged as a compelling solution for reconfigurable and flexible RF circuits, particularly in wearable and conformal applications [210]. These materials, which remain liquid at or near room temperature, offer several advantages, including controllable flow within microfluidic cavities and superior mechanical elasticity compared to conventional conductors such as copper. Liquid metals can be patterned and integrated using modern fabrication techniques such as 3D printing [211], injection molding [212], or spraying [213] onto rigid or flexible substrates.

Movement or reconfiguration of liquid metal within hollow channels can be achieved via micropumps or electrochemically controlled capillary forces [210], enabling enhanced tunability and high power-handling capabilities in RF devices. Applications include tunable filters [214], reconfigurable antennas [211], and frequency-selective surfaces [198], as shown in Figure 10e. Among available options, eutectic gallium–indium (EGaIn) and galinstan are the most commonly used liquid metals due to their low melting points, high thermal conductivities, and low viscosities [210].

Despite these advantages, integrating liquid metals into RF systems presents several challenges. These include the need for improved manufacturing precision and more accurate flow control, as discrepancies between simulated and measured performance often arise due to nonuniform distribution of metal within the channels [169]. Furthermore, many liquid metals are toxic or reactive, necessitating robust packaging to prevent leakage and ensure long-term device reliability [215]. Advancements in precision manufacturing and encapsulation technologies will be crucial to unlocking the full potential of liquid metal-based RF components.

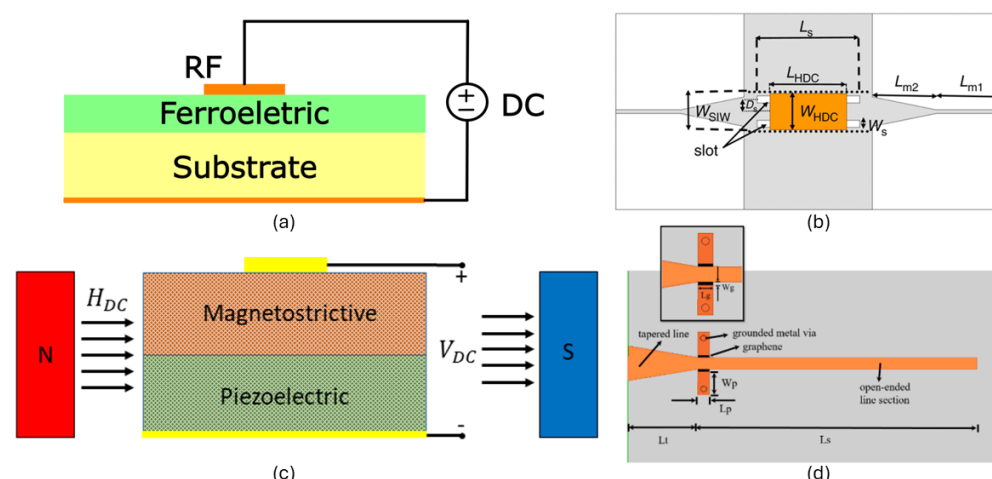


**Figure 11.** Examples of tunable phase shifters with (a) ferroelectric material, (b) ferrite [179], (c) multiferroic, and (d) graphene [180].

### 3.7. On Digital Twins and Communications

As discussed in Section 1, next-generation communication systems will form an interconnected ecosystem, linking everything to everything, everyone to everything, and everyone to everyone. A key component of this ecosystem will rely on emerging technologies, particularly AI and ML. These technologies will be crucial in developing a cyber space that mirrors the physical space (e.g., user equipment, core networks, base stations, point-to-point communications, etc.), with the goal of predicting behavior, simplifying the management and orchestration of complex network infrastructures (e.g., [216]), and optimizing performance in real-time. This cyber space will operate as a closed-loop system capable of (1) collecting real-time data from various applications (e.g., vehicular, terrestrial, and satellite networks), involving any technological components connected to the Internet or future networks, (2) diagnosing system performance, (3) identifying deficiencies, (4) predicting failures, and (5) preventing negative outcomes. This cyber space is what has been referred to as a digital twin (DT), and it is a system that will enable the optimal performance of next-generation communication systems. Although DTs are not traditionally part of the physical layer, they depend on continuous, real-time interaction with physical systems, making them a natural extension of it. The authors consider that their inclusion in this paper is essential, as they represent an application domain that directly influences the development and optimization of physical layer technologies. Essentially, a bi-directional communication link will be established between the digital twin and the physical space, where the events of the physical space are captured in near-real-time, and the tasks performed within the cyber space, such as modeling, learning, data analytics, prediction, and simulation, provide feedback to the physical space [217,218].

To the authors' understanding, DT technology is expected to impact multiple disciplines within the broader framework of next-generation communication systems. By creating real-time, data-driven virtual replicas of physical systems, DTs will enable optimization, predictive analysis, and autonomous decision making across various domains. One prominent application of DTs is in satellite communications, particularly with the rapid expansion of low Earth orbit (LEO) satellite constellations. Companies such as Starlink, Kuiper, and OneWeb have already launched, or plan to launch, thousands of satellites to provide global connectivity. As of today, Starlink operates over 3000 satellites, serving more than 400,000 customers worldwide [219]. To optimize satellite-to-satellite and satellite-to-Earth/user communication links, highly efficient computational models are required. A DT framework, leveraging learning-by-example algorithms [220], can dynamically predict and optimize system performance. For instance, in Starlink's Ku-band operation, satellite beam steering is limited to 40-degree scan angles with an EIRP of 5 dBW/MHz [221]. Moreover, with an average line-of-sight connection of only 10 min per satellite, users must continuously switch between satellites for uninterrupted connectivity. A DT model that maps the entire communication ecosystem, incorporating satellite availability, frequency bands, modulation schemes, and antenna polarization, is expected to be able to provide real-time recommendations to user terminals, ensuring optimal connectivity. Furthermore, DTs will be critical in mitigating latency challenges in space communications. The one-way propagation delay between a user and a satellite varies from 1 ms to 140 ms, depending on the satellite's altitude [222]. It is these authors' intuition that a DT engine will help minimize this delay by optimizing packet error rates and maximizing data burst efficiency.

DTs will also play a transformative role in vehicular networks, particularly with the rapid deployment of autonomous vehicles (AVs). In cities like San Francisco and Singapore, AVs are already in operation by companies like Waymo [223], Cruise [224], and A\*STAR [225], Aptiv [226], and MooVita [227], respectively. Establishing intelligent networks that integrate AVs with conventional vehicles is essential for ensuring safe and

efficient transportation. It is well-understood that the realization of a large-scale human-machine ecosystem within cities is not feasible without such networks. A DT model, continuously updated with real-time data from various cities and driving conditions, can make decisions with near-zero statistical error, guiding autonomous navigation in real-world environments. For example, a DT-powered system can make critical decisions regarding (a) when a vehicle is to stop, accelerate, or decelerate, (b) how to safely overtake another vehicle, (c) how to avoid collisions with vehicles or pedestrians, and (d) decision making in high-risk scenarios, such as choosing between colliding with another vehicle or risking harm to a pedestrian. By continuously learning from real-world driving scenarios, we believe that a living DT network will be instrumental in improving safety, efficiency, and decision-making autonomy in AVs.

A similar, but even more complex, application of DTs is in unmanned aerial vehicle (UAV) navigation, particularly in commercial drone delivery services. Companies such as Amazon, DHL, FedEx, and Zipline are already using drones for logistics, including medical supply transport, package delivery, and food distribution, e.g., [228]. For example, (a) Meituan, a Chinese company, has 30 drone delivery routes, handling over 300,000 orders [229], (b) Amazon operates drone delivery services in College Station, Texas, and Phoenix, Arizona [230], and (c) food delivery by drones is now part of daily life in Shenzhen, China [231]. Notably, the drone package delivery market is projected to reach 8.57 billion USD by 2032 [232]. Therefore, it is expected that in the near future, thousands of drones will be deployed for last-mile deliveries [233], creating an extremely complex air traffic management challenge. It is these authors' position that traditional human-controlled air traffic systems will not be able to scale for managing these thousands of drones. Current aviation accident data indicate that 69% of general aviation accidents are due to pilot error [234]. Therefore, the DT-powered UAV navigation systems takeover is expected, with the goal to dramatically improve safety by reducing human intervention and optimizing flight paths in real-time. Moreover, in highly populated cities, where spectrum congestion is already a major issue, drones are required to be able to efficiently communicate with base stations. Currently, FCC regulations restrict drone operations to unlicensed frequency bands, including 2.4 GHz, 5.8 GHz, 900 MHz, and 433 MHz [235]. If these regulations pertain, a DT engine is expected to dynamically allocate spectrum, optimize routing, and ensure robust, interference-free communications in these environments.

Additionally, as data demand continues to skyrocket, traditional communication networks will struggle to process massive amounts of real-time information from these thousands UAVs as well as other autonomous systems connected to the same communication network. We expect DTs to alleviate this challenge by training machine learning models for predicting, optimizing, and guiding device performance, thus improving overall network performance.

As expected, security and privacy are critical concerns in communication systems. Malicious users may attempt to intercept data, manipulate control signals, or disrupt information. A DT-enhanced security framework can address these challenges by improving (a) precoding schemes for secure transmission, (b) cooperative secure communication strategies, (c) the mitigation of pilot contamination, (d) robustness against hardware impairments, and (e) energy-efficient communication.

Finally, we expect DT to revolutionize hardware development. Existing full-wave electromagnetic simulators, based on analytical and numerical methods, can be seen as early precursors of DT technology. Future DT engines will integrate these simulators with machine learning algorithms, creating multiphysics, multi-fidelity models capable of predicting device performance and optimizing new designs [236]. This simulation-hardware co-design approach will significantly reduce costs and enhance device maintenance.

DTs will play a transformative role in next-generation communication systems, from LEO satellite networks and autonomous vehicles to drone-based delivery services and system-level design. It is these authors' opinion that by continuously collecting and analyzing real-world data, DTs will enable unparalleled optimization, decision making, and security, ultimately shaping the future of wireless communication systems and not only. Table 3 summarizes the application areas and anticipated key benefits of DTs as discussed in this section.

**Table 3.** Digital twin applications.

Application Area	Description	Key Benefits
Satellite Communications	DT models dynamically predict and optimize satellite-to-satellite and satellite-to-Earth links, accounting for variables like frequency bands and modulation schemes.	Improved connectivity, reduced packet error rates, and minimized latency.
Autonomous Vehicles (AVs)	DT models guide AV navigation by learning from real-world driving conditions to improve safety and efficiency.	Enhanced traffic control, collision avoidance, and improved decision making in complex scenarios.
Drone Delivery Systems (UAV Navigation)	DT models manage large-scale drone navigation in crowded urban environments and ensure robust communication despite spectrum congestion.	Improved air traffic management, reduced human error, and optimized delivery efficiency.
Mobile Edge Computing	DT frameworks predict and improve data offloading, latency reduction, and performance in distributed networks.	Reduced failure rates and enhanced resource management.
Network Security	DT frameworks secure communication systems by improving precoding schemes, mitigating pilot contamination, and enhancing robustness against attacks.	Enhanced security, improved transmission strategies, and energy-efficient communication.
Hardware Development	DT-integrated simulators improve device design, incorporating machine learning for performance prediction.	Accelerated development cycles, cost reduction, and enhanced system reliability.

#### 4. Antennas and Antenna Related Technologies for Future Internet

In the current section, we attempt a classification of antenna and antenna-related technologies, identifying, as a key driving force, the tendency of antennas to become more and more competent. Indeed, independent of how potent the given version of a radiator can be, there is, deterministically, the need for the newer prototype to excel and expand on every key performance indicator (KPI) used to describe the specific targeted use case or application [237]. An easy example, to advocate in favor of this point of view, is, of course, the quantitative evolution of the MIMO concept and relative implementation. To increase in competence, antenna link systems, focused on wireless communications, started as SISO to evolve to multi-element array formations. Indeed, this is verified by the quantitative MIMO evolution across the wireless communication generations (Generation, (max) Number of Digital Ports): (3, 1(No-MIMO==SISO)), (4, (2)4—legacy MIMO)), (5,16), (5.5,64—massive-

MIMO), (6, 256 g-MIMO). In the next table (Table 4), we present the historical series of events in a more compact way [238].

**Table 4.** MIMO prototype evolution towards gMIMO.

Ref.	Frequency (GHz)	No. of Antennas	No. of Ports
[239]	2.4	64	16
[240]	3.7	100	100 (10)
[241]	5.8	256	64
[242]	3.5	128	128 (12)
[243]	3.5	64	32
[244]	3.5	288	72
[245]	5.8	120	120
[246]	3.5	240	60
[247]	13	4096	256

Thus, having verified, at least partially, the radiators' evolution towards multi-competent designs, we unfold our point of view on the classification of antennas and antenna-related technologies, as shown in Figure 12.

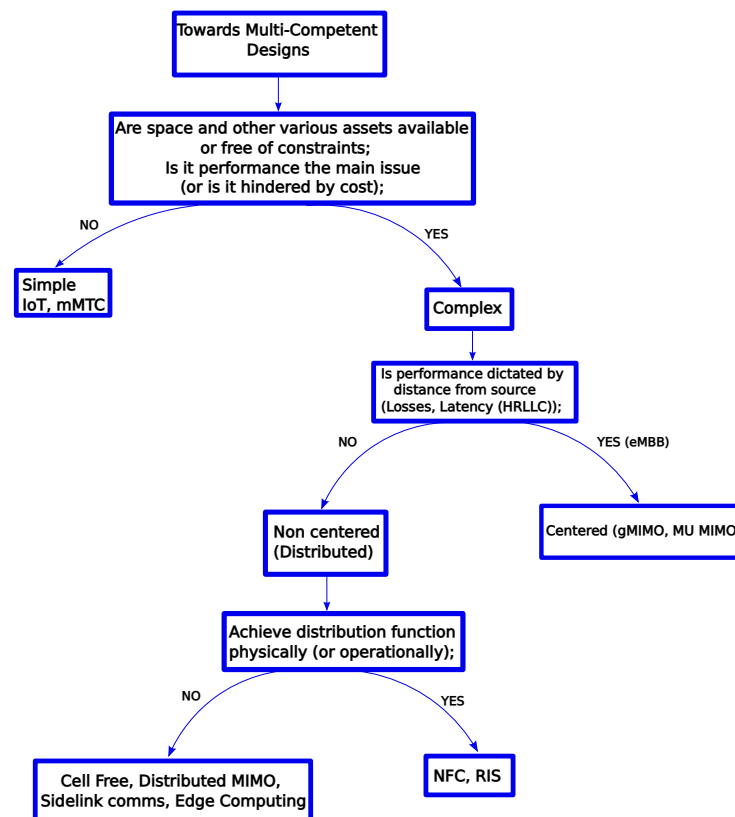


**Figure 12.** Antennas and antenna-related technologies classification.

While achieving multi-competent designs is the goal, there are challenges ahead that dictate the route of the path forward. The first bifurcation point takes place under the pressure of assets availability and whether performance or cost is the driving factor. In the term ‘assets’, we include factors like available area and volume size of the host, access to it, power supply availability and thermal dissipation ability, available technologies, and so on. In case performance is the determining force, the delivered system can become more complex and expensive. In this case, it is the technology level that sets the upper limit of

the design's competence. For example, the systems provided tend to be multifunctional, complex, and very elaborate.

On the other hand, when cost is the main issue, the designs tend to be simple but nevertheless thoughtful. In this case, the goal is that relevant devices can be produced in great numbers, usually via automated procedures, and be of low profile while retaining the necessary degree of merit and minimum functionality to work seamlessly, integrated into the targeted system. In this category, we include antennas for UEs, where available space, MIMO function, and reduced SAR control the design process. Also, we include IoT devices' radiators working under the umbrella of mMTCs in smart homes, factories, cities, or sensor network applications. These antennas are designed to achieve high scores on diverse KPIs from multiband operation to multi-polarization and DoA functionality, from body networks to wireless power transfer and super-directivity, from frequency coding to sensor and RFID applications, and, of course, many more.

In the case where complex designs are allowable, the next factor is whether the system's performance is critically impaired or limited by the distance between the communicating nodes (with well-known examples being propagation losses and system latency). If this is not the case, then centralized designs (meaning non-peer node communication where a coordinating-serving access point, such as a base station, LEO satellite, or IoT reader station, connects with a set of numerous users, such as UEs or IoTs, whose spatial positioning is angularly represented into the utilized wireless channel) can be employed. These are well suited to the eMBB use case of 5G and 6G communications. A notable example of this case is the base station MIMO antenna system, which has been covered in Table 4.

On the other hand, if performance is critically impaired or limited by Tx-Rx distance, distributed solutions are employed. The aim here is more uniform coverage or reduced latency between the communicating nodes. In this case, one can distinguish between the ways this distribution is attained. If the distributed operation is based on physics-level principles, we can refer to near field communications (NFC) and RIS-assisted communications. Alternatively, if antenna distribution is achieved by choosing a distributed operation paradigm for the communication network, we can include cell-free communications (distributed MIMO), side-link communications, and edge computing.

In NFC, the distributed function is achieved by adding an extra dimension to the space that surrounds the main antenna. Before NFC, the space around an antenna was conceived as functioning only in the far field and, thus, described only by angular dimensions. By adopting NFC, antennas become electrically large, and this pushes the Fraunhofer boundary (the far-field boundary) outward from the antenna. To access any receiver immersed into this extra, near-field space, one needs the additional Tx-Rx distance dimension, since the angular one alone is no longer sufficient. This increases capacity, a major KPI concern in 5G and 6G wireless communications.

In the RIS case, a reflective (or even a transmissive) array antenna structure is employed as a relay to assist NLOS (or, in general, unreliable) wireless communication. Reconfigurability and, thus, adaptability to varying link conditions is achieved via controlled lumped loads attached to each of the reflecting elements. This technology, which allows for a multibeamforming response, is considered a key ingredient for future wireless internet communications.

Let us now steer our attention to the case when the angular representation of the channel is altered by employing enhanced network operation structures. Here, we will focus on antenna systems evolved in cell-free (or distributed MIMO) communications, side-link communications, and edge computing solutions.

In the next subsections, we list some notable examples relative to the classification stated in Figure 12. The application-focused antenna designs identified here include simple

(e.g., UE, IoT) and complex devices, both centralized (gMIMO) and distributed. In the latter case, both physics-based (e.g., NFC, RIS) and network/system-based (e.g., cell-free, side-link, edge computing) solutions are discussed.

#### 4.1. Antennas for User Devices, (IoT—mMTC and UEs)

Antennas for user devices can be studied based on design goals, novelty and merit, manufacturing process and evaluation, and the focus of the specific application, and they are grouped here into two main categories: the IoT and user equipment (UE) serving antennas. A summary of indicative works is listed in Table 5 where various antenna characteristics are depicted for user devices, including IoT devices and UE. The table details various parameters for each antenna technology, such as the element type, number of elements, size, frequency band, beamforming utilization, number of beams, gain, beamwidth, and number of MIMO ports used. Key challenges that must be addressed for the upcoming 6G communication include miniaturization, polarization diversity, and energy efficiency with respect to antennas for user devices.

**Table 5.** Summary of antenna technologies for IOT and UE.

Ref.	Type of Element	Elements No.	Size (mm <sup>3</sup> )	Frequency (GHz)	No. of Beams	Gain (dBi)
[248]	Circular Patch	4	40.17 × 40.17 × 0.57	5.75	4	6.41
[249]	Square Ring Patch	1	77.9 × 73.2 × 0.2	1.1–2.3	1	1.5
[250]	Γ-Dipoles	4	75 × 75 × 1	2.4	2–4	6.84
[251]	Sector Patch	4	27.4 × 27.4 × 1.34	4.16	Multiple	4.62
[252]	Circular/Annular Patch	3	60 × 60 × 0.7	2.43–2.467	3	6
[253]	Circular Patch	3	41.6 × 41.6 × 3	3.5	3	N/A
[254]	Rhombohedral Patch	3	75 × 70.2 × 6	4.18–6.76	Multiple	7.8
[255]	Half-Mode Patch	1	22.55 × 23.95 × 3	2.45 & 5.5	2	4.53 & 9.1
[256]	Lateral Cross-Dipoles	4	21 × 5 × 1.622	28–38	2	11.5/9.7
[257]	Multi-Branch Patch	10 × 10	60 × 10 × 0.8	0.8–1.04, 4.69–11.5	1.6–2.71, Multiple	6.49
[258]	π and L Patch	12	150 × 80 × 0.8	3.4–3.6, 5.1–5.9	3.6–3.8, 12	N/A
[259]	Dipoles and T-Monopole	3	30.5 × 1 × 0.8	3.5	3	5
[260]	Slotted Patch	8 × 8	27 × 27 × 1.6	3.3–3.8	Multiple	10
[261]	Planar Monopole with EBG	4	64 × 64 × 1.6	3.25–3.5, 4.2–5.1	4	5.6
[262]	Slotted Patch	2	35.5 × 25.0 × 0.75	3.3–4.2	Multiple	2–4

For the IoT case, one can identify antennas for wearable, polarization beamforming, DoA-focused, MIMO, wireless power transfer, super-directivity-based, and multiband applications. Wearable antennas are the focus of [248,249], where 3D beam-steering MIMO antenna for on-body IoT applications and lightweight flexible, wearable, circularly polarized antenna for navigation and positioning in IoT applications are contributed, respectively. Multi-polarization focus, beamforming, and DoA functions are the quest of [250,251,263]. There, an all-polarization, beamforming, and DoA-ready  $\Gamma$ -dipole antenna, an all-polarization rectenna, and a multi-sector annular antenna for IoT applications are contributed. An example of an all-polarization  $\Gamma$ -dipoles antenna array is depicted in Figure 13.

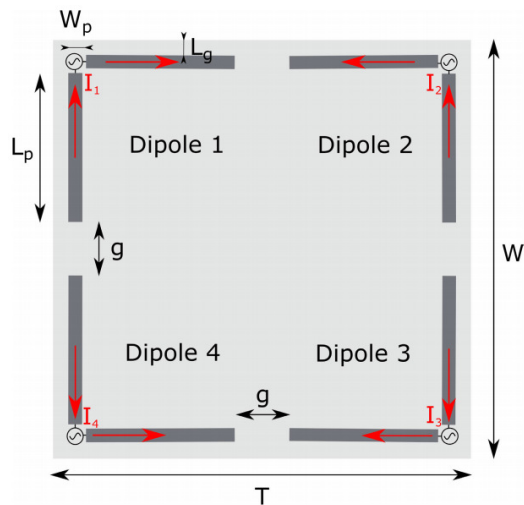


**Figure 13.** An all-polarization, beamforming, and DoA-ready,  $\Gamma$ -Dipole Antenna [250].

MIMO functionality is extensively studied, designed, and implemented in numerous works [252,253,264]. Rectenna designs for simultaneous wireless information and power transfer (SWIPT), with optimized energy efficiency especially for low-power IoT sensors, are presented in [254,265]. Superdirective, endfire, and broadside array configurations are discussed in [266], while a multiband patch antenna design covering the WiFi 6 bands is introduced in [255].

Various antennas focusing on UE applications are presented in the following references. In [256], lateral cross-dipole elements are integrated into a compact antenna-in-package design for 5G UE applications. The design exhibits dual polarization and dual-band operation in the 28 GHz and 38 GHz millimeter-wave bands, with a total bandwidth ranging from 27 GHz to 40 GHz. In [257,258,267], 8-, 10-, and 12-port UE antenna arrays operating at various multiband frequencies are presented. Novel techniques for enhancing MIMO antenna array performance in the sub-7 GHz band are introduced in [268].

A shared-aperture three-antenna module utilizing a single floating metal structure with minimal clearance is the focus of [259]. This design maximizes space efficiency while maintaining high performance, making it ideal for compact 5G mobile terminals. A dual characteristic mode antenna design integrated into the smartphone back cover is proposed in [260], supporting multiple 5G frequency bands efficiently.

Photonic reconfigurable electromagnetic band gap (EBG) antenna arrays focused on beam-steering enhancement are presented in [261]. Furthermore, other works focus on topics such as heat dissipation [269], user interaction mitigation [270], which refers to strategies aimed at improving handset antenna performance when affected by the human body, which can degrade radiation efficiency metasurface-based phone cases [271], and extremely low-profile tunable multiport handset antennas [262]. The photonic reconfigurable electromagnetic band gap antenna arrays discussed in [261] are illustrated in Figure 14.

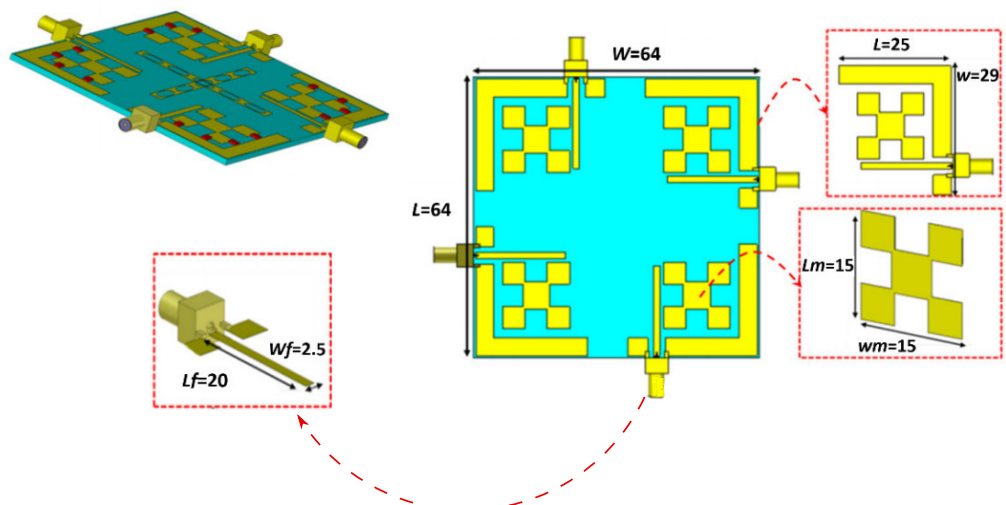


**Figure 14.** Photonic reconfigurable electromagnetic band gap antenna arrays [261].

#### 4.2. Antennas for Centralized Solutions

In the current section, antennas for centralized solutions are presented, including antennas for TN base stations and for NTN as well.

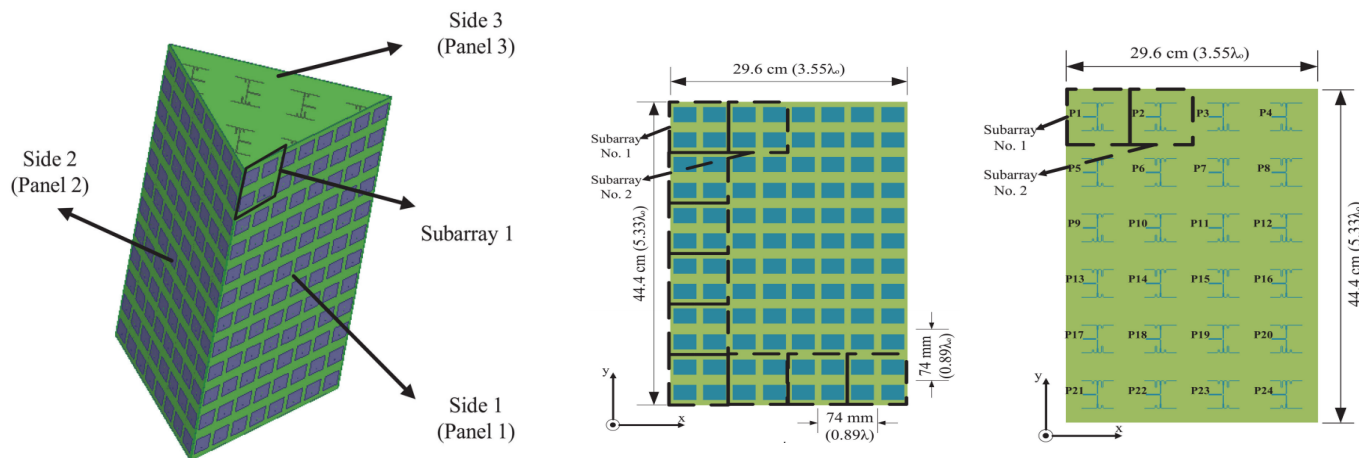
Indicative antenna arrays for TN and NTN are summarized in Table 6, where their main characteristics are depicted. Some of their essential characteristics are discussed next.

**Table 6.** Summary of antennas for base stations.

Ref.	Elements Type	No. *	Size (mm <sup>3</sup> )	Frequency (GHz)	Beamforming	No. of Beams	Gain (dBi)	Beamwidth
[244]	2 × 2 Rectangular Patch Array	72	444 × 296 × 1.524	3.45–3.55	Switched	13	19.5	±34°
[241]	1 × 4 Rectangular Patch Array	8	320 × 215 × 1	5.7–5.9	Digital	Multiple	13	90°
[272]	Elliptical, Bowtie Dipoles	2	220 × 220 × 100	0.7–0.96, 1.7–3, 3.3–3.8	N/A	N/A	8	73°, 65°, 80°
[273]	Dual-Polarized Bent Dipoles	4	330 × 105 × 31	2.5–2.7 & 3.3–3.6	N/A	N/A	8.6 (LB)/ 7.8 (UB)	61° (LB)/ 66° (UB)
[274]	Bowtie Dipoles	2	110 × 52 × 34	2.3–2.69	N/A	2	8	50
[275]	Magneto-Electric Dipole	3	96 × 95 × 21.1	1.68–2.93, 3.32–3.64	N/A	3	7.2	102–160°
[276]	Evanescence Quadridge	4	96 × 95 × 21.1	1.68–2.93, 3.32–3.64	Analog	Multiple	5.93	N/A
[277]	Brick Horn	64	5.61 × 4.85 × N/A	Tx: 37.5–42.5, Rx: 47.2–51.4	Analog	8	24.4	N/A
[278]	Square Patch	32	82.42 × 30	34.8–37.6	Digital	Multiple	8.7	N/A

\* Number of elements.

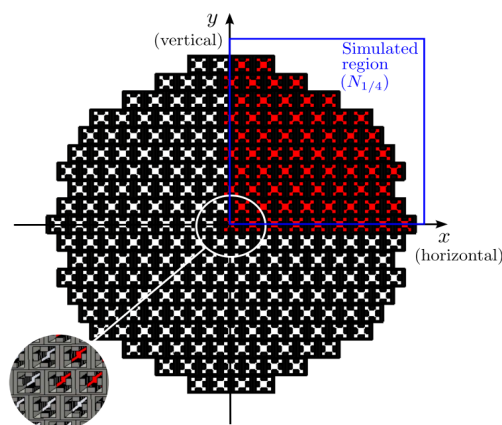
Massive MIMO antenna systems for 5G base stations [244] (shown in Figure 15) and active multibeam antenna systems [241] contribute significantly to advancements in beam steering and multibeam management. The massive MIMO system features a 72-port triangular structure supporting 288 elements with beam-switching capabilities, producing 13 beams and a gain of 19.5 dBi. Its adaptability to varied environmental conditions through both MIMO and beam-switching modes is commendable. The active multibeam antenna system, with 64 RF channels and 256 antenna elements operating in the 5.7–5.9 GHz range, efficiently manages multiple beams via digital beamforming with a gain of 13 dBi, making it ideal for large-scale MIMO deployments.



**Figure 15.** Base station antenna with 288 elements [244].

Other noteworthy designs include the triple-band dual-polarized indoor base station antenna [272], which offers multiband support across 2G, 3G, 4G, and Sub-6 GHz 5G networks. Its stable gain and reliable radiation patterns make it a strong candidate for indoor applications. The compact dual-band dual-polarized antenna [273] integrates filtering structures to reduce mutual coupling, enhancing stability with gains of up to 8.6 dBi in the lower band and up to 7.8 dBi in the upper band. Innovative designs like the metasurface decoupling antenna [274] utilize a metasurface superstrate to improve isolation by over 25 dB and enhance efficiency by approximately 10%. The conformal magneto-electric dipole antenna [275] offers a compact design and improved MIMO performance through the integration of metamaterials.

Another promising development concerning NTN is the use of multibeam antennas based on 3D discrete lenses [276] (Figure 16), which feature Evanescent Quadridge Antennas (EQA) and achieve an impressive beam-scanning range of  $\pm 70^\circ$  while maintaining a gain of 5.93 dBi. Additionally, the highly integrated Q/V-band multibeam phased-array antenna [277], designed for LEO satellite applications, leverages an advanced beamformer chip and hybrid construction for efficient power management and thermal control, achieving an effective gain of 24.4 dBi. The reconfigurable multibeam holographic antenna [278] employs liquid-crystal technology to achieve low power consumption, independent beam control, and flexible beam steering, making it suitable for Ka-band LEO satellite communication. In [279–281], direct radiating array solutions for MEO satellites, combined with digital or hybrid beamforming, are analyzed and studied.

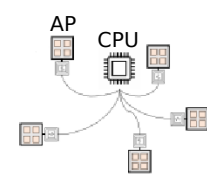
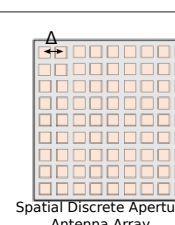
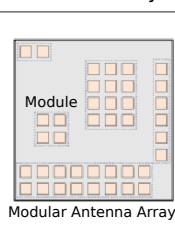
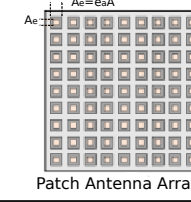
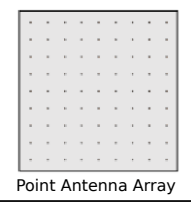
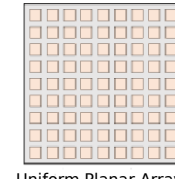
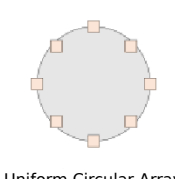


**Figure 16.** Additive manufactured 3D discrete lenses antenna, with beam scanning  $\pm 70^\circ$  and gain of 5.93 dBi [276].

The development of 6G networks will introduce several critical challenges for base station antenna systems. Higher frequency operation at THz bands will require improved materials and designs to manage increased signal attenuation and path loss. Extreme beamforming requirements will necessitate advanced phased-array and metasurface technologies. Energy efficiency will become increasingly important to ensure sustainable deployments as data rates and frequency ranges grow. Finally, the demand for compact and lightweight designs will require innovative engineering to accommodate denser urban environments while maintaining optimal performance.

#### 4.3. Physics-Assisted Distributed Solutions

A number of review papers focus on electrically large antennas (ELAs) for near-field communications [282–284]. The near field of an antenna extends to a distance equal to  $2D/\lambda^2$ , known as the Rayleigh distance, which is used to distinguish between near- and far-field regions. The extension of the near field is defined by both the wavelength (ranging from a few millimeters down to a fraction of a millimeter) and the maximum dimension  $D$  of the antenna (or the array of a RIS). Thus, structures with relatively small physical dimensions (e.g., a window supporting a RIS) may behave as an electrically extremely large antenna. In the near-field region, electromagnetic waves exhibit spherical wavefronts rather than planar ones. For mmWave and THz communications, the near-field distance varies from hundreds of meters to a few centimeters. Figure 17 depicts different configurations of ELAs, which are categorized according to antenna array distribution, antenna spacing, antenna element size modeling, and array geometry. Many studies demonstrate the importance of ELAs in improving communication reliability, security, and efficiency in near-field wireless systems.

Category	Architecture		
Element Distribution	 Co-located Antenna Array	 Distributed Antenna Array	
Antenna Spacing	 Spatial Discrete Aperture Antenna Array	 Spatial Continuous Aperture Antenna Array	 Modular Antenna Array
Element Size	 Patch Antenna Array	 Point Antenna Array	
Geometry	 Uniform Linear Array	 Uniform Planar Array	 Uniform Circular Array

**Figure 17.** Large antenna array configurations for near-field communications [283].

In [285], a switched-beam system serving a high-speed train is studied, enhancing connectivity through dynamic beam design. In [286,287], near-field beam focusing is explored, aiming to enhance spatial resolution, reduce interference, and improve physical layer security in near-field communications. Improved accuracy in complex environments through range estimation is investigated in [288] with regard to near-field multistatic radar. In [289], sparse arrays are used to harness the benefits of near-field multiuser communication, achieving better spatial selectivity and improved user separation, while in [290], a novel theoretical model for received power estimation in phased-array-based wireless power transfer systems is studied, optimizing energy delivery in the near-field region. A true time delay system is utilized in [291] to improve wideband MIMO system performance in near-field environments. In [292], the study focuses on extremely large cylindrical antenna array systems, optimizing beamforming patterns for improved coverage and capacity in near-field systems. Fluid and movable near-field antenna systems are discussed in [293,294], aiming to enhance adaptability, flexibility, and spatial diversity for multiuser near-field communication systems.

#### 4.4. Antennas for Distributed Solutions Based on Network Structure

##### 4.4.1. Antennas in Cell-Free Communications

Cell-free communications is an emerging wireless technology where multiple distributed access points (APs) collaborate to serve all UEs in a given area without relying on cell boundaries. This technology aims to improve network performance by leveraging beamforming and interference management. Key advantages include improved coverage [295], as multiple APs are distributed across the area and serve all UEs simultaneously, significantly reducing dead zones and weak coverage areas. A better user experience is also achieved, since unlike traditional cellular systems where performance degrades at cell edges, cell-free systems ensure consistent data rates across the entire coverage area. Robustness to user mobility is another key benefit, as the absence of fixed cell boundaries minimizes handover procedures, reducing latency and service interruptions for moving users.

Major drawbacks include complexity in signal processing; coordinating multiple APs for coherent transmission requires sophisticated algorithms and significant computational resources. Deployment costs are another key challenge, as cell-free architectures often require more APs and additional infrastructure and incur higher operational costs than traditional cellular systems [296,297]. The coordination and communication between various APs in the infrastructure of cell-free communication systems also present significant challenges.

The merits of cell-free communications are supported in numerous publications [295,298,299]. An example of a radio stripe system design is shown in Figure 18. Each radio stripe sends and receives data to or from one or multiple CPUs through a shared bus.

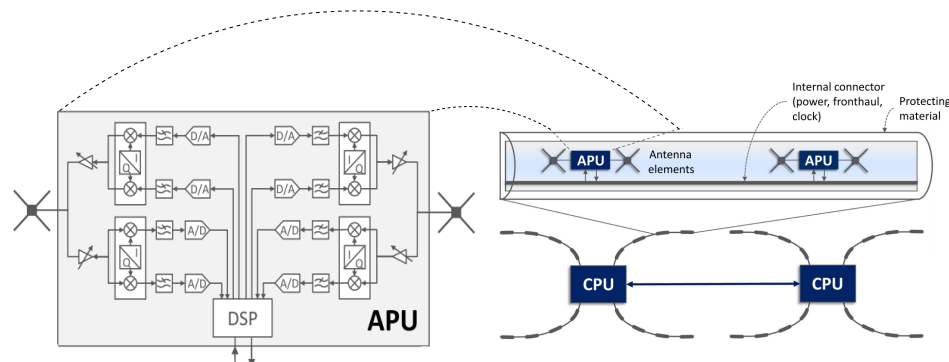


**Figure 18.** Efficient radio stripe system [295].

In [300,301], a cost-efficient radio stripe system architecture is presented. In such a system, the antennas and the associated antenna processing units (APUs) are serially located inside the same cable, which also provides synchronization, data transfer, and power supply. This approach significantly improves performance by minimizing signal degradation caused by environmental obstacles. In [302], the cell-free concept is extended by integrating LEO satellites with terrestrial antenna systems. This hybrid model enables seamless connectivity in remote and underserved regions. The combination of satellite and terrestrial antennas enhances the reliability and scalability of cell-free networks. Radio stripe antennas are utilized for wireless energy transfer in [303]. This solution provides improved indoor coverage and supports energy-efficient designs, especially for IoT and smart building applications.

#### 4.4.2. Antennas for Side-Link Communications

Several innovative antenna designs have been introduced to enhance UAV and vehicular communication systems. The quad-polarization reconfigurable conformal array antenna [304] employs a patch radiator with edge slots and shorting pins, arranged in a  $3 \times 3$  subarray configuration. This design achieves a gain greater than 14 dBi and enables wide beam-scanning coverage ( $50^\circ \times 180^\circ$ ), making it suitable for UAV platforms requiring flexible polarization control. The balloon conformal heterogeneous array antenna [305] integrates dumbbell-shaped and size-tapered dipoles (see Figure 19a) to achieve  $360^\circ$  azimuthal coverage and dynamic beam switching. This feature makes it highly adaptable for aerial communication scenarios. Another significant innovation is the planar dual-mode dipole antenna (Figure 19b) [306], which combines dipole and monopole radiation characteristics using H-slot-loaded microstrip arms. Operating across the 0.94–1.57 GHz range, it offers stable vertically polarized radiation patterns, ensuring reliable long-range UAV communications. For improved UAV coverage, the null-filled axisymmetric secant square-shaped beam antenna [307] employs a patch radiator with a grooved circular structure and four monopoles (Figure 19c), efficiently mitigating null formations while ensuring stable connectivity.

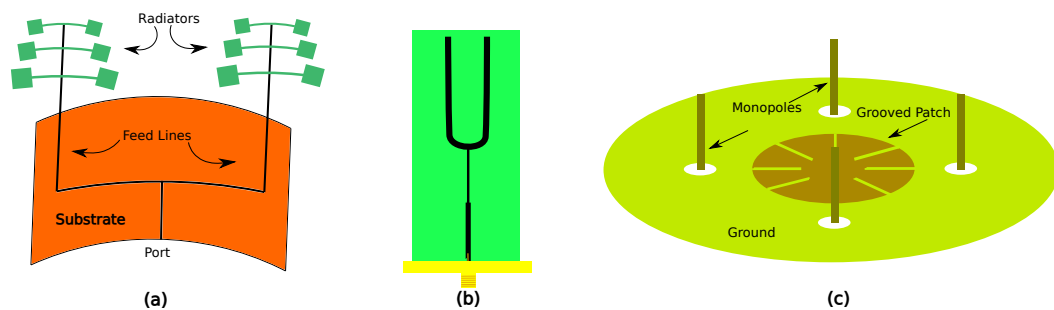


**Figure 19.** UAV antenna designs: (a) size tapered dipoles, (b) U-shaped dipoles, and (c) grooved patch.

Meanwhile, the airborne flexible rectifying metasurface system [308] utilizes metasurface structures with rectifying diodes to maximize power absorption efficiency and maintain stable wide-angle reception, enhancing UAV applications that require power harvesting capabilities. Table 7 summarizes, in more detail, various antenna characteristics for side-link communications.

**Table 7.** Summary of antenna characteristics for side link communications.

Ref.	Element Type	No. *	Size (mm <sup>3</sup> )	Frequency Band (GHz)	No. of Beams	Gain
[304]	Slotted Circular Patch	9	930 × 340 × 5.8	1.5	3	14
[305]	Conformal Dumbbell-Shaped Dipoles	18	400 × 1462 × 55	2.4	9	12
[306]	H-Slot Loaded Dipole	1	90 × 10 × 1	0.94–1.57	1	4.76
[307]	Grooved Circular Patch with Monopoles	1	225 × 225 × 2.8	5.4–5.8	1	9
[308]	Slotted Rectangular Patch	16	36.2 × 36.2 × 0.3	5.8	N/A	N/A
[309]	Monopolar Stacked Circular Patch	1	170 × 170 × 4.175	2.24–2.53, 5.42–5.98	N/A	6/7.5
[310]	Hexagonal Fern-Fractal Patch	1	29.38 × 29.38 × 17.95	3.49–3.9	N/A	5.16
[311]	Circular Patch with L-Shaped Stubs	1	135 × 135 × 15.27	2.6–2.98	N/A	5.1
[312]	Hybrid Quasi-Circular and Square Monopole	1	24 × 16 × 0.8	3.1–10.9	N/A	3.5
[313]	Slot Patch	4	20 × 10 × 20	3.25–6.7	N/A	4.97
[314]	Annular Arc Monopole	4	32 × 15 × 32	2.8–9.5	N/A	3.2–5.41
[315]	Dielectric Resonator	4	100 × 100 × 50	2.5–3	N/A	2–5
[316]	Dielectric-Loaded Horn Antenna	4	152 × 152 × 20	0.7–6	4	8–8.7
[317]	F Monopole Antenna	4	50 × 50 × 33.3	1.95–6.25	4	3.3–6.16
[318]	Rectangular Patch with Lens	1	73.4 × 73.4 × 87.03	5.85–5.92	1	14.3
[319]	Square Monopole with Defected Ground	32	142 × 142 × 114.25	3.03–15.33	N/A	12.1

\* Number of elements.

In vehicular communication, the low-profile dual-band stacked microstrip monopolar patch antenna [309] leverages stacked microstrip patches and conductive vias to enhance bandwidth while preserving stable omnidirectional patterns. A compact circularly polarized wide-beamwidth microstrip antenna [310] for vehicular communication provides improved blind spot detection capabilities, utilizing a miniaturized patch size and achieving a 410 MHz impedance bandwidth. The dual-band dual-CP all-metal antenna [311] enhances vehicular communication systems by combining circular polarization with metal structures for improved isolation and mechanical robustness. For wideband automotive communication, a compact UWB monopole antenna [312] features a hybrid quasi-circular and square monopole structure, ensuring stable radiation patterns across a wide frequency range. The broadband slot-based MIMO antenna array [313] integrates slot-based structures and microstrip line feeding, optimizing gain performance and pattern diversity with low envelope correlation coefficient (ECC) values. Similarly, the interlocked four-port MIMO antenna [314] achieves improved isolation and wideband performance, enhancing connectivity in dynamic automotive environments.

Another key advancement is the circularly polarized quad-port MIMO dielectric resonator antenna [315], shown in Figure 20a, which enhances polarization diversity and beam tilting for stable vehicular connectivity. A compact four-channel MIMO 5G sub-6 GHz antenna (Figure 20b) [316] further optimizes element placement to improve pattern diversity and gain in advanced vehicular applications.

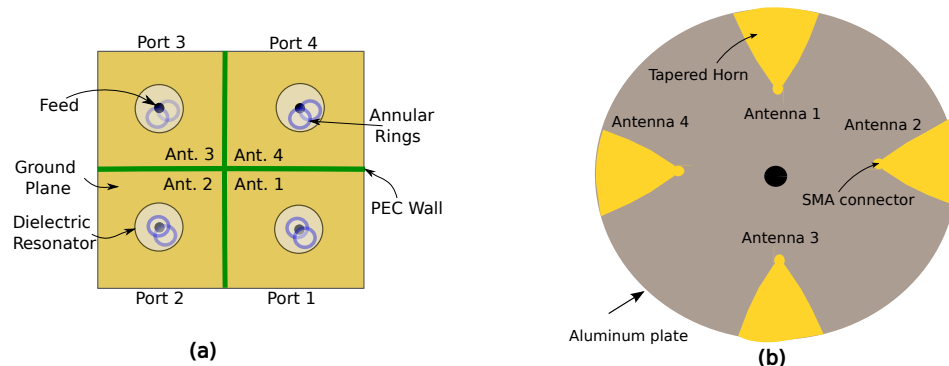


**Figure 20.** Antenna designs for vehicular communications: (a) MIMO dielectric resonator antenna; (b) MIMO tapered horn antenna.

The compact quad-element vertically polarized MIMO antenna [317] achieves high isolation and wideband performance by reducing mutual coupling and ensuring stable gain across frequencies. Lastly, the low-cost 3D-printed circularly polarized lens antenna [318] combines a linearly polarized patch radiator with a 3D-printed lens to achieve a low axial ratio and high gain for improved V2X communication, while the wideband 32-element 3D-MIMO antenna [319] expands performance across 3.03 GHz to 16 GHz, providing multi-directional beamforming capabilities that enhance data throughput and vehicular connectivity.

A major challenge for UAV platforms will be the need for highly adaptive beamforming and tracking systems to maintain stable links during rapid movement and altitude changes. Moreover, the integration of energy-efficient designs will be critical, particularly for UAV antennas with power harvesting requirements. For vehicular communications, achieving ultra-reliable low-latency communication (URLLC) will require robust MIMO designs that maintain performance in high-mobility environments. Enhanced interference management techniques will be essential to mitigate signal degradation in dense urban areas. Additionally, compact and lightweight antenna designs must be developed to ensure efficient integration into modern vehicles without compromising performance. These

challenges will drive innovation in materials, signal processing algorithms, and advanced antenna architectures.

#### 4.4.3. Antennas for Edge-Computing Solutions

It is common practice, when latency is a key factor, to employ edge computing solutions. Various relevant reviews exist [320–322]. Notable antenna designs include edge computing antennas for rail [323], 5G [324], and MIMO systems [325]. Nevertheless, particularly noteworthy examples include movable and fluid antenna solutions [326,327]. While the massive MIMO UAV-aided approach in [326] emphasizes energy optimization for vehicular networks, the fluid antenna concept in [327] offers adaptability and improved connectivity in dynamic environments. Figure 21 illustrates the concept of a fluid antenna.

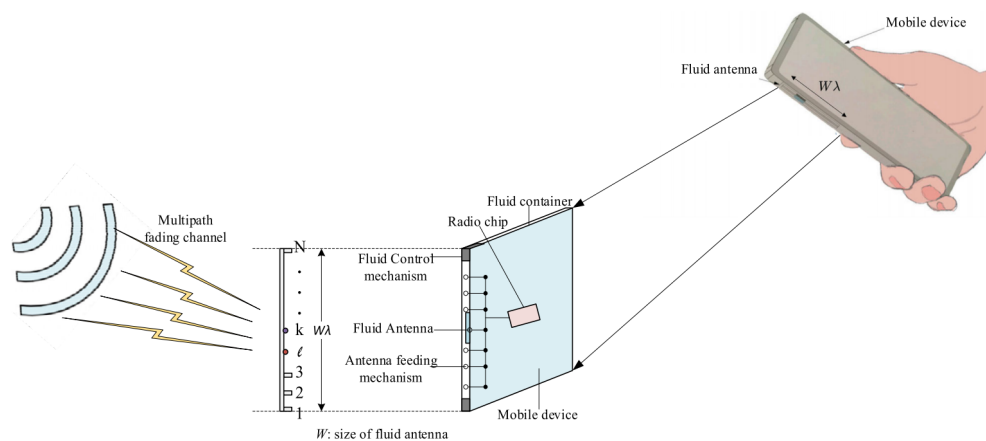


**Figure 21.** Concept of fluid antenna [327].

This novel antenna design dynamically adjusts its configuration to optimize signal quality and coverage.

## 5. Discussion

This review provides a comprehensive consolidation of the key enabling technologies necessary for realizing the Future Internet and 6G wireless networks. The technologies examined, including beamforming, massive MIMO, reconfigurable intelligent surfaces (RIS), terahertz communications, wireless energy harvesting, digital twins, and advanced antenna systems, each contribute uniquely to the evolving landscape of wireless communication. However, significant interdisciplinary challenges persist.

Beamforming techniques have advanced substantially, with hybrid and adaptive solutions enabling efficient wideband communication. Nevertheless, real-world deployment faces major hurdles, including architectural complexity, beam squint effects due to the lack of wideband tunable devices, and the need for ultra-fast beam management in dynamic environments. These limitations underscore the urgent need for novel beamforming methods that combine low complexity and power consumption with precise, multibeam control to achieve scalable, low-latency, energy-efficient performance.

Massive MIMO systems are foundational to the capacity and reliability gains envisioned for 6G. However, practical implementations remain constrained by energy consumption and hardware complexity. In mmWave communications, a compromise between high-gain beams and MIMO diversity is necessary to overcome the highly lossy environment. These challenges highlight the need for intelligent hybrid analog–digital designs and machine learning-driven beam management strategies to enable feasible massive MIMO deployments.

RIS technologies offer promising means for cost-effective manipulation of the wireless environment. However, the realization of dynamically controllable metasurfaces or selective frequency surfaces at practical scales remains nontrivial. Key challenges include low-latency reconfiguration, seamless integration with existing infrastructure, power optimization, and accurate channel estimation. Furthermore, the absence of standardized deployment models limits wide adoption. Embedding sensing capabilities and simplifying unit cell control will be crucial for real-time adaptability and computational efficiency.

Terahertz communications open access to vast underutilized spectral resources but introduce fundamental challenges, including high propagation losses, sensitivity to blockages, and atmospheric absorption. Addressing these constraints requires not only high-gain antenna innovations but also the development of efficient channel models, transceiver architectures, and multiple access schemes tailored to the impairments of THz bands.

Wireless energy harvesting and power transfer are pivotal for sustainable Internet of Everything (IoE) applications. Yet, existing solutions are limited by poor energy conversion efficiency and matching losses, especially under variable received power conditions. Novel energy harvester topologies and advanced nonlinear techniques are needed to optimize utilization of the vast RF spectrum and ensure efficient power transfer.

Digital twins hold transformative potential for wireless network design, offering real-time predictive management, virtual prototyping, and enhanced operational resilience. However, they introduce challenges such as real-time data synchronization, massive data handling, and scalable virtualization. Addressing these issues will require novel architectural frameworks and AI-enhanced analytics.

Antennas, fundamental to all the technologies discussed, face increasing demands for efficiency, miniaturization, reconfigurability, and integration. Innovations are required across user equipment, base stations, satellites, UAVs, and RIS-based systems to support multiband, multibeam, energy-efficient operation at mmWave and THz frequencies. Persistent challenges include phase noise, nonlinearities, THz miniaturization, and massive array integration, all under constraints of real-time adaptability, ultra-low latency, and high reliability. These demands necessitate disruptive circuit-level innovations and smarter, more resilient hardware paradigms.

Realizing the full potential of the Future Internet and 6G wireless networks demands a paradigm shift from incremental progress to a holistic, interdisciplinary approach that addresses performance, scalability, and sustainability simultaneously. This entails developing integrated solutions that balance system complexity with operational efficiency, enabling intelligent, adaptive, and energy-aware communication across all network layers. Overcoming the outlined challenges will require advances in hardware, cross-layer optimization, and machine learning-driven control, along with seamless integration of diverse technologies into a unified framework. The path to 6G will be shaped by the convergence of these technologies into a cohesive, resilient, and scalable infrastructure capable of supporting the stringent demands of future wireless ecosystems.

## 6. Conclusions

This review has explored the key perspectives and research challenges in wireless communication hardware, focusing on the evolving landscape of next-generation networks beyond 5G and towards 6G. The seamless integration of terrestrial and non-terrestrial networks, including satellite and HAPS, presents a fundamental shift in communication infrastructure, enabling global connectivity and ultra-reliable low-latency communications. Advancements in mmWave and sub-terahertz technologies, massive MIMO, beamforming networks, and RIS are essential to overcoming the limitations of current networks and ensuring enhanced performance.

Additionally, challenges such as high power consumption, spectrum efficiency, and thermal management must be addressed to develop more sustainable and energy-efficient wireless systems. The deployment of AI and ML in optimizing beamforming, digital twin technology for network orchestration, and WPT solutions for IoT networks further underscore the importance of interdisciplinary innovation. As we move towards the 6G era, it is evident that collaboration among industry stakeholders, researchers, and policy makers is crucial for realizing the full potential of these emerging technologies. Future research should focus on bridging the gap between theoretical advancements and practical implementations, ensuring that next-generation wireless networks are not only faster and more reliable but also energy-efficient, scalable, and seamlessly integrated into our digital society.

**Author Contributions:** Conceptualization, G.A.K.; methodology, D.G.A. and T.N.F.K.; validation T.M.E.; formal analysis, D.G.A. and C.L.Z.; investigation, D.G.A., T.N.F.K. and T.M.E.; resources, D.G.A. and T.M.E.; data curation, C.L.Z.; writing—original draft preparation, D.G.A., T.M.E. and T.N.F.K.; writing—review and editing, G.A.K. and C.L.Z.; visualization, D.G.A. and T.M.E.; supervision, G.A.K. All authors have read and agreed to the published version of the manuscript.

**Funding:** This research received no external funding.

**Data Availability Statement:** No new data were created or analyzed in this study.

**Conflicts of Interest:** The authors declare no conflicts of interest.

## Glossary

ADC	Analog to Digital Converter
AI	Artificial Intelligence
BM	Beamformer
DAC	Digital to Analog Converter
DT	Digital Twins
EIRP	Equivalent Isotropic Radiated Power
EM-EH	Electromagnetic Energy Harvesting
eMBB	Enhanced Mobile Broadband
FCC	Federal Commission of Communications
GEO	Geosynchronous Earth Orbit
HAPS	High-Altitude Platform Stations
HPA	High Power Amplifiers
IEEE	Institute of Electrical and Electronic Engineers
ITU	International Telecommunication Union
IoT	Internet of Things
IoV	Internet of Vehicles
LEO	Low Earth Orbit
LNA	Low Noise Amplifier
LOS	Line-of-Sight
MEMS	Microelectromechanical Systems
MIMO	Multiple Input Multiple Output
ML	Machine Learning
mMTC	Massive Machine Type Communications
NTN	Non-Terrestrial Networks
OAT	Over-the-Air
PAE	Power Added Efficiency
PCB	Printed Circuit Board

PCM	Phase Change Material
QoE	Quality of Experience
QoS	Quality of Service
RIS	Reconfigurable Intelligence Surfaces
SATCOM	Satellite Communications
SDMA	Spatial Division Multiple Access
SDVN	Software-Defined Vehicular Networks
SIW	Substrate Integrated Waveguide
SPDT	Single Pole Dual Through
UAV	Unmanned Aerial Vehicle
URLLC	Ultra-Reliable and Low Latency Communication
VR	Virtual Reality
WPT	Wireless Power Transfer
XR	Extended Reality

## References

- Pegoraro, R. What Is 5G, and Does It Actually Make a Difference? Available online: <https://www.nytimes.com/wirecutter/guides/what-is-5g/> (accessed on 30 December 2024).
- Patel, B.; Yarlagadda, V.K.; Dhameliya, N.; Mullangi, K.; Vennapusa, S.C.R. Advancements in 5G Technology: Enhancing Connectivity and Performance in Communication Engineering. *Eng. Int.* **2022**, *10*, 117–130. [[CrossRef](#)]
- European Commision. The Next Generation Internet of Things. Available online: <https://digital-strategy.ec.europa.eu/en/policies/next-generation-internet-things> (accessed on 30 December 2024).
- Frequencychecker: 5G NR N258 (mmWave 26 GHz). Available online: <https://www.frequencycheck.com/bands/5g-nr-band-25-8-26G> (accessed on 30 December 2024).
- Yarali, A. Future 6G Networks. In *From 5G to 6G: Technologies, Architecture, AI, and Security*; Wiley-IEEE Press: New York, NY, USA, 2023; pp. 185–201. [[CrossRef](#)]
- Kim, J.; Park, K. 6G and the Internet of Things: Topic Analysis. *J. Ind. Integr. Manag.* **2022**, *7*, 535–553. [[CrossRef](#)]
- Dala Pegorara Souto, V.; Dester, P.S.; Soares Pereira Facina, M.; Gomes Silva, D.; de Figueiredo, F.A.P.; Rodrigues de Lima Tejerina, G.; Silveira Santos Filho, J.C.; Silveira Ferreira, J.; Mendes, L.L.; Souza, R.D.; et al. Emerging MIMO Technologies for 6G Networks. *Sensors* **2023**, *23*, 1921. [[CrossRef](#)]
- Hajiyat, Z.R.; Ismail, A.; Sali, A.; Hamidon, M.N. Antenna in 6G wireless communication system: Specifications, challenges, and research directions. *Optik* **2021**, *231*, 166415. [[CrossRef](#)]
- Tuzi, D.; Delamotte, T.; Knopp, A. Beamforming Schemes for 6G Direct-to-Cell Connectivity Using Satellite Swarms. In Proceedings of the 2024 18th European Conference on Antennas and Propagation (EuCAP), Glasgow, UK, 17–22 March 2024; pp. 1–5. [[CrossRef](#)]
- Deguchi, A.; Hirai, C.; Matsuoka, H.; Nakano, T.; Oshima, K.; Tai, M.; Tani, S. What Is Society 5.0? In *Society 5.0: A People-Centric Super-Smart Society*; Springer: Singapore, 2020; pp. 1–23. [[CrossRef](#)]
- Dange, S.; Patil, S.; Patil, V.; Mulla, S.; Husainy, A. A Review on 5G Technology: Evolution, Features and Challenges. *Asian J. Sci. Appl. Technol.* **2021**, *10*, 15–21. [[CrossRef](#)]
- Akyildiz, I.F.; Kak, A.; Nie, S. 6G and Beyond: The Future of Wireless Communications Systems. *IEEE Access* **2020**, *8*, 133995–134030. [[CrossRef](#)]
- Dangi, R.; Choudhary, G.; Dragoni, N.; Lalwani, P.; Khare, U.; Kundu, S. 6G Mobile Networks: Key Technologies, Directions, and Advances. *Telecom* **2023**, *4*, 836–876. [[CrossRef](#)]
- Abe, Y.; Hiroshi, A.; Hitoshi, A.; Mitsuhiro, A.; Daniel, C.; Miwako, D.; Tomoyuki, E.; Katsumi, F.; Satoshi, F.; Mikio, F.; et al. *White Paper: Beyond 5G/6G*; Technical Report; National Institute of Information and Communications Technology (NICT): Tokyo, Japan, 2023.
- Bertenyi, B.; Kunzmann, G.; Nielsen, S.; Pedersen, K. *White Paper: Transforming the 6G Vision to Action*; Technical Report; Nokia Bell Labs: Espoo, Finland, 2024.
- Kim, H. Enhanced Mobile Broadband Communication Systems. In *Design and Optimization for 5G Wireless Communications*; Wiley-IEEE Press: New York, NY, USA, 2020; pp. 239–302. [[CrossRef](#)]
- Maghsoudnia, A.; Vlad, E.; Gong, A.; Dumitriu, D.M.; Hassanieh, H. Ultra-Reliable Low-Latency in 5G: A Close Reality or a Distant Goal? In Proceedings of the HotNets '24—23rd ACM Workshop on Hot Topics in Networks, Irvine, CA, USA, 18–19 November 2024; pp. 111–120. [[CrossRef](#)]
- Sachs, J.; Popovski, P.; Höglund, A.; Gozalvez-Serrano, D.; Fertl, P. Machine-type communications. In *5G Mobile and Wireless Communications Technology*; Osseiran, A., Monserrat, J.F., Marsch, P., Eds.; Cambridge University Press: Cambridge, UK, 2016; pp. 77–106.

19. Kota, S.; Giambene, G. IEEE International Network Generations Roadmap-Satellite. Available online: <https://futurenetworks.ieee.org/roadmap> (accessed on 30 December 2024).
20. Hong, W.; Jiang, Z.H.; Yu, C.; Hou, D.; Wang, H.; Guo, C.; Hu, Y.; Kuai, L.; Yu, Y.; Jiang, Z.; et al. The Role of Millimeter-Wave Technologies in 5G/6G Wireless Communications. *IEEE J. Microwaves* **2021**, *1*, 101–122. [CrossRef]
21. Tripathi, S.; Sabu, N.V.; Gupta, A.K.; Dhillon, H.S. Millimeter-Wave and Terahertz Spectrum for 6G Wireless. In *6G Mobile Wireless Networks*; Wu, Y., Singh, S., Taleb, T., Roy, A., Dhillon, H.S., Kanagarathinam, M.R., De, A., Eds.; Springer International Publishing: Cham, Switzerland, 2021; pp. 83–121. [CrossRef]
22. International Telecommunication Union (ITU), 2025. Available online: <https://www.itu.int/en/Pages/default.aspx> (accessed on 11 February 2025).
23. Balanis, C. *Antenna Theory: Analysis and Design*; Wiley: New York, NY, USA, 2015.
24. Marcus, M.; Pattan, B. Millimeter wave propagation: Spectrum management implications. *IEEE Microw. Mag.* **2005**, *6*, 54–62. [CrossRef]
25. Lialis, D.I.; Ntetsikas, N.; Paschaloudis, K.D.; Zekios, C.L.; Georgakopoulos, S.V.; Kyriacou, G.A. Design of True Time Delay Millimeter Wave Beamformers for 5G Multibeam Phased Arrays. *Electronics* **2020**, *9*, 1331. [CrossRef]
26. Cahoon, N.; Srinivasan, P.; Guarin, F. 6G Roadmap for Semiconductor Technologies: Challenges and Advances. In Proceedings of the 2022 IEEE International Reliability Physics Symposium (IRPS), Dallas, TX, USA, 27–31 March 2022; pp. 11B.1–1–11B.1–9. [CrossRef]
27. Yu, Y.; Yu, L.; Chen, P.; Yu, C. Behavioral Modeling of Millimeter Wave GaN Power Amplifiers for 6G Integrated Sensing and Communications Application. In Proceedings of the 2024 IEEE/MTT-S International Microwave Symposium—IMS 2024, Washington, DC, USA, 16–21 June 2024; pp. 653–656. [CrossRef]
28. Komatsuzaki, Y.; Sakata, S.; Saiki, K.; Yamashita, A.; Shinjo, S.; Yamanaka, K. Advanced GaN Wideband/Multiband Power Amplifier for Sub-6 GHz 5G and Beyond Wireless Communication: Toward Future Flexible Base Station by AI-Based Digital Assisted PA. *IEEE Microw. Mag.* **2024**, *25*, 32–43. [CrossRef]
29. Wang, J.; Zhang, W.; Chen, Y.; Liu, Z.; Sun, J.; Wang, C.X. Time-Varying Channel Estimation Scheme for Uplink MU-MIMO in 6G Systems. *IEEE Trans. Veh. Technol.* **2022**, *71*, 11820–11831. [CrossRef]
30. Zhang, H.; Tong, W. Channel Coding for 6G Extreme Connectivity—Requirements, Capabilities, and Fundamental Tradeoffs. *IEEE BITS Inf. Theory Mag.* **2023**, *3*, 54–66. [CrossRef]
31. Fang, X.; Feng, W.; Chen, Y.; Ge, N.; Zhang, Y. Joint Communication and Sensing Toward 6G: Models and Potential of Using MIMO. *IEEE Internet Things J.* **2023**, *10*, 4093–4116. [CrossRef]
32. Gautam, A.; Thakur, P.; Singh, G. Advanced channel coding schemes for B5G/6G networks: State-of-the-art analysis, research challenges and future directions. *Int. J. Commun. Syst.* **2024**, *37*, e5855.
33. Elbadawy, H.M.; Sadek, R.A. B5G/6G Service Planning Process for the Deployment of Smart Cities as a Model for Massive Urban Area Applications. In Proceedings of the 2022 39th National Radio Science Conference (NRSC), Cairo, Egypt, 29 November–1 December 2022; Volume 1, pp. 332–341. [CrossRef]
34. Bojovic, P.D.; Malbasic, T.; Vujosevic, D.; Martic, G.; Bojovic, Z. Dynamic QoS Management for a Flexible 5G/6G Network Core: A Step toward a Higher Programmability. *Sensors* **2022**, *22*, 2849. [CrossRef] [PubMed]
35. Kisseleff, S.; Martins, W.A.; Al-Hraishawi, H.; Chatzinotas, S.; Ottersten, B. Reconfigurable Intelligent Surfaces for Smart Cities: Research Challenges and Opportunities. *IEEE Open J. Commun. Soc.* **2020**, *1*, 1781–1797. [CrossRef]
36. Jian, M.; Alexandropoulos, G.C.; Basar, E.; Huang, C.; Liu, R.; Liu, Y.; Yuen, C. Reconfigurable intelligent surfaces for wireless communications: Overview of hardware designs, channel models, and estimation techniques. *Intell. Converg. Netw.* **2022**, *3*, 1–32. [CrossRef]
37. Siddiqi, M.Z.; Mir, T. Reconfigurable intelligent surface-aided wireless communications: An overview. *Intell. Converg. Netw.* **2022**, *3*, 33–63. [CrossRef]
38. Rana, B.; Cho, S.S.; Hong, I.P. Review Paper on Hardware of Reconfigurable Intelligent Surfaces. *IEEE Access* **2023**, *11*, 29614–29634. [CrossRef]
39. Tortora, P.; Modenini, D.; Zannoni, M.; Gramigna, E.; Strollo, E.; Togni, A.; Paolini, E.; Valentini, L.; Coccilillo, O.; Simone, L. Ground and Space Hardware for Interplanetary Communication Networks. In *A Roadmap to Future Space Connectivity: Satellite and Interplanetary Networks*; Sacchi, C., Granelli, F., Bassoli, R., Fitzek, F.H.P., Ruggieri, M., Eds.; Springer International Publishing: Cham, Switzerland, 2023; pp. 107–138. [CrossRef]
40. Guo, F.; Yu, F.R.; Zhang, H.; Li, X.; Ji, H.; Leung, V.C.M. Enabling Massive IoT Toward 6G: A Comprehensive Survey. *IEEE Internet Things J.* **2021**, *8*, 11891–11915. [CrossRef]
41. Arnaoutoglou, D.G.; Empliouk, T.M.; Kaifas, T.N.F.; Chryssomallis, M.T.; Kyriacou, G. A Review of Multifunctional Antenna Designs for Internet of Things. *Electronics* **2024**, *13*, 3200. [CrossRef]
42. Sandoval, R.M.; Garcia-Sanchez, A.J.; Garcia-Sanchez, F.; Garcia-Haro, J. Evaluating the More Suitable ISM Frequency Band for IoT-Based Smart Grids: A Quantitative Study of 915 MHz vs. 2400 MHz. *Sensors* **2017**, *17*, 76. [CrossRef] [PubMed]

43. Queralta, J.P.; Gia, T.; Zou, Z.; Tenhunen, H.; Westerlund, T. Comparative Study of LPWAN Technologies on Unlicensed Bands for M2M Communication in the IoT: Beyond LoRa and LoRaWAN. *Procedia Comput. Sci.* **2019**, *155*, 343–350.
44. Yu, X.; Li, G.; Lu, W. Power consumption based on 5G communication. In Proceedings of the 2021 IEEE 5th Information Technology, Networking, Electronic and Automation Control Conference (ITNEC), Xi'an, China, 15–17 October 2021; Volume 5, pp. 910–914. [CrossRef]
45. Frenger, P.; Jading, Y.; Bengtsson, J. 5G Energy Consumption: What's the Impact of 5G NR in Real Networks? Available online: <https://www.ericsson.com/en/blog/2021/10/5g-energy-consumption-impact-5g-nr> (accessed on 30 December 2024).
46. Takagi, Y.; Hirakawa, T.; Konishi, M.; Ohta, Y. Power Consumption and Reduction of High-Power Amplifier in 5G NR Downlink. *IEEE Access* **2024**, *12*, 55051–55061. [CrossRef]
47. Taneja, A.; Saluja, N.; Taneja, N.; Alqahtani, A.; Elmagzoub, M.A.; Shaikh, A.; Koundal, D. Power Optimization Model for Energy Sustainability in 6G Wireless Networks. *Sustainability* **2022**, *14*, 7310. [CrossRef]
48. Wu, W.; Yang, C.S.; Fu, I.K.; Liao, P.K.; Calin, D.; Fan, M. Revisiting the System Energy Footprint and Power Efficiency on the Way to Sustainable 6G Systems. *IEEE Wirel. Commun.* **2022**, *29*, 6–8. [CrossRef]
49. Naser, S.; Bariah, L.; Muhamadat, S.; Basar, E. Zero-Energy Devices Empowered 6G Networks: Opportunities, Key Technologies, and Challenges. *IEEE Internet Things Mag.* **2023**, *6*, 44–50. [CrossRef]
50. Garg, N.; Garg, R. Energy harvesting in IoT devices: A survey. In Proceedings of the 2017 International Conference on Intelligent Sustainable Systems (ICISS), Palladam, India, 7–8 December 2017; pp. 127–131. [CrossRef]
51. Zeadally, S.; Shaikh, F.K.; Talpur, A.; Sheng, Q.Z. Design architectures for energy harvesting in the Internet of Things. *Renew. Sustain. Energy Rev.* **2020**, *128*, 109901. [CrossRef]
52. Makhetha, M.J.; Markus, E.D.; Abu-Mahfouz, A.M. Integration of wireless power transfer and low power wide area networks in IoT applications—A review. *Sens. Int.* **2024**, *5*, 100284. [CrossRef]
53. Going Green: Energy Efficiency in Telecoms. Available online: <https://www.gsmaintelligence.com/product-news/going-green-energy-efficiency-in-telecoms/> (accessed on 30 December 2024).
54. Kolta, E.; Hatt, T.; Moore, S. *Going Green: Benchmarking the Energy Efficiency of Mobile Networks*, 2nd ed.; Technical Report; GSMA Intelligence: London, UK 2023.
55. Rijs, F. Next generation of efficient 6G power amplifiers. In Proceedings of the CWTe 6G Symposium, Eindhoven, The Netherlands, 15 September 2023.
56. Bordel, B.; Alcarria, R.; Chung, J.; Voinov, I.A. Spatial Multiplexing Techniques and Multifrequency Cells for Massive Machine-type Communications in Future 6G Networks. In *Proceedings of the Mobile Internet Security*; You, I., Kim, H., Angin, P., Eds.; Springer: Singapore, 2023; pp. 48–62.
57. Heydari, P. Transceivers for 6G Wireless Communications: Challenges and Design Solutions. In Proceedings of the 2021 IEEE Custom Integrated Circuits Conference (CICC), 25–30 April 2021; pp. 1–8. [CrossRef]
58. Lambrechts, J.W.; Sinha, S.; Sengupta, K.; Bimana, A.; Kadam, S.; Bhandari, S.; Preez, J.D.; Shao, Z.; Huang, X.; Liu, Z.; et al. Intelligent Integrated Circuits and Systems for 5G/6G Telecommunications. *IEEE Access* **2024**, *12*, 21402–21419. [CrossRef]
59. Liu, Y.; Liu, X.; Mu, X.; Hou, T.; Xu, J.; Di Renzo, M.; Al-Dhahir, N. Reconfigurable Intelligent Surfaces: Principles and Opportunities. *IEEE Commun. Surv. Tutor.* **2021**, *23*, 1546–1577. [CrossRef]
60. Gros, J.B.; Popov, V.; Odit, M.A.; Lenets, V.; Lerosey, G. A Reconfigurable Intelligent Surface at mmWave Based on a Binary Phase Tunable Metasurface. *IEEE Open J. Commun. Soc.* **2021**, *2*, 1055–1064. [CrossRef]
61. Hwang, M.; An, D.; Chang, S.; Youn, Y.; Kim, D.; Lee, C.; Hong, W. Demonstration of Millimeter-Wave Reconfigurable Intelligent Surface (RIS) with Built-In Sensors for Automatic Tracking of Direction-of-Arrival (DOA). *IEEE Sens. Lett.* **2023**, *7*, 1–4. [CrossRef]
62. Griva, A.I.; Boursianis, A.D.; Koulouridis, S.; Sarigiannidis, P.; Karagiannidis, G.; Goudos, S.K. Reconfigurable Intelligent Surfaces: A Brief Review on Design Specifications. In Proceedings of the 2024 13th International Conference on Modern Circuits and Systems Technologies (MOCAST), Sofia, Bulgaria, 26–28 June 2024; pp. 01–04. [CrossRef]
63. Li, J. Roadmap of 6G Reconfigurable Intelligent Surfaces with Nematic Liquid Crystals: Fundamentals, State-of-the-Art, and Challenges. In Proceedings of the 2024 10th International Conference on Control, Decision and Information Technologies (CoDIT), Valletta, Malta, 1–4 July 2024; pp. 802–807. [CrossRef]
64. Kim, J.; Choi, S.; Chung, H. Moving Reconfigurable Intelligent Surfaces: A Promising Frontier for 6G Communications. In Proceedings of the 2024 Fifteenth International Conference on Ubiquitous and Future Networks (ICUFN), Budapest, Hungary, 2–5 July 2024; pp. 233–237. [CrossRef]
65. Farashahi, M.; Seet, B.C.; Li, X.J. Dual-Polarized Reconfigurable Intelligent Surface Unit Cell with Single Varactor Diode. In Proceedings of the 2024 IEEE International Mediterranean Conference on Communications and Networking (MeditCom), Madrid, Spain, 8–11 July 2024; pp. 447–452. [CrossRef]

66. Saikia, M.; García-Fernández, M.; Álvarez Narciandi, G.; Babar Abbasi, M.A.; Cotton, S.; Yurduseven, O. A Polarization Insensitive and Angularly Stable Reconfigurable Unit Cell for Reconfigurable Intelligent Surfaces. In Proceedings of the 2024 IEEE International Symposium on Antennas and Propagation and INC/USNC-URSI Radio Science Meeting (AP-S/INC-USNC-URSI), Florence, Italy, 14–19 July 2024; pp. 1961–1962. [[CrossRef](#)]
67. Baki, A.K.M.; Roy Chowdhury, A.; Hasan, M.S. Toward the Realization of an Intelligent Reflecting Surface with Full 360° Phase Variation for Beam Steering Applications at C and X Bands. *IEEE Access* **2024**, *12*, 113178–113192. [[CrossRef](#)]
68. Zhang, Z.; Wei Zhang, J.; Juan Lv, Y.; Dong Li, H.; Luo, J.; Wei Wu, J.; Cheng, Q. A Novel Design Approach Using Zero-Pole-Based Multiport Model for Reconfigurable Intelligent Surfaces. *IEEE Trans. Antennas Propag.* **2024**, *72*, 8564–8574. [[CrossRef](#)]
69. Ahmed, M.; Wahid, A.; Khan, W.U.; Khan, F.; Ihsan, A.; Ali, Z.; Rabie, K.M.; Shongwe, T.; Han, Z. A Survey on RIS Advances in Terahertz Communications: Emerging Paradigms and Research Frontiers. *IEEE Access* **2024**, *12*, 173867–173901. [[CrossRef](#)]
70. Papazafeiropoulos, A.; Kourtessis, P.; Chatzinotas, S.; Kaklamani, D.I.; Venieris, I.S. Performance of Double-Stacked Intelligent Metasurface-Assisted Multiuser Massive MIMO Communications in the Wave Domain. *IEEE Trans. Wirel. Commun.* **2025**, *24*, 4205–4218. [[CrossRef](#)]
71. Darsena, D.; Verde, F.; Iudice, I.; Galdi, V. Design of Stacked Intelligent Metasurfaces With Reconfigurable Amplitude and Phase for Multiuser Downlink Beamforming. *IEEE Open J. Commun. Soc.* **2025**, *6*, 531–550. [[CrossRef](#)]
72. Mo, Z.; Ni, Y.; Liu, Y.; Zhao, H.; Li, L.; Cai, Y. Active RIS-assisted Communication Systems with Discrete Phase Shifts. *IEEE Commun. Lett.* **2025**, *29*, 674–678. [[CrossRef](#)]
73. Tishchenko, A.; Khalily, M.; Shojaeifard, A.; Burton, F.; Björnson, E.; Di Renzo, M.; Tafazolli, R. The Emergence of Multi-Functional and Hybrid Reconfigurable Intelligent Surfaces for Integrated Sensing and Communications—A Survey. *IEEE Commun. Surv. Tutor.* **2024**. [[CrossRef](#)]
74. Zheng, X.; Cheng, W.; Wang, J.; Zhang, W. Location-Driven Beamforming for RIS-Assisted Near-Field Communications. *IEEE Commun. Mag.* **2025**, *63*, 44–50. [[CrossRef](#)]
75. de Sena, S.; Rasti, M.; Mahmood, N.H.; Latva-aho, M. Beyond Diagonal RIS for Multi-Band Multi-Cell MIMO Networks: A Practical Frequency-Dependent Model and Performance Analysis. *IEEE Trans. Wirel. Commun.* **2025**, *24*, 749–766. [[CrossRef](#)]
76. Ozden, B.A.; Aydin, E. Antenna Selection for Receive Spatial Modulation System Empowered by Reconfigurable Intelligent Surface. *IEEE Trans. Veh. Technol.* **2025**, *74*, 1169–1179. [[CrossRef](#)]
77. Marasco, I.; Cantore, C.; Bianco, G.V.; Bruno, G.; D’Orazio, A.; Magno, G. Transparent Graphene-Based RIS for 6G Communications in the THz Spectrum. *IEEE OOpen J. Antennas Propag.* **2025**, *6*, 193–200. [[CrossRef](#)]
78. Heath, R.W., Jr.; Lozano, A. *Foundations of MIMO Communication*; Cambridge University Press: Cambridge, UK, 2018.
79. Chataut, R.; Akl, R. Massive MIMO Systems for 5G and beyond Networks—Overview, Recent Trends, Challenges, and Future Research Direction. *Sensors* **2020**, *20*, 2753. [[CrossRef](#)]
80. Saini, M.; Grewal, S.K. MIMO Systems in Wireless Communications: State of the Art. In Proceedings of the Information and Communication Technology for Competitive Strategies (ICTCS 2020), Rajasthan, India, 11–12 December 2020; pp. 1141–1153.
81. Tan, J.; Luan, T.H.; Guan, W.; Wang, Y.; Peng, H.; Zhang, Y.; Zhao, D.; Lu, N. Beam Alignment in mmWave V2X Communications: A Survey. *IEEE Commun. Surv. Tutor.* **2024**, *26*, 1676–1709. [[CrossRef](#)]
82. Xia, X.; Zhao, J.; Ni, X.; Wang, Y.; Zhou, J. Multiple-User Full-Duplex Hybrid Beamforming Design for mmWave Systems with a Joint Interference Cancellation Design. In Proceedings of the 2024 18th European Conference on Antennas and Propagation (EuCAP), Glasgow, UK, 17–22 March 2024; pp. 1–5. [[CrossRef](#)]
83. Jin, X.; Lv, T.; Ni, W.; Lin, Z.; Zhu, Q.; Hossain, E.; Poor, H.V. A Reconfigurable Subarray Architecture and Hybrid Beamforming for Millimeter-Wave Dual-Function-Radar-Communication Systems. *IEEE Trans. Wirel. Commun.* **2024**, *23*, 12594–12607. [[CrossRef](#)]
84. Hong, J.; Sun, J.; He, Y.; Zhang, W.; Wang, C.X. A Tensor-Based Millimeter Wave Wideband Massive MIMO Channel Estimation Technique Using Uniform Planar Arrays. *IEEE Wirel. Commun. Lett.* **2024**, *13*, 1458–1462. [[CrossRef](#)]
85. Zhu, X.; Liu, Y.; Wang, C.X. Sub-Array-Based Millimeter Wave Massive MIMO Channel Estimation. *IEEE Wirel. Commun. Lett.* **2023**, *12*, 1608–1612. [[CrossRef](#)]
86. Redondi, A.E.C.; Innamorati, C.; Gallucci, S.; Fiocchi, S.; Matera, F. A Survey on Future Millimeter-Wave Communication Applications. *IEEE Access* **2024**, *12*, 133165–133182. [[CrossRef](#)]
87. Satoshi, S.; Tatsuki, O.; Yuki, I.; Yoshihisa, K. 5G Multi-Antenna Technology and Experimental Trials, 2016. Available online: <https://ieeexplore.ieee.org/document/7833602> (accessed on 4 February 2025).
88. Khalaf, A.A.M.; El-Daly, A.R.B.M.; Hamed, H.F.A. Different adaptive beamforming algorithms for performance investigation of smart antenna system. In Proceedings of the 2016 24th International Conference on Software, Telecommunications and Computer Networks (SoftCOM), Split, Croatia, 22–24 September 2016; pp. 1–6. [[CrossRef](#)]
89. Kaur, S.; Kumar, N.; Dubey, S. Investigation of Adaptive Beam-forming Algorithms for Smart Antennas System. *IOP Conf. Ser. Mater. Sci. Eng.* **2021**, *1033*, 012015. [[CrossRef](#)]
90. Butler, J. Beam-forming matrix simplifies design of electronically scanned antennas. *Electron. Des.* **1961**, *9*, 170–173.
91. Nolen, J. *Synthesis of Multiple Beam Networks for Arbitrary Illuminations*; Bendix Corp.: Elyria, OH, USA, 1965.

92. Blass, J. Multidirectional antenna—A new approach to stacked beams. In Proceedings of the 1958 IRE International Convention Record, New York, NY, USA, 21–25 March 1966; Volume 8, pp. 48–50. [CrossRef]
93. Rotman, W.; Turner, R. Wide-angle microwave lens for line source applications. *IEEE Trans. Antennas Propag.* **1963**, *11*, 623–632. [CrossRef]
94. Shallah, A.B.; Zubir, F.; Rahim, M.K.A.; Majid, H.A.; Ullah Sheikh, U.; Murad, N.A.; Yusoff, Z. Recent Developments of Butler Matrix From Components Design Evolution to System Integration for 5G Beamforming Applications: A Survey. *IEEE Access* **2022**, *10*, 88434–88456. [CrossRef]
95. Kerjee, H.; Rahim, M.K.A.; Ayop, O.; Nayyef, N.A. Beamforming networks using the Nolen matrix for 5G applications. *Waves Random Complex Media* **2023**, *1*–21.
96. Lialisios, D.I.; Zekios, C.L.; Georgakopoulos, S.V. A New Class of Full-Dimensional Planar True-Time-Delay Beamforming Networks. *IEEE Trans. Antennas Propag.* **2024**, *72*, 2337–2346. [CrossRef]
97. Lialisios, D.I.; Zekios, C.L.; Georgakopoulos, S.V. Nonorthogonal Multibeam Network Synthesis Achieving Stein’s Limit and Implementation Based on RGW Technology. *IEEE Trans. Antennas Propag.* **2024**, *72*, 8184–8198. [CrossRef]
98. Ericsson. Base Stations and Networks. Available online: <https://www.ericsson.com/en/about-us/sustainability-and-corporate-responsibility/responsible-business/radio-waves-and-health/base-stations-and-networks> (accessed on 27 February 2025).
99. Boussad, Y.; Mahfoudi, M.N.; Legout, A.; Lizzi, L.; Ferrero, F.; Dabbous, W. Evaluating Smartphone Accuracy for RSSI Measurements. *IEEE Trans. Instrum. Meas.* **2021**, *70*, 1–12. [CrossRef]
100. Silver, S. *Microwave Antenna Theory and Design*; Radiation Laboratory Series; McGraw-Hill: New York, NY, USA, 1949; Volume 12.
101. Du, Y.; Cao, C.; Zou, X.; He, J.; Yan, H.; Wang, G.; Steer, D. Measurement and Modeling of Penetration Loss in the Range from 2 GHz to 74 GHz. In Proceedings of the 2016 IEEE Globecom Workshops (GC Wkshps), Washington, DC, USA, 4–8 December 2016; pp. 1–6. [CrossRef]
102. Joseph, W.; Roelens, L.; Martens, L. Path Loss Model for Wireless Applications at 3500 MHz. In Proceedings of the 2006 IEEE Antennas and Propagation Society International Symposium, Albuquerque, NM, USA, 9–14 July 2006; pp. 4751–4754. [CrossRef]
103. Anderson, C.; Rappaport, T. In-building wideband partition loss measurements at 2.5 and 60 GHz. *IEEE Trans. Wirel. Commun.* **2004**, *3*, 922–928. [CrossRef]
104. Sun, S.; Thomas, T.A.; Rappaport, T.S.; Nguyen, H.; Kovacs, I.Z.; Rodriguez, I. Path Loss, Shadow Fading, and Line-of-Sight Probability Models for 5G Urban Macro-, Cellular Scenarios. In Proceedings of the 2015 IEEE Globecom Workshops (GC Wkshps), San Diego, CA, USA, 6–10 December 2015; pp. 1–7. [CrossRef]
105. Empliouk, T.; Kapetanidis, P.; Arnaoutoglou, D.; Kolitsidas, C.; Lialisios, D.; Koutinos, A.; Kaifas, T.N.F.; Georgakopoulos, S.V.; Zekios, C.L.; Kyriacou, G.A. Compact, Ultra-Wideband Butler Matrix Beamformers for the Advanced 5G Band FR3—Part I. *Electronics* **2024**, *13*, 2763. [CrossRef]
106. Low, K.K.W.; Zihir, S.; Kanar, T.; Rebeiz, G.M. A 27–31-GHz 1024-Element Ka-Band SATCOM Phased-Array Transmitter With 49.5-dBW Peak EIRP, 1-dB AR, and  $\pm 70^\circ$  Beam Scanning. *IEEE Trans. Microw. Theory Tech.* **2022**, *70*, 1757–1768. [CrossRef]
107. Kebe, M.; Yagoub, M.C.E.; Amaya, R.E. A Survey of Phase Shifters for Microwave Phased Array Systems. *Int. J. Circuit Theory Appl.* **2024**.
108. Tagliapietra, G.; Giacomozzi, F.; Michelini, M.; Marcelli, R.; Sardi, G.M.; Iannacci, J. Discussion and Demonstration of RF-MEMS Attenuators Design Concepts and Modules for Advanced Beamforming in the Beyond-5G and 6G Scenario—Part 1. *Sensors* **2024**, *24*, 2308. [CrossRef] [PubMed]
109. Lee, Y.; Suh, B.; Min, B.W. A Ka-Band Bi-Directional Reconfigurable Switched Beam-Forming Network Based on  $4 \times 4$  Butler Matrix in 28-nm CMOS. *IEEE Trans. Microw. Theory Tech.* **2023**, *71*, 2479–2487. [CrossRef]
110. Niu, Y.; Li, Y.; Jin, D.; Su, L.; Vasilakos, A. A Survey of Millimeter Wave (mmWave) Communications for 5G: Opportunities and Challenges. *Wirel. Netw.* **2015**, *21*, 2657–2676. [CrossRef]
111. Yang, B.; Yu, Z.; Lan, J.; Zhang, R.; Zhou, J.; Hong, W. Digital Beamforming-Based Massive MIMO Transceiver for 5G Millimeter-Wave Communications. *IEEE Trans. Microw. Theory Tech.* **2018**, *66*, 3403–3418. [CrossRef]
112. Kim, D.C.; Park, S.J.; Kim, T.W.; Minz, L.; Park, S.O. Fully Digital Beamforming Receiver With a Real-Time Calibration for 5G Mobile Communication. *IEEE Trans. Antennas Propag.* **2019**, *67*, 3809–3819. [CrossRef]
113. Dutta, S.; Barati, C.N.; Ramirez, D.; Dhananjay, A.; Buckwalter, J.F.; Rangan, S. A Case for Digital Beamforming at mmWave. *IEEE Trans. Wirel. Commun.* **2020**, *19*, 756–770. [CrossRef]
114. Zhang, J.; Yu, X.; Letaief, K.B. Hybrid Beamforming for 5G and Beyond Millimeter-Wave Systems: A Holistic View. *IEEE Open J. Commun. Soc.* **2020**, *1*, 77–91. [CrossRef]
115. Sohrabi, F.; Yu, W. Hybrid Analog and Digital Beamforming for mmWave OFDM Large-Scale Antenna Arrays. *IEEE J. Sel. Areas Commun.* **2017**, *35*, 1432–1443. [CrossRef]
116. Li, A.; Masouros, C. Energy-Efficient SWIPT: From Fully Digital to Hybrid Analog–Digital Beamforming. *IEEE Trans. Veh. Technol.* **2018**, *67*, 3390–3405. [CrossRef]

117. Ardah, K.; Fodor, G.; Silva, Y.C.B.; Freitas, W.C.; de Almeida, A.L.F. Hybrid Analog-Digital Beamforming Design for SE and EE Maximization in Massive MIMO Networks. *IEEE Trans. Veh. Technol.* **2020**, *69*, 377–389. [CrossRef]
118. Hosking, R.H. Software Defined R Ware Defined Radio Handbook. Available online: <https://www.pentek.com/sftradhandbook/sftradhandbook.cfm> (accessed on 30 December 2024).
119. Han, C.; Yan, L.; Yuan, J. Hybrid Beamforming for Terahertz Wireless Communications: Challenges, Architectures, and Open Problems. *IEEE Wirel. Commun.* **2021**, *28*, 198–204. [CrossRef]
120. Abdalrazak, M.Q.; Majeed, A.H.; Abd-Alhameed, R.A. A Critical Examination of the Beam-Squinting Effect in Broadband Mobile Communication: Review Paper. *Electronics* **2023**, *12*, 400. [CrossRef]
121. Heng, Y.; Andrews, J.G.; Mo, J.; Va, V.; Ali, A.; Ng, B.L.; Zhang, J.C. Six Key Challenges for Beam Management in 5.5G and 6G Systems. *IEEE Commun. Mag.* **2021**, *59*, 74–79. [CrossRef]
122. Fanourios Fakoukakis, G.K. Novel Nolen Matrix Based Beamforming Networks For Series-Fed Low SII Multibeam Antennas. *Prog. Electromagn. Res. B* **2013**, *51*, 33–64. [CrossRef]
123. Brilhante, D.d.S.; Manjarres, J.C.; Moreira, R.; de Oliveira Veiga, L.; de Rezende, J.F.; Müller, F.; Klautau, A.; Leonel Mendes, L.; de Figueiredo, F.A.P. A Literature Survey on AI-Aided Beamforming and Beam Management for 5G and 6G Systems. *Sensors* **2023**, *23*, 4359. [CrossRef]
124. Chatzoglou, E.; Goudos, S.K. Beam-Selection for 5G/B5G Networks Using Machine Learning: A Comparative Study. *Sensors* **2023**, *23*, 2967. [CrossRef]
125. Nwajana, A.O.; Obi, E.R. A Review on SIW and Its Applications to Microwave Components. *Electronics* **2022**, *11*, 1160. [CrossRef]
126. Sahu, A.; Devabhaktuni, V.; Mishra, R.; Aaen, P. Recent advances in theory and applications of substrate-integrated waveguides: A review. *Int. J. Microw. Comput.-Aided Eng.* **2015**, *26*, 129–145. [CrossRef]
127. Bozzi, M.; Pasian, M.; Perregini, L.; Wu, K. On the losses in substrate-integrated waveguides and cavities. *Int. J. Microw. Wirel. Technol.* **2009**, *1*, 395–401. [CrossRef]
128. Parment, F.; Ghiotto, A.; Vuong, T.P.; Duchamp, J.M.; Wu, K. Air-filled SIW transmission line and phase shifter for high-performance and low-cost U-Band integrated circuits and systems. In Proceedings of the Global Symposium on Millimeter-Waves (GSMM), Montreal, QC, Canada, 25–27 May 2015; pp. 1–3. [CrossRef]
129. Messem, L.; Sinha, S.; Ocket, I.; Trischler, H.; Schlaffer, E.; Schlick, D.; Rogier, H.; Lemey, S. Air-filled SIW technology for mass-manufacturable and energy-efficient terahertz systems. *Sci. Rep.* **2023**, *13*, 16714. [CrossRef] [PubMed]
130. Valero-Nogueira, A.; Alfonso, E. How gap waveguides were conceived. In Proceedings of the 2017 11th European Conference on Antennas and Propagation (EUCAP), Paris, France, 19–24 March 2017; pp. 242–246. [CrossRef]
131. Sahu, A.; Aaen, P.H.; Devabhaktuni, V.K. Advanced technologies for next-generation RF front-end modules. *Int. J. Microw. Comput.-Aided Eng.* **2019**, *29*, e21700.
132. Shady, M.; Sifat, S.M.; Ali, M.M. Exploring Gap Waveguide Solutions: A Review of Millimeter-Wave Beamforming Components and Antennas for Advanced Applications. *J. Electron. Electr. Eng.* **2024**, *3*, 236–254. [CrossRef]
133. Tzounis, A.; Katsoulas, N.; Bartzanas, T.; Kittas, C. Internet of Things in agriculture, recent advances and future challenges. *Biosyst. Eng.* **2017**, *164*, 31–48. [CrossRef]
134. Hammi, B.; Khatoun, R.; Zeadally, S.; Fayad, A.; Khoukhi, L. Internet of Things (IoT) Technologies for Smart Cities. *IET Netw.* **2017**, *7*, 1–13. [CrossRef]
135. Ge, Y.; Zhang, G.; Meqdad, M.N.; Chen, S. A systematic and comprehensive review and investigation of intelligent IoT-based healthcare systems in rural societies and governments. *Artif. Intell. Med.* **2023**, *146*, 102702. [CrossRef] [PubMed]
136. Mateu, L.; Moll, F. Review of energy harvesting techniques and applications for microelectronics. In *Proceedings of the VLSI Circuits and Systems II*; Lopez, J.F., Fernandez, F.V., Lopez-Villegas, J.M., de la Rosa, J.M., Eds.; International Society for Optics and Photonics, SPIE: Philadelphia, PA, USA, 2005; Volume 5837, pp. 359–373. [CrossRef]
137. Matiko, J.W.; Grabham, N.J.; Beeby, S.P.; Tudor, M.J. Review of the application of energy harvesting in buildings. *Meas. Sci. Technol.* **2013**, *25*, 012002. [CrossRef]
138. Shaikh, F.K.; Zeadally, S. Energy harvesting in wireless sensor networks: A comprehensive review. *Renew. Sustain. Energy Rev.* **2016**, *55*, 1041–1054. [CrossRef]
139. Cansiz, M.; Altinel, D.; Kurt, G.K. Efficiency in RF energy harvesting systems: A comprehensive review. *Energy* **2019**, *174*, 292–309. [CrossRef]
140. Detka, K.; Górecki, K. Wireless Power Transfer—A Review. *Energies* **2022**, *15*, 7236. [CrossRef]
141. Liu, Z.; Li, T.; Li, S.; Mi, C.C. Advancements and challenges in wireless power transfer: A comprehensive review. *Nexus* **2024**, *1*, 100014. [CrossRef]
142. Nnamdi, U.; Asianuba, I. Wireless Power Transfer: A Review of Existing Technologies. *Eur. J. Eng. Technol. Res.* **2023**, *8*, 59–66. [CrossRef]

143. Lefki, M.; Baccar, S.; Shall, H.; Ghorbel, M.; Kadi, M. 5G Ambient Backscatter Communications: Achievable Range and Power Levels in an Urban Environment. In Proceedings of the 2022 IEEE 12th International Conference on RFID Technology and Applications (RFID-TA), Cagliari, Italy, 12–14 September 2022; pp. 74–77. [[CrossRef](#)]
144. Ahmed, M.; Khan, W.U.; Ihsan, A.; Li, X.; Li, J.; Tsiftsis, T.A. Backscatter Sensors Communication for 6G Low-Powered NOMA-Enabled IoT Networks Under Imperfect SIC. *IEEE Syst. J.* **2022**, *16*, 5883–5893. [[CrossRef](#)]
145. Disharoon, W.; Lee, S.Y.; Ramsey, J.; Ghalichechian, N. Overview of Reconfiguration Technologies for Reflectarrays and Trasmitarrays. In Proceedings of the 2023 17th European Conference on Antennas and Propagation (EuCAP), Florence, Italy, 26–31 March 2023; pp. 1–5. [[CrossRef](#)]
146. Mahdi, S.; Raheema, M.; Hammed, R. Design and analysis of reconfigurable filters employing varactor and PIN diodes. *Eng. Technol. J.* **2024**, *43*, 115–136. [[CrossRef](#)]
147. Messaoudi, E.; Sánchez de Rojas, J.V.; Martínez, J.D.; Boria, V.E. Miniaturized Fully Reconfigurable Bandpass Filter with Automated Varactor Biasing. In Proceedings of the 2024 IEEE International Microwave Filter Workshop (IMFW), Cocoa Beach, FL, USA, 21–23 February 2024; pp. 18–20. [[CrossRef](#)]
148. Sangmahamad, P.; Janpugdee, P.; Zhao, Y. A Metasurface-Based Electronically Reconfigurable and Dual-Polarized Reflectarray Antenna for Beam-Steering Applications. *IEEE Access* **2023**, *11*, 137414–137425. [[CrossRef](#)]
149. Agasti, R.; Nichols, D.C.; Eck, A.M.; Sigmarsson, H.H.; Ruyle, J.E. Varactor-Tuned Superstrate-Loaded Antenna and Filtenna for X-Band Applications. *IEEE Trans. Antennas Propag.* **2024**, *72*, 7651–7663. [[CrossRef](#)]
150. Wang, Z.; Dong, Y. Phase and Polarization Digitally Modulated Array Using Reconfigurable DR Element: Proposal, Design, and Verification. *IEEE Trans. Antennas Propag.* **2023**, *71*, 4102–4114. [[CrossRef](#)]
151. Wu, J.; Lu, X.; Wang, W.; Han, J.; Xu, G.; Huang, Z. Design of a Compact Polarization-Agile and Frequency-Tailored Array Antenna with Digital-Controllable Radiation Beams. *IEEE Trans. Antennas Propag.* **2022**, *70*, 813–822. [[CrossRef](#)]
152. Panaia, P.; Luxey, C.; Jacquemod, G.; Staraj, R.; Kossiavas, G.; Dussopt, L.; Vacherand, F.; Billard, C. MEMS-based reconfigurable antennas. In Proceedings of the 2004 IEEE International Symposium on Industrial Electronics, Ajaccio, France, 4–7 May 2004; Volume 1, pp. 175–179. [[CrossRef](#)]
153. Nadh, B.P.; Madhav, B.T.P.; Kumar, M.S.; Kumar, T.A.; Rao, M.V.; Reddy, S.M. MEMS-based reconfigurable and flexible antenna for body-centric wearable applications. *J. Electromagn. Waves Appl.* **2022**, *36*, 1389–1403. [[CrossRef](#)]
154. Khaira, N.K.; Singh, T.; Mansour, R.R. Monolithically Integrated RF MEMS-Based Variable Attenuator for Millimeter-Wave Applications. *IEEE Trans. Microw. Theory Tech.* **2019**, *67*, 3251–3259. [[CrossRef](#)]
155. G, A.; M, S.K.; Ayyadurai, M.; C, S.K.; Ramkumar, G. Design of Miniaturized Single Bit MEMS Phase Shifter using MEMS Switches. In Proceedings of the 2021 5th International Conference on Trends in Electronics and Informatics (ICOEI), Tirunelveli, India, 3–5 June 2021; pp. 235–239. [[CrossRef](#)]
156. Abumunshar, A.J.; Nahar, N.K.; Hyman, D.; Sertel, K. 18–40GHz low-profile phased array with integrated MEMS phase shifters. In Proceedings of the 2017 11th European Conference on Antennas and Propagation (EUCAP), Paris, France, 19–24 March 2017; pp. 2800–2801. [[CrossRef](#)]
157. Raeesi, A.; Abdel-Wahab, W.M.; Palizban, A.; Gigoyan, S.; Safavi-Naeini, S. A Bidirectional MEMS-Like Passive Beamformer for Emerging Millimeter-Wave Applications. *IEEE Trans. Microw. Theory Tech.* **2022**, *70*, 3741–3752. [[CrossRef](#)]
158. Zhang, Y.; Liu, H.; Sun, J.; Liu, Z. Scalable Contact-Capacitive MEMS Switches with High Capacitance Ratio for Millimeter-Wave Applications. *IEEE Access* **2022**, *10*, 37360–37368. [[CrossRef](#)]
159. Xu, J.; Yang, R.; Fan, Y.; Fu, Q.; Zhang, F. A Review of Tunable Electromagnetic Metamaterials with Anisotropic Liquid Crystals. *Front. Phys.* **2021**, *9*, 633104. [[CrossRef](#)]
160. Huang, Y.; Wen, G.; Zhu, W. Tunable metamaterials based on ferrites and the applications. In Proceedings of the 2012 International Workshop on Metamaterials (Meta), Nanjing, China, 8–10 October 2012; pp. 1–4. [[CrossRef](#)]
161. Bozorgi, M.; Rafaei-Booket, M. Metallic Array on a Biased Ferrite Substrate as a Reconfigurable Reflectarray Antenna. In Proceedings of the 2018 9th International Symposium on Telecommunications (IST), Tehran, Iran, 17–19 December 2018; pp. 80–85. [[CrossRef](#)]
162. Zhang, W.; Li, Y.; Zhang, Z. A Reconfigurable Reflectarray Antenna With an 8  $\mu\text{m}$ -Thick Layer of Liquid Crystal. *IEEE Trans. Antennas Propag.* **2022**, *70*, 2770–2778. [[CrossRef](#)]
163. Goelden, F.; Gaebler, A.; Karabey, O.; Goebel, M.; Manabe, A.; Jakoby, R. Tunable band-pass filter based on Liquid Crystal. In Proceedings of the German Microwave Conference Digest of Papers, Berlin, Germany, 15–17 March 2010; pp. 98–101.
164. Du, S.; Yang, Q.; Fan, X.; Wang, M.; Zhang, H. A Compact and Low-Loss Tunable Bandpass Filter Using YIG/GGG Film Structures. *IEEE Microw. Wirel. Technol. Lett.* **2023**, *33*, 259–262. [[CrossRef](#)]
165. Sheikh, S.I.M.; Gibson, A.A.P.; Basorrah, M.; Alhulwah, G.; Alanizi, K.; Alfarsi, M.; Zafar, J. Analog/Digital Ferrite Phase Shifter for Phased Array Antennas. *IEEE Antennas Wirel. Propag. Lett.* **2010**, *9*, 319–321. [[CrossRef](#)]
166. Wang, Q.; Su, Z.; Li, S.; Zhao, H.; Yin, X. Electrically tunable liquid crystal phase shifter with excellent phase shift capability per wavelength based on opposed coplanar waveguide. *J. Phys. D Appl. Phys.* **2022**, *55*, 405001. [[CrossRef](#)]

167. How, H.; Shi, P.; Vittoria, C.; Hokanson, E.; Champion, M.; Kempel, L.; Trott, K. Steerable phased array antennas using single-crystal YIG phase shifters-theory and experiments. *IEEE Trans. Microw. Theory Tech.* **2000**, *48*, 1544–1549. [CrossRef]
168. Liu, J.; Liang, F.; Wang, Y.; Ni, X.; Wang, X.; Zhao, D.; Wang, B.Z. Circularly Polarized High-Gain K-Band Liquid Crystal Phased Array Antenna. *IEEE Trans. Antennas Propag.* **2024**, *72*, 7341–7346. [CrossRef]
169. Suryapaga, V.; Khairnar, V.V. Review on Multifunctional Pattern and Polarization Reconfigurable Antennas. *IEEE Access* **2024**, *12*, 90218–90251. [CrossRef]
170. Tumarkin, A.; Sapego, E.; Gagarin, A.; Karamov, A. High Tunable BaTi<sub>x</sub>Zr<sub>1-x</sub>O<sub>3</sub> Films on Dielectric Substrate for Microwave Applications. *Molecules* **2022**, *27*, 6086. [CrossRef]
171. Borderon, C.; Ginestar, S.; Gundel, H.W.; Haskou, A.; Nadaud, K.; Renoud, R.; Sharaiha, A. Design and Development of a Tunable Ferroelectric Microwave Surface Mounted Device. *IEEE Trans. Ultrason. Ferroelectr. Freq. Control* **2020**, *67*, 1733–1737. [CrossRef]
172. Gagarin, A.; Platonov, R.; Legkova, T.; Altynnikov, A. Estimation of Ferroelectric Material Properties and Phase-Shifter Design Key Parameters Influence on Its Figure of Merit for Optimization of Development Process. *Crystals* **2021**, *11*, 538. [CrossRef]
173. Yao, K.; Chen, S.; Lai, S.C.; Yousry, Y.M. Enabling Distributed Intelligence with Ferroelectric Multifunctionalities. *Adv. Sci.* **2022**, *9*, 2103842. [CrossRef]
174. Gupta, D.; Kotnala, R. A review on current status and mechanisms of room-temperature magnetoelectric coupling in multiferroics for device applications. *J. Mater. Sci.* **2022**, *57*, 1–28. [CrossRef]
175. Yang, X.; Gao, Y.; Wu, J.; Zhou, Z.; Beguhn, S.; Nan, T.; Sun, N.X. Voltage Tunable Multiferroic Phase Shifter with YIG/PMN-PT Heterostructure. *IEEE Microw. Wirel. Components Lett.* **2014**, *24*, 191–193. [CrossRef]
176. Popov, M.A.; Zavisljak, I.V.; Zhou, P.; Li, T.; Shah, P.J.; Howe, B.M.; McConney, M.E.; Srinivasan, G.; Page, M.R. An electric field controlled dual resonator magneto-electric band-stop filter. *Microw. Opt. Technol. Lett.* **2019**, *61*, 873–877. [CrossRef]
177. Gaire, P.; Jaiswal, V.; Sayeed, S.Y.B.; Volakis, J.L.; Pulugurtha, M.R.; Bhardwaj, S. Tunable Multiferroics for Reconfigurable RF System Packages. In Proceedings of the 2021 IEEE 16th Nanotechnology Materials and Devices Conference (NMDC), Vancouver, BC, Canada, 12–15 December 2021; pp. 1–4. [CrossRef]
178. Bichurin, M.; Sokolov, O.; Ivanov, S.; Ivasheva, E.; Leontiev, V.; Lobekin, V.; Semenov, G. Modeling the Composites for Magnetoelectric Microwave Devices. *Sensors* **2023**, *23*, 1780. [CrossRef]
179. Rahimian Omam, Z.; Abdel-Wahab, W.; Gigoyan, S.; Safavi-Naeini, S. Continuously tunable 360° phase shifter based on planar waveguide technology for MM-wave applications. *Electron. Lett.* **2020**, *56*, 776–777.
180. Yasir, M.; Peinetti, F.; Savi, P. Enhanced Graphene Based Electronically Tunable Phase Shifter. *Micromachines* **2023**, *14*, 1877. [CrossRef] [PubMed]
181. Sounas, D.L.; Caloz, C. Graphene for highly tunable non-reciprocal electromagnetic devices. In Proceedings of the 2012 IEEE International Symposium on Antennas and Propagation, Chicago, IL, USA, 8–14 July 2012; pp. 1–2. [CrossRef]
182. Mutepfe, C.D.K.; Srivastava, V.M. Design and Implementation of Graphene-Based Tunable Microwave Filter for THz Applications. *Nanomaterials* **2022**, *12*, 4443. [CrossRef]
183. Ullah, Z.; Witjaksono, G.; Nawi, I.; Tansu, N.; Irfan Khattak, M.; Junaid, M. A Review on the Development of Tunable Graphene Nanoantennas for Terahertz Optoelectronic and Plasmonic Applications. *Sensors* **2020**, *20*, 1401. [CrossRef]
184. Zakrajsek, L.; Einarsson, E.; Thawdar, N.; Medley, M.; Jornet, J.M. Design of graphene-based plasmonic nano-antenna arrays in the presence of mutual coupling. In Proceedings of the 2017 11th European Conference on Antennas and Propagation (EUCAP), Paris, France, 19–24 March 2017; pp. 1381–1385. [CrossRef]
185. Singh, T.; Mansour, R.R. Miniaturized Reconfigurable 28 GHz PCM-Based 4-bit Latching Variable Attenuator for 5G mmWave Applications. In Proceedings of the 2020 IEEE/MTT-S International Microwave Symposium (IMS), Los Angeles, CA, USA, 4–6 August 2020; pp. 53–56. [CrossRef]
186. Hong, Q.; Luo, J.; Wen, C.; Zhang, J.; Zhu, Z.; Qin, S.; Yuan, X. Hybrid metal-graphene plasmonic sensor for multi-spectral sensing in both near- and mid-infrared ranges. *Opt. Express* **2019**, *27*, 35914–35924. [CrossRef] [PubMed]
187. Ibanez-Labiano, I.; Alomainy, A. Hybrid Metal-Graphene Ultra-Wideband Antenna. In Proceedings of the 2020 International Conference on UK-China Emerging Technologies (UCET), Glasgow, UK, 20–21 August 2020; pp. 1–3. [CrossRef]
188. Rong, X.S.; Wan, Q.M.; Peng, H.L.; Zhang, Y.P.; Mao, J.F. A Graphene Loaded THz Patch Antenna with Tunable Frequency. In Proceedings of the 2018 IEEE World Symposium on Communication Engineering (WSCE), Singapore, 28–30 December 2018; pp. 76–79. [CrossRef]
189. Yu, R.; Pruneri, V.; Garcia de Abajo, J. Active modulation of visible light with graphene-loaded ultrathin metal plasmonic antennas. *Sci. Rep.* **2016**, *6*, 32144. [CrossRef]
190. Hosseini, P.; Oraizi, H. Analysis and design of terahertz reflectarrays based on graphene cell clusters. *Sci. Rep.* **2022**, *12*, 22117. [CrossRef]
191. Li, J.; He, M.; Wu, C.; Zhang, C. Radiation-Pattern-Reconfigurable Graphene Leaky-Wave Antenna at Terahertz Band Based on Dielectric Grating Structure. *IEEE Antennas Wirel. Propag. Lett.* **2017**, *16*, 1771–1775. [CrossRef]

192. Abbasi, M.I.; Dahri, M.H.; Jamaluddin, M.H.; Seman, N.; Kamarudin, M.R.; Sulaiman, N.H. Millimeter Wave Beam Steering Reflectarray Antenna Based on Mechanical Rotation of Array. *IEEE Access* **2019**, *7*, 145685–145691. [[CrossRef](#)]
193. Hu, A.; Konno, K.; Chen, Q. A 2-bit 3-D-Printed Reflectarray Antenna Using Cylindrical Rotation-Based Phase-Tunable Elements. *IEEE Trans. Antennas Propag.* **2024**, *72*, 7774–7782. [[CrossRef](#)]
194. Hu, A.; Konno, K.; Chen, Q. A Novel Electromagnet-Controlled Reflectarray Element Employing 1-Bit Height Locking System with Low Power Consumption. *IEICE Commun. Express* **2024**, *13*, 285–288. [[CrossRef](#)]
195. Baena-Molina, M.; Palomares-Caballero, A.; Martinez-Garcia, G.; Padial-Allue, R.; Padilla, P.; Valenzuela-Valdes, J.F. 1-bit RIS Unit Cell with Mechanical Reconfiguration at 28 GHz. In Proceedings of the 2024 18th European Conference on Antennas and Propagation (EuCAP), Glasgow, UK, 17–22 March 2024; pp. 1–5. [[CrossRef](#)]
196. Cao, Z.; Li, Y.; Zhang, Z.; Iskander, M.F. Single Motor-Controlled Mechanically Reconfigurable Reflectarray. *IEEE Trans. Antennas Propag.* **2023**, *71*, 190–199. [[CrossRef](#)]
197. Ramer, R.; Chan, K.Y. Developing PCM-Based Microwave and Millimetre-Wave Switching Networks by Optimised Building Blocks. *Electronics* **2022**, *11*, 3683. [[CrossRef](#)]
198. Li, P.; Liu, W.; Ren, Z.; Meng, W.; Song, L. A High-Temperature and Frequency-Reconfigurable Multilayer Frequency Selective Surface Using Liquid Metal. *IEEE Access* **2022**, *10*, 9446–9454. [[CrossRef](#)]
199. Chen, P.; Wang, D.; Wang, L.; Liu, L.; Gan, Z. Liquid crystal-based reconfigurable antenna for 5G millimeter-wave. *Sci. Rep.* **2024**, *14*, 16646. [[CrossRef](#)] [[PubMed](#)]
200. Sun, P.; Liu, P.; Upadhyaya, P.; Jeong, D.; Heo, D.; Mina, E. Silicon-based PIN SPST RF switches for improved linearity. In Proceedings of the 2010 IEEE MTT-S International Microwave Symposium, Anaheim, CA, USA, 23–28 May 2010; pp. 948–951. [[CrossRef](#)]
201. Singh, T.; Hummel, G.; Vaseem, M.; Shamim, A. Recent Advancements in Reconfigurable mmWave Devices Based on Phase-Change and Metal Insulator Transition Materials. *IEEE J. Microwaves* **2023**, *3*, 827–851. [[CrossRef](#)]
202. Singh, T.; Khaira, N.K.; Repeta, M.; Mansour, R.R. Phase-Change RF Devices for Future Communications: Phase-Change Materials and Devices for Reconfigurable RF Front-Ends: State-of-the-Art and Future Perspectives. *IEEE Microw. Mag.* **2024**, *25*, 18–38. [[CrossRef](#)]
203. Singh, T.; Mansour, R.R. Symmetrical Multiport mmWave Chalcogenide Phase-Change RF Switches. In Proceedings of the 2023 IEEE/MTT-S International Microwave Symposium—IMS 2023, San Diego, CA, USA, 11–16 June 2023; pp. 1017–1020. [[CrossRef](#)]
204. Shuai, C.; Zheng, Y.; Chen, Q.; Fu, Y. Wideband Single-Pole Double-Throw Switch Based on Phase Change Material GeTe for Millimeter-Wave Applications. In Proceedings of the 2024 IEEE International Symposium on Radio-Frequency Integration Technology (RFIT), Chengdu, China, 28–30 August 2024; pp. 1–3. [[CrossRef](#)]
205. Wainstein, N.; Orren, A.; Nir-Harwood, R.G.; Yalon, E.; Kvatincky, S. Asymmetric and Symmetric Single-Pole Double-Throw With Improved Power Handling Using Indirectly Heated Phase-Change Switches. *IEEE Trans. Electron Devices* **2025**, *72*, 344–349. [[CrossRef](#)]
206. Singh, T.; Mansour, R.R. Ultra-Compact Phase-Change GeTe-Based Scalable mmWave Latching Crossbar Switch Matrices. *IEEE Trans. Microw. Theory Tech.* **2022**, *70*, 938–949. [[CrossRef](#)]
207. Yang, S.; Li, W.; Vaseem, M.; Shamim, A. Additively Manufactured Dual-Mode Reconfigurable Filter Employing VO<sub>2</sub>-Based Switches. *IEEE Trans. Components Packag. Manuf. Technol.* **2020**, *10*, 1738–1744. [[CrossRef](#)]
208. Su, Z.; Vaseem, M.; Li, W.; Yang, S.; Shamim, A. Additively Manufactured Frequency/Radiation Pattern Reconfigurable Antenna Based on Monolithically Printed VO<sub>2</sub> Switch. In Proceedings of the 2019 13th European Conference on Antennas and Propagation (EuCAP), Krakow, Poland, 31 March–5 April 2019; pp. 1–4.
209. El-Hinnawy, N.; Slovin, G.; Moen, K.; Masse, C.; Howard, D. A Tale of Two Phases: An Overview of Phase-Change Material RF Switch Technology: Sub-20-fs RON\*COFF RF Switch Technology for the Mm-Wave and 5G/6G Revolutions. *IEEE Microw. Mag.* **2024**, *25*, 57–76. [[CrossRef](#)]
210. Dong, J.; Zhu, Y.; Liu, Z.; Wang, M. Liquid Metal-Based Devices: Material Properties, Fabrication and Functionalities. *Nanomaterials* **2021**, *11*, 3400. [[CrossRef](#)] [[PubMed](#)]
211. Zhou, J.; Dong, J.; Wang, M.; Luo, H. A 3D printed dual-band antenna using liquid metal for wearable bracelets communications. In Proceedings of the 2020 IEEE MTT-S International Wireless Symposium (IWS), Shanghai, China, 20–23 September 2020; pp. 1–3. [[CrossRef](#)]
212. Liu, Z.F.; Zhu, Y.Y.; Ma, M.Y.; Wang, M.; Dong, J. Liquid Metal Antenna: Application and Fabrication. In Proceedings of the 2022 Photonics & Electromagnetics Research Symposium (PIERS), Hangzhou, China, 25–29 April 2022; pp. 715–717. [[CrossRef](#)]
213. Bharambe, V.; Adams, J.J.; Joshipura, I.D.; Ayers, H.R.; Dickey, M.D. Reversibly Reconfigurable Liquid Metal Patch Antenna Using A Superhydrophobic Spray-Coating. In Proceedings of the 2018 IEEE International Symposium on Antennas and Propagation & USNC/URSI National Radio Science Meeting, Boston, MA, USA, 8–13 July 2018; pp. 287–288. [[CrossRef](#)]

214. Pham, A.H.; Saeedi, S.; Sigmarsson, H.H. Continuously-Tunable Substrate Integrated Waveguide Bandpass Filter Actuated by Liquid Metal. In Proceedings of the 2019 IEEE MTT-S International Microwave Symposium (IMS), Boston, MA, USA, 2–7 June 2019; pp. 21–23. [CrossRef]
215. Chen, S.; Zhao, R.; Sun, X.; Wang, H.; Li, L.; Liu, J. Toxicity and Biocompatibility of Liquid Metals. *Adv. Healthc. Mater.* **2023**, *12*, 2201924. [CrossRef] [PubMed]
216. Zeb, S.; Mahmood, A.; Hassan, S.A.; Piran, M.J.; Gidlund, M.; Guizani, M. Industrial digital twins at the nexus of NextG wireless networks and computational intelligence: A survey. *J. Netw. Comput. Appl.* **2022**, *200*, 103309. [CrossRef]
217. Tao, F.; Zhang, H.; Liu, A.; Nee, A.Y.C. Digital Twin in Industry: State-of-the-Art. *IEEE Trans. Ind. Inform.* **2019**, *15*, 2405–2415. [CrossRef]
218. Barricelli, B.R.; Casiraghi, E.; Fogli, D. A Survey on Digital Twin: Definitions, Characteristics, Applications, and Design Implications. *IEEE Access* **2019**, *7*, 167653–167671. [CrossRef]
219. Starlink. Starlink—High-Speed Satellite Internet, 2025. Available online: <https://www.starlink.com/> (accessed on 4 February 2025).
220. Alpaydin, E. *Introduction to Machine Learning*, 4th ed.; MIT Press: Cambridge, MA, USA, 2020.
221. Federal Communications Commission (FCC). FCC Report on Starlink Modification Application; Federal Communications Commission (FCC): Washington, DC, USA, 2020.
222. IEEE Future Networks. Satellite Working Group—IEEE Future Networks Roadmap; IEEE Future Networks: Washington, DC, USA, 2025.
223. Waymo. Waymo—The Future of Driving, 2025. Available online: <https://waymo.com/intl/zh-tw/> (accessed on 4 February 2025).
224. Cruise LLC. Cruise—Driverless Rides | Autonomous Vehicles | Self-Driving Cars, 2025. Available online: <https://www.reuters.com/company/cruise-llc/> (accessed on 11 February 2025).
225. Agency for Science, Technology and Research (A\*STAR). A\*STAR—Advancing Science, Engineering, and Technology, 2025. Available online: <https://www.a-star.edu.sg/> (accessed on 4 February 2025).
226. Aptiv. Aptiv—Advancing Mobility, 2025. Available online: <https://www.aptiv.com/en/ces-2025> (accessed on 27 February 2025).
227. MooVita Pte Ltd. MooVita—Autonomous Driving Solutions, 2025. Available online: <https://www.moovita.com/> (accessed on 4 February 2025).
228. Ye, Z. In China, Drones Are Now Delivering Takeout to the Great Wall. *Sixth Tone*, 19 August 2024. Available online: <https://www.sixthtone.com/news/1015714> (accessed on 11 February 2025).
229. Meituan. Meituan—About Us, 2025. Available online: <https://www.meituan.com/en-US/about-us> (accessed on 4 February 2025).
230. Amazon. Amazon Drone Delivery—Help & Customer Service, 2025. Available online: <https://www.amazon.com/gp/help/customer/display.html?nodeId=T3jxhuvPfQ629BOIL4> (accessed on 4 February 2025).
231. Yang, Z. Food Delivery by Drone Is Just Part of Daily Life in Shenzhen. *MIT Technology Review* 2023. Available online: <https://www.technologyreview.com/2023/05/23/1073500/drone-food-delivery-shenzhen-meituan/> (accessed on 11 February 2025).
232. Polaris Market Research & Consulting LLP. Drone Package Delivery Market Size Poised to Hit USD 8,572.49 Million by 2032, Driven by a 37% CAGR, 2024. Available online: <https://www.polarismarketresearch.com/press-releases/drone-package-delivery-market> (accessed on 11 February 2025).
233. Eskandarpour, H.; Boldsaikhan, E. Last-Mile Drone Delivery: Past, Present, and Future. *Drones* **2023**, *7*, 77. [CrossRef]
234. Pilot Institute. Aviation Accident Causes—Pilot Error Statistics, 2020. Available online: <https://pilotinstitute.com/aviation-accident-causes/> (accessed on 11 February 2025).
235. Federal Communications Commission. FCC Adopts Initial Rules for ‘Drone’ Operations in the 5 GHz Band, 2024. Available online: <http://www.fcc.gov/document/fcc-adopts-initial-rules-drone-operations-5-ghz-band> (accessed on 11 February 2025).
236. Sendrea, R.E.; Zekios, C.L.; Georgakopoulos, S.V. A Review of Multi-Fidelity Learning Approaches for Electromagnetic Problems. *Electronics* **2025**, *14*, 89. [CrossRef]
237. Saad, W.; Bennis, M.; Chen, M. A Vision of 6G Wireless Systems: Applications, Trends, Technologies, and Open Research Problems. *IEEE Netw.* **2020**, *34*, 134–142. [CrossRef]
238. Tsafaras, A.C.; Mpatargias, P.; Karakilidis, A.; Giouros, G.; Gavriilidis, I.; Katsinelis, V.; Sarinakis, G.; Kaifas, T. Radiator Enablers for Wireless Communication Evolution. *Electronics* **2025**, *14*, 1081. [CrossRef]
239. Shepard, C.; Yu, H.; Anand, N.; Li, E.; Marzetta, T.; Yang, R.; Zhong, L. Argos: Practical many-antenna base stations. In Proceedings of the Mobicom ’12—18th Annual International Conference on Mobile Computing and Networking, Istanbul, Turkey, 22–26 August 2012; pp. 53–64. [CrossRef]
240. Vieira, J.; Malkowsky, S.; Nieman, K.; Miers, Z.; Kundargi, N.; Liu, L.; Wong, I.; Öwall, V.; Edfors, O.; Tufvesson, F. A flexible 100-antenna testbed for Massive MIMO. In Proceedings of the 2014 IEEE Globecom Workshops (GC Wkshps), Austin, TX, USA, 8–12 December 2014; pp. 287–293. [CrossRef]

241. Pang, X.; Hong, W.; Yang, T.; Li, L. Design and implementation of an active multibeam antenna system with 64 RF channels and 256 antenna elements for massive MIMO application in 5G wireless communications. *China Commun.* **2014**, *11*, 16–23. [CrossRef]
242. Harris, P.; Hasan, W.B.; Brice, H.; Chitambira, B.; Beach, M.; Mellios, E.; Nix, A.; Armour, S.; Doufexi, A. An overview of massive MIMO research at the University of Bristol. In Proceedings of the Radio Propagation and Technologies for 5G (2016), Durham, UK, 3 October 2016; pp. 1–5. [CrossRef]
243. Wirth, T.; Mehlhose, M.; Thiele, L.; Haustein, T. Proof-of-concept of flexible massive MIMO beamforming at 2.4 GHz. In Proceedings of the 2017 51st Asilomar Conference on Signals, Systems, and Computers, Pacific Grove, CA, USA, 29 October–1 November 2017; pp. 1061–1065. [CrossRef]
244. Al-Tarifi, M.A.; Sharawi, M.S.; Shamim, A. Massive MIMO antenna system for 5G base stations with directive ports and switched beamsteering capabilities. *IET Microwaves, Antennas Propag.* **2018**, *12*, 1709–1718.
245. Gröschel, P.; Hehn, M.; Sippel, E.; Schober, R.; Weigel, R.; Vossiek, M.; Carlowitz, C. An Ultra-Versatile Massive MIMO Transceiver Testbed for Multi-Gb/s Communication. In Proceedings of the 2019 IEEE 2nd 5G World Forum (5GWF), Dresden, Germany, 30 September–2 October 2019; pp. 1–6. [CrossRef]
246. el Mrini, M.; Mchbal, A.; Touhami, N. Design of a 240 elements antenna system for 5G massive MIMO applications with an inclined beam and two operating modes. *J. Electromagn. Waves Appl.* **2024**, *38*, 1–15. [CrossRef]
247. Qualcomm. Giga-MIMO Is the Foundation for Wide-Area 6G, 2025. Available online: <https://www.rcrwireless.com/20240325/5g/giga-mimo-is-the-foundation-for-wide-area-6g> (accessed on 27 February 2025).
248. Zandamela, A.; Marchetti, N.; Ammann, M.J.; Narbudowicz, A. 3-D Beam-Steering MIMO Antenna for On-Body IoT Applications. *IEEE Trans. Antennas Propag.* **2024**, *72*, 2241–2251. [CrossRef]
249. Gao, G.P.; Bai, J.M.; Jin, L.J.; Deng, W.Z.; Xu, H.; Peng, H.; Zou, Q.; Sun, Y.; Li, G. A Lightweight Flexible Wearable Circularly Polarized Antenna for Navigation and Positioning in IoT Applications. *IEEE Internet Things J.* **2025**, *12*, 16720–16734. [CrossRef]
250. Arnaoutoglou, D.G.; Kyriakou, A.A.G.; Kaifas, T.N.F.; Sirakoulis, G.C.; Kyriacou, G.A. An All-Polarization, Beamforming, and DoA Ready, G-Dipole Antenna Array. *IEEE Trans. Antennas Propag.* **2024**, *72*, 2323–2336. [CrossRef]
251. Zandamela, A.; Marchetti, N.; Ammann, M.J.; Narbudowicz, A. Pattern and Polarization Diversity Multisector Annular Antenna for IoT Applications. *IEEE Trans. Antennas Propag.* **2023**, *71*, 7241–7249. [CrossRef]
252. Guo, D.; Ma, G.; Hu, B. A Compact Tri-Port MIMO Antenna With High Isolation for Broadside and Conical Radiation. *IEEE Internet Things J.* **2024**, *12*, 12219–12225. [CrossRef]
253. Piao, D.; Wang, M.; Zuo, J.; Zhang, L.; Wang, Y. Compact and low coupled tripolarized microstrip MIMO antenna based on parasitic patch loading. *IEEE Trans. Antennas Propag.* **2021**, *69*, 5992–5997. [CrossRef]
254. Cao, C.; Zhang, X.; Song, C.; Georgiadis, A.; Goussetis, G. A Highly Integrated Multi-polarization Wideband Rectenna for Simultaneous Wireless Information and Power Transfer (SWIPT). *IEEE Trans. Antennas Propag.* **2023**, *71*, 7980–7991. [CrossRef]
255. Gao, S.; Chang, L.; Zhang, A.; Li, Y.; Zhang, Z. Small-Volume Microstrip Patch Antennas Exactly Covering Wi-Fi 6 Bands of 2.4–2.5 GHz and 5.15–5.85 GHz. *IEEE Trans. Antennas Propag.* **2023**, *71*, 5739–5748. [CrossRef]
256. Chou, H.T.; Yan, Z.D. Antenna-in-Package of Lateral Cross-Dipole Elements for Endfire Dual-Polarized Radiation at Dual Millimeter-Wave Frequency Bands for 5G FR2 User Equipment Applications. *IEEE Trans. Antennas Propag.* **2025**, *73*, 74–86. [CrossRef]
257. Chung, M.A.; Chen, K.X.; Hsu, C.C.; Lin, C.W. A  $10 \times 10$  Multi-Band MIMO Antenna System for LTE, 5G, Wi-Fi 7, and X-Band Communication Applications. *IEEE Access* **2025**, *13*, 28693–28710. [CrossRef]
258. Li, Y.; Sim, C.Y.D.; Luo, Y.; Yang, G. 12-Port 5G Massive MIMO Antenna Array in Sub-6GHz Mobile Handset for LTE Bands 42/43/46 Applications. *IEEE Access* **2018**, *6*, 344–354. [CrossRef]
259. Han, M.; Chang, L.; Zhang, A. Shared-Aperture Three-Antenna Module Using a Single Floating Metal With Small Clearance for 5G Mobile Terminals. *IEEE Antennas Wirel. Propag. Lett.* **2024**, *23*, 3053–3057. [CrossRef]
260. Hu, W.; Chen, Z.; Qian, L.; Wen, L.; Luo, Q.; Xu, R.; Jiang, W.; Gao, S. Wideband Back-Cover Antenna Design Using Dual Characteristic Modes With High Isolation for 5G MIMO Smartphone. *IEEE Trans. Antennas Propag.* **2022**, *70*, 5254–5265. [CrossRef]
261. Elwi, T.A.; Taher, F.; Virdee, B.S.; Alibakhshikenari, M.; Zuazola, I.J.G.; Krasniqi, A.; Kamel, A.S.; Tokan, N.T.; Khan, S.; Parchin, N.O. On the Performance of a Photonic Reconfigurable Electromagnetic Band Gap Antenna Array for 5G Applications. *IEEE Access* **2024**, *12*, 60849–60862. [CrossRef]
262. Luomaniemi, R.; Lehtovuori, A.; Ilvonen, J.; Khripkov, A.; Viikari, V. Extremely Low-Profile Tunable Multiport Handset Antenna. *IEEE Trans. Antennas Propag.* **2022**, *70*, 911–921. [CrossRef]
263. Wang, S.; Chang, H.Y. A 3D rectenna with all-polarization and omnidirectional capacity for IoT applications. In Proceedings of the IEEE MTT-S International Microwave Symposium, Los Angeles, CA, USA, 4–6 August 2020; pp. 1188–1190.
264. Wang, Y.; Piao, D.; Song, J. Implementation and MIMO performance assessment of two quad-polarized antennas. *IEEE Antennas Wirel. Propag. Lett.* **2022**, *21*, 2332–2336. [CrossRef]
265. Malav, V.K.; Sharma, A. A Miniaturized Coupler-Integrated Rectenna Element to Eliminate Hybrid-Coupler Circuit for Polarization-Insensitive Wireless Power Transmission. *IEEE Trans. Microw. Theory Tech.* **2024**, *73*, 2453–2460. [CrossRef]

266. Ziolkowski, R.W. Superdirective Unidirectional Mixed-Multipole Antennas: Designs, Analysis, and Simulations. *IEEE Trans. Antennas Propag.* **2023**, *71*, 5566–5581. [[CrossRef](#)]
267. Thakur, V.; Jaglan, N. Eight-Element Low-Profile MIMO System for Thin 5G Smartphone Applications. In Proceedings of the 2023 9th International Conference on Signal Processing and Communication (ICSC), Noida, India, 21–23 December 2023; pp 557–561. [[CrossRef](#)]
268. Sim, C.Y.D. Novel Techniques Applied to MIMO Antenna Array for 5G Sub-7 GHz Smartphone Applications. In Proceedings of the 2023 International Workshop on Antenna Technology (iWAT), Aalborg, Denmark, 15–17 May 2023; pp. 1–2. [[CrossRef](#)]
269. Chen, M.; Chang, L.; Zhang, A. Heat-Dissipating Mobile Antenna: A Novel Mobile Antenna Concept with Extremely Small Clearance and Integrated Heat-Dissipating Function. *IEEE Trans. Antennas Propag.* **2024**, *72*, 7480–7492. [[CrossRef](#)]
270. Li, H.; Zheng, W.; Diao, Y.; Wu, Q. Alleviating User Interaction for Handset Antennas With Reactive Loads. *IEEE Trans. Antennas Propag.* **2024**, *72*, 6069–6074. [[CrossRef](#)]
271. Sufian, M.A.; Hussain, N. Metasurface-Based Phone Case for the SAR Reduction of the 5G Mobile Phones. *IEEE Trans. Electromagn. Compat.* **2024**, *66*, 417–426. [[CrossRef](#)]
272. Alieldin, A.; Huang, Y.; Boyes, S.J.; Stanley, M.; Joseph, S.D.; Hua, Q.; Lei, D. A Triple-Band Dual-Polarized Indoor Base Station Antenna for 2G, 3G, 4G and Sub-6 GHz 5G Applications. *IEEE Access* **2018**, *6*, 49209–49216. [[CrossRef](#)]
273. Liu, Y.; Wang, S.; Li, N.; Wang, J.B.; Zhao, J. A Compact Dual-Band Dual-Polarized Antenna With Filtering Structures for Sub-6 GHz Base Station Applications. *IEEE Antennas Wirel. Propag. Lett.* **2018**, *17*, 1764–1768. [[CrossRef](#)]
274. Liu, F.; Guo, J.; Zhao, L.; Shen, X.; Yin, Y. A Meta-Surface Decoupling Method for Two Linear Polarized Antenna Array in Sub-6 GHz Base Station Applications. *IEEE Access* **2019**, *7*, 2759–2768. [[CrossRef](#)]
275. Feng, B.; Chung, K.L.; Lai, J.; Zeng, Q. A Conformal Magneto-Electric Dipole Antenna With Wide H-Plane and Band-Notch Radiation Characteristics for Sub-6-GHz 5G Base-Station. *IEEE Access* **2019**, *7*, 17469–17479. [[CrossRef](#)]
276. Berretti, L.; Loison, R.; Menargues, E.; Polo-López, L.; Toso, G.; García-Vigueras, M. Multibeam Antennas Based on 3-D Discrete Lenses With Magnified Field-of-View. *IEEE Open J. Antennas Propag.* **2025**, *6*, 98–109. [[CrossRef](#)]
277. Yang, Y.Q.; Jin, S.; Liu, D.; Yang, B.; Huang, J.; Cheng, Y.; Fei, C.; Zhou, B.; Mei, C.; Liu, L. Highly Integrated Q/V-Band Multi-Beam Phased Array Antenna for LEO Communication Satellite. In Proceedings of the 2022 IEEE MTT-S International Microwave Workshop Series on Advanced Materials and Processes for RF and THz Applications (IMWS-AMP), Guangzhou, China, 27–29 November 2022; pp. 1–3. [[CrossRef](#)]
278. Yoo, Y.; Park, J.; Lee, C.; Yoon, D.K.; Park, S.O. Reconfigurable Multibeam Holographic Antenna Based on Liquid-Crystal Technology for Ka-Band LEO Satellite Application. *IEEE Access* **2025**, *13*, 27141–27149. [[CrossRef](#)]
279. Vidal, F.; Legay, H.; Goussetis, G.; Ströber, T.; Gayrard, J.D. Benchmark of MEO Multibeam Satellite Adaptive Antenna and Payload Architectures for Broadband Systems. In Proceedings of the 2020 10th Advanced Satellite Multimedia Systems Conference and the 16th Signal Processing for Space Communications Workshop (ASMS/SPSC), Graz, Austria, 20–21 October 2020; pp. 1–8. [[CrossRef](#)]
280. Palisetty, R.; Socarras, L.M.G.; Chaker, H.; Singh, V.; Eappen, G.; Martins, W.A.; Ha, V.N.; Vásquez-Peralvo, J.A.; Rios, J.L.G.; Duncan, J.C.M. FPGA Implementation of Efficient Beamformer for On-Board Processing in MEO Satellites. In Proceedings of the 2023 IEEE 34th Annual International Symposium on Personal, Indoor and Mobile Radio Communications (PIMRC), Toronto, ON, Canada, 5–8 September 2023; pp. 1–7. [[CrossRef](#)]
281. Vidal, F.; Legay, H.; Goussetis, G.; Fraysse, J.P. Joint Precoding and Resource Allocation Strategies Applied to a Large Direct Radiating Array for GEO Telecom Satellite Applications. In Proceedings of the 2021 15th European Conference on Antennas and Propagation (EuCAP), Dusseldorf, Germany, 22–26 March 2021; pp. 1–5. [[CrossRef](#)]
282. Liu, Y.; Wang, Z.; Xu, J.; Ouyang, C.; Mu, X.; Schober, R. Near-Field Communications: A Tutorial Review. *IEEE Open J. Commun. Soc.* **2023**, *4*, 1999–2049. [[CrossRef](#)]
283. Ye, S.; Xiao, M.; Kwan, M.W.; Ma, Z.; Huang, Y.; Karagiannidis, G.; Fan, P. Extremely Large Aperture Array (ELAA) Communications: Foundations, Research Advances and Challenges. *IEEE Open J. Commun. Soc.* **2024**, *5*, 7075–7120. [[CrossRef](#)]
284. Cui, M.; Wu, Z.; Lu, Y.; Wei, X.; Dai, L. Near-Field MIMO Communications for 6G: Fundamentals, Challenges, Potentials, and Future Directions. *IEEE Commun. Mag.* **2023**, *61*, 40–46. [[CrossRef](#)]
285. Huang, J.; Qi, C.; Dobre, O.A.; Li, G.Y. Beam Switching Based Beam Design for High-Speed Train mmWave Communications. *IEEE Trans. Wirel. Commun.* **2025**, *24*, 1355–1370. [[CrossRef](#)]
286. Sun, L.; Chen, Z.; Huang, T.; Shu, F.; Yan, S. Near-Field Communication With Random Frequency Diverse Array. *IEEE Wirel. Commun. Lett.* **2025**, *14*, 213–217. [[CrossRef](#)]
287. Droulias, S.; Stratidakis, G.; Alexiou, A. Beam-focusing in near-field communications: Enhancing the physical layer security. In Proceedings of the 2024 IEEE 25th International Workshop on Signal Processing Advances in Wireless Communications (SPAWC), Lucca, Italy, 10–13 September 2024; pp. 216–220. [[CrossRef](#)]

288. Moulin, F.D.S.; Thiran, G.; Craeye, C.; Vandendorpe, L.; Oestges, C. Near-Field EM-Based Multistatic Radar Range Estimation. In Proceedings of the 2024 32nd European Signal Processing Conference (EUSIPCO), Lyon, France, 26–30 August 2024; pp. 2407–2411. [CrossRef]
289. Chen, K.; Qi, C.; Li, G.Y.; Dobre, O.A. Near-Field Multiuser Communications Based on Sparse Arrays. *IEEE J. Sel. Top. Signal Process.* **2024**, *18*, 619–632. [CrossRef]
290. Saha, N.; Alvarez, E.P.; Mahbub, I. A Novel Theoretical Modeling of the Received Power for Phased Array-Based Wireless Power Transfer System in the Near-Field Region. *IEEE Open J. Antennas Propag.* **2024**, *5*, 1476–1488. [CrossRef]
291. Hu, X.; Zhang, Y.; Yang, L.; Li, Y.; Li, K.; Yi, Y.; Kai, C. Securing Near-Field Wideband MIMO Communications via True-Time Delayer-Based Hybrid Beamfocusing. *IEEE Trans. Wirel. Commun.* **2024**, *23*, 13562–13578. [CrossRef]
292. Wang, X.; Zhang, C.; Zhang, H.; Xu, Y.; Zheng, F.C. Near-Field Codebook Design for Extremely Large Cylindrical Antenna Array Systems. *IEEE Trans. Commun.* **2024**, *72*, 5380–5395. [CrossRef]
293. Chen, Y.; Chen, M.; Xu, H.; Yang, Z.; Wong, K.K.; Zhang, Z. Joint Beamforming and Antenna Design for Near-Field Fluid Antenna System. *IEEE Wirel. Commun. Lett.* **2025**, *14*, 415–419. [CrossRef]
294. Ding, J.; Zhu, L.; Zhou, Z.; Jiao, B.; Zhang, R. Near-Field Multiuser Communications Aided by Movable Antennas. *IEEE Wirel. Commun. Lett.* **2025**, *14*, 138–142. [CrossRef]
295. Interdonato, G.; Björnson, E.; Ngo, H.Q.; Frenger, P.; Larsson, E.G. Ubiquitous cell-free Massive MIMO communications. *J. Wirel. Commun. Netw.* **2019**, *2019*, 197. [CrossRef]
296. Ngo, H.Q.; Ashikhmin, A.; Yang, H.; Larsson, E.G.; Marzetta, T.L. Cell-Free Massive MIMO Versus Small Cells. *IEEE Trans. Wirel. Commun.* **2017**, *16*, 1834–1850. [CrossRef]
297. Zhang, J.; Chen, S.; Lin, Y.; Zheng, J.; Ai, B.; Hanzo, L. Cell-Free Massive MIMO: A New Next-Generation Paradigm. *IEEE Access* **2019**, *7*, 99878–99888. [CrossRef]
298. Kassam, J.; Castanheira, D.; Silva, A.; Dinis, R.; Gameiro, A. Cell-Free Massive MIMO Technology and Applications in 6G. In *Massive MIMO for Future Wireless Communication Systems: Technology and Applications*; IEEE: New York, NY, USA, 2025; pp. 95–122. [CrossRef]
299. Femenias, G.; Riera-Palou, F. From Cells to Freedom: 6G’s Evolutionary Shift with Cell-Free Massive MIMO. *IEEE Trans. Mob. Comput.* **2025**, *24*, 812–829. [CrossRef]
300. Frenger, P.; Hederen, J.; Hessler, M.; Interdonato, G. Improved Antenna Arrangement for Distributed Massive MIMO. WO2018103897, 14 June 2018.
301. Shaik, Z.H.; Björnson, E.; Larsson, E.G. Cell-Free Massive MIMO with Radio Stripes and Sequential Uplink Processing. In Proceedings of the 2020 IEEE International Conference on Communications Workshops (ICC Workshops), Dublin, Ireland, 7–11 June 2020; pp. 1–6. [CrossRef]
302. Riera-Palou, F.; Femenias, G.; Caus, M.; Shaat, M.; Pérez-Neira, A.I. Scalable Cell-Free Massive MIMO Networks With LEO Satellite Support. *IEEE Access* **2022**, *10*, 37557–37571. [CrossRef]
303. López, O.L.A.; Kumar, D.; Souza, R.D.; Popovski, P.; Tölli, A.; Latva-Aho, M. Massive MIMO With Radio Stripes for Indoor Wireless Energy Transfer. *IEEE Trans. Wirel. Commun.* **2022**, *21*, 7088–7104. [CrossRef]
304. Tang, W.; Gao, X.; Ding, C.; Zhu, C.; Li, R.; Tian, B.; Bu, X.; An, J. A Quad-Polarization Reconfigurable Conformal Array of Wide Coverage Range and High Gain for Unmanned Aerial Vehicle Communications. *IEEE Trans. Antennas Propag.* **2024**, *72*, 3795–3800. [CrossRef]
305. Ding, C.; Gao, X.; Tang, W.; Liu, H.; Zhu, C.; Bu, X.; An, J. A Balloon Conformal Heterogeneous Array Antenna with Ultrawide Bandwidth and Half-Space Beam Coverage. *IEEE Trans. Antennas Propag.* **2024**, *72*, 7077–7088. [CrossRef]
306. Chou, H.T.; Lin, D.B.; Chiu, H.L. Planar Dual-Mode Dipole Antenna Formed by Artificial Microstrip Arms Loaded With Multiple H-Slots for Broadband Operation of Vertically Polarized Radiation on UAV Platform. *IEEE Trans. Antennas Propag.* **2022**, *70*, 7869–7877. [CrossRef]
307. Diao, W.; Li, Y.; Zhang, Z. A Null-Filled Axisymmetric Secant-Square-Shaped Beam Antenna for Unmanned Aerial Vehicles. *IEEE Antennas Wirel. Propag. Lett.* **2023**, *22*, 1937–1941. [CrossRef]
308. Lu, P.; Xia, Y.; Lei, E.; Wang, Y.; Song, C. Airborne Flexible Rectifying Metasurface System for Wirelessly Powered Unmanned Aerial Vehicles (UAVs). *IEEE Trans. Antennas Propag.* **2024**, *72*, 7710–7721. [CrossRef]
309. Gao, S.; Ge, L.; Zhang, D.; Qin, W. Low-profile dual-band stacked microstrip monopolar patch antenna for WLAN and car-to-car communications. *IEEE Access* **2018**, *6*, 69575–69581. [CrossRef]
310. Mondal, T.; Maity, S.; Ghatak, R.; Chaudhuri, S.R.B. Compact circularly polarized wide-beamwidth fern-fractal-shaped microstrip antenna for vehicular communication. *IEEE Trans. Veh. Technol.* **2018**, *67*, 5126–5134. [CrossRef]
311. Wang, S.; Zhu, L.; Zhang, G.; Yang, J.; Wang, J.; Wu, W. Dual-band dual-CP all-metal antenna with large signal coverage and high isolation over two bands for vehicular communications. *IEEE Trans. Veh. Technol.* **2020**, *69*, 1131–1135. [CrossRef]
312. Alsath, M.G.N.; Kanagasabai, M. Compact UWB monopole antenna for automotive communications. *IEEE Trans. Antennas Propag.* **2015**, *62*, 4204–4208. [CrossRef]

313. Bactavatchalame, P.; Rajakani, K. Compact broadband slot-based MIMO antenna array for vehicular environment. *Microw. Opt. Technol. Lett.* **2020**, *62*, 2024–2032. [[CrossRef](#)]
314. Saravanan, M.; Kalidoss, R.; Partibane, B.; Vishvaksenan, K.S. Design of an interlocked four-port MIMO antenna for UWB automotive communications. *Int. J. Microw. Wirel. Technol.* **2021**, *14*, 239–246. [[CrossRef](#)]
315. Dwivedi, A.K.; Sharma, A.; Singh, A.K.; Singh, V. Circularly polarized quad-port MIMO dielectric resonator antenna with beam tilting feature for vehicular communication. *IETE Tech. Rev.* **2020**, *39*, 389–401. [[CrossRef](#)]
316. Che, J.K.; Chen, C.C.; Locke, J.F. A compact 4-channel MIMO 5G Sub-6 GHz/LTE/WLAN/V2X antenna design for modern vehicles. *IEEE Trans. Antennas Propag.* **2021**, *69*, 7290–7297. [[CrossRef](#)]
317. Wang, W.; Zhao, Z.; Sun, Q.; Liao, X.; Fang, Z.; See, K.Y.; Zheng, Y. Compact quad-element vertically-polarized high isolation wideband MIMO antenna for vehicular base station. *IEEE Trans. Veh. Technol.* **2020**, *69*, 10000–10008. [[CrossRef](#)]
318. Kalista, W.; Leszkowska, L.; Rzymowski, M.; Nyka, K.; Kulas, L. Low-cost 3D Printed Circularly Polarized Lens Antenna for 5.9 GHz V2X Applications. In Proceedings of the 2023 17th European Conference on Antennas and Propagation (EuCAP), Florence, Italy, 26–31 March 2023; pp. 1–4. [[CrossRef](#)]
319. Saurabh, A.K.; Bharati, R.; Meshram, M.K. Wideband 32-Element 3D-MIMO antenna for vehicular applications. *AEU—Int. J. Electron. Commun.* **2024**, *186*, 155475. [[CrossRef](#)]
320. Kong, X.; Wu, Y.; Wang, H.; Xia, F. Edge Computing for Internet of Everything: A Survey. *IEEE Internet Things J.* **2022**, *9*, 23472–23485. [[CrossRef](#)]
321. Zhang, Q.; Luo, Y.; Jiang, H.; Zhang, K. Aerial Edge Computing: A Survey. *IEEE Internet Things J.* **2023**, *10*, 14357–14374. [[CrossRef](#)]
322. Yin, Z.; Wu, C.; Guo, C.; Li, Y.; Xu, M.; Gao, W.; Chi, C. A comprehensive survey of orbital edge computing: Systems, applications, and algorithms. *Chin. J. Aeronaut.* **2024**, *in press*. [[CrossRef](#)]
323. McLaren Applied. The First 5G Edge Computing Rail Antenna, 2024. Available online: <https://mclarenapplied.com/solutions/active-antenna> (accessed on 5 April 2025).
324. McLaren Applied. 5G Intelligent Edge Antenna (HALO 300), 2024. Available online: <https://mclarenapplied.com/products/halo-300-antenna> (accessed on 5 April 2025).
325. Michailidis, E.T.; Miridakis, N.I.; Michalas, A.; Skondras, E.; Vergados, D.J.; Vergados, D.D. Energy Optimization in Massive MIMO UAV-Aided MEC-Enabled Vehicular Networks. *IEEE Access* **2021**, *9*, 117388–117403. [[CrossRef](#)]
326. Zuo, Y.; Guo, J.; Sheng, B.; Dai, C.; Xiao, F.; Jin, S. Fluid Antenna for Mobile Edge Computing. *IEEE Commun. Lett.* **2024**, *28*, 1728–1732. [[CrossRef](#)]
327. Shah, A.F.M.S.; Karabulut, M.A.; Cinar, E.; Rabie, K.M. A Survey on Fluid Antenna Multiple Access for 6G: A New Multiple Access Technology That Provides Great Diversity in a Small Space. *IEEE Access* **2024**, *12*, 88410–88425. [[CrossRef](#)]

**Disclaimer/Publisher’s Note:** The statements, opinions and data contained in all publications are solely those of the individual author(s) and contributor(s) and not of MDPI and/or the editor(s). MDPI and/or the editor(s) disclaim responsibility for any injury to people or property resulting from any ideas, methods, instructions or products referred to in the content.